Novel Design Methodology for Variable Stiffness Laminates

Master Thesis

Daniel Ladomerszki

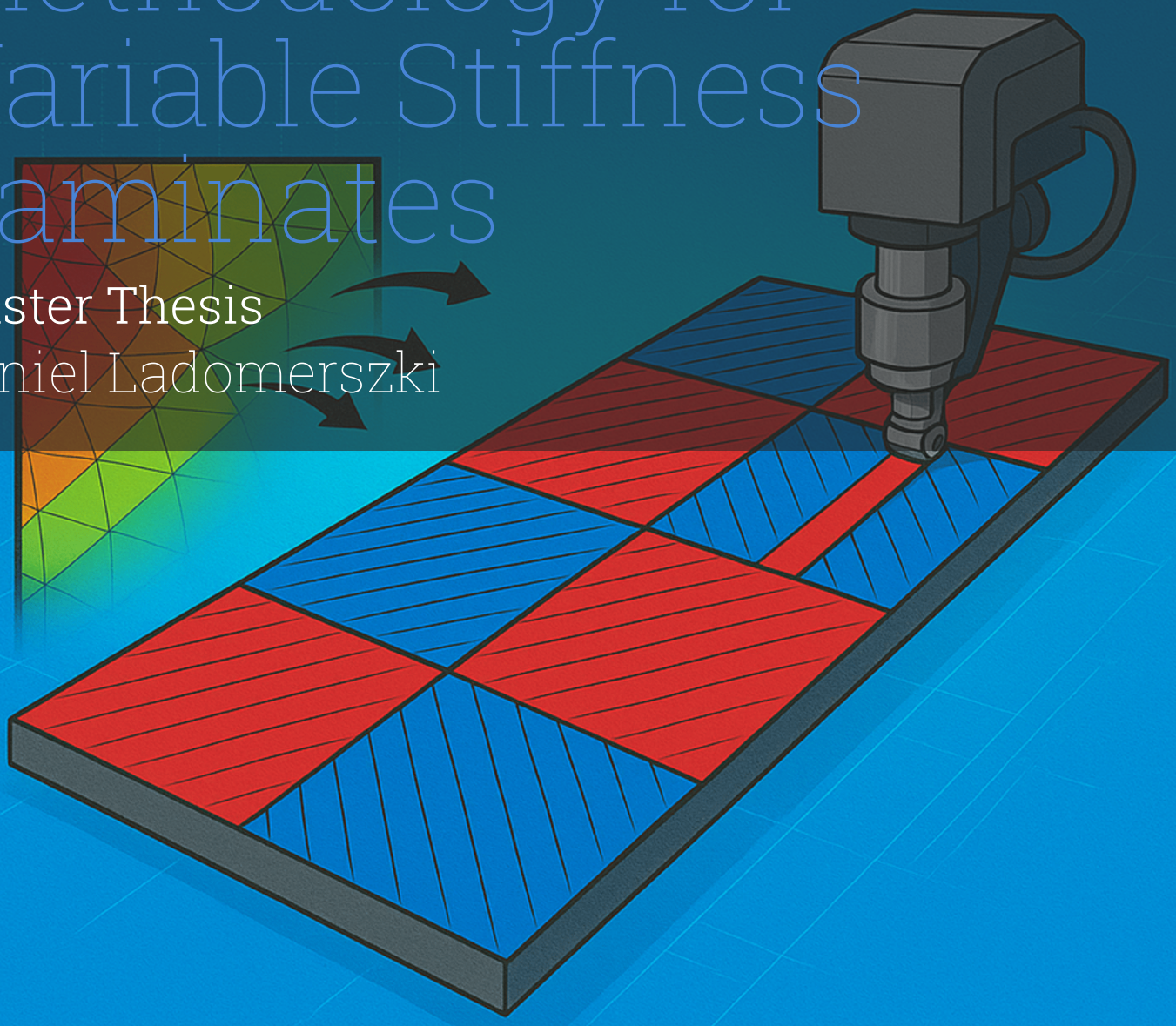

Delft University of Technology & Collins Aerospace

TU Delft

Collins Aerospace

Novel Design Methodology for Variable Stiffness Laminates

by

Daniel Ladomerszki

Daniel Ladomerszki(5222346)

Supervisor:	Daniel Peeters
Company Supervisor:	Ismet Baran
Project Duration:	February, 2025 - September, 2025
Faculty:	Faculty of Aerospace Engineering-Aerospace Structures and Materials, Delft

Cover:	Chat Gpt
Style:	TU Delft Report Style, with modifications by Daan Zwaneveld

TU Delft

Collins Aerospace

Preface

This thesis marks the end of a master program at the Technical University of Delft. This long journey provided valuable knowledge and experience in engineering for personal and proffessional growth. The thesis was conducted at Collins Aerospace Advanvced Materials Design Methods and Simulation team located at Houten. The topic involves a vide variety of knowledge areas and topics.

First of all I am grateful for the supervision provided by my responsible supervisor Daniel Peeters and company supervisor Ismet Baran. Their supervision provided valuable outside perspective and hope in the future further collaboration on new projects will be possible. Furthermore, I want to thank my friends who provided support during late night study sessions during the masters.

Lastly I want to thank my family. My sister and brother supported me along the way and without them this thesis and masters degree would have been not possible.

”Gratitude is not only the greatest of virtues, but the parent of all the others.” — Cicero

Daniel Ladomerszki
Delft, September 2025

Summary

Global warming has created new incentives for innovation in the aerospace industry. Among the most promising developments for aerospace are technologies such as sustainable aviation fuels and the use of advanced composite materials. Weight reduction remains one of the most direct and effective strategies for lowering emissions in aerospace applications. In this regard, composite materials with thermoset or thermoplastic matrices have become a major focus of research. The industry has increasingly pushed toward employing composites in more structural components [10].

In recent years, interest in thermoplastic composites has grown, particularly due to their potential for recyclability. Moreover, these materials are compatible with advanced automated manufacturing techniques, such as automated fiber placement (AFP), automated tape placement (ATP), and welding. The potential for automation further strengthens the relevance of thermoplastic composites in industrial applications. Nevertheless, most current composite designs continue to rely on constant-thickness laminates. With the flexibility offered by automated manufacturing processes, however, it is now possible to produce variable stiffness laminates (VSLs) by varying thickness or steering fiber during placement. By enabling stiffness to vary across a component, VSLs provide opportunities for further weight reduction while maintaining structural performance.

This research aims to develop a multi-step design methodology that translates optimized variable stiffness laminate designs into geometries suitable for automated manufacturing. First a free-size optimization is used to generate a variable thickness design. The free-size result is imported in PyMAPDL and processed through self-written code. The methodology employs a two-level clustering process based on total element thickness and in-plane principal stresses. The clustered results are then converted into manufacturable geometries and expressed as patchwise definitions. A genetic algorithm is applied to minimize the average error in lamination parameters by matching the patch model definition with the clustered design. The proposed methodology is demonstrated on a beam structure, with variations in the number of clusters and tape widths used to evaluate performance and identify potential limitations.

The results of the clustering based on total element thickness indicate that automatic zone definition is feasible. However, some elements deviate significantly from their respective clusters, suggesting that additional parameter tuning is necessary to achieve improved initial zone definitions. The second clustering level, based on principal stresses, shows promise in translating highly variable thickness and element definitions into more uniform regions. Nevertheless, the results reveal that the thickness-based assignment does not consistently align with the structural load paths. Further refinement is therefore required to ensure that element definitions follow load paths while maintaining uniform zone distribution.

The application of the genetic algorithm demonstrates that increasing design complexity leads to higher error percentages. Moreover, for a given manufacturing dimension, the error percentage tends to converge to similar values regardless of cluster configuration. Analysis of the final designs produced by the genetic algorithm also shows a significant increase in weight. This suggests that, although the genetic algorithm effectively reduces mismatches in lamination parameters, the resulting designs are not suitable for weight-saving purposes.

In conclusion, this research proposes a novel methodology for the design of variable stiffness laminates. While the study demonstrates the feasibility of the approach, it also highlights several limitations and areas for improvement in the clustering and patching processes. These findings provide a foundation for further refinement and development of the methodology, advancing the potential for practical implementation of variable stiffness laminates in the aerospace industry.

Contents

Preface 1

Summary 2

List of Figures 8

List of Tables 9

Nomenclature 10

1 Introduction 12

2 Literature review 13
2.1 Composites in the Aerospace industry . . . 13
2.2 Manufacturing methods . . . 13
2.3 Optimization methods and Design for Manufacturing . . . 15
2.3.1 Optimization methods . . . 15
2.3.2 Design for Manufacturing . . . 17
2.4 Research Objective and research questions . . . 21

3 Methodology 22
3.1 Free-size Optimization . . . 23
3.2 Two level clustering . . . 25
3.3 Patching Algorithm . . . 27
3.3.1 Manufacturing mesh generation . . . 27
3.3.2 Patch generation . . . 32
3.4 Optimization Employing a genetic algorithm . . . 33

4 Results 35
4.1 Test cases and free-size optimization input . . . 35
4.2 Initial Test Results . . . 36
4.3 MBB Beam . . . 42
4.3.1 Test Plan . . . 44
4.3.2 MBB Beam Thickness and Stress Clustering Variation . . . 45
4.3.3 Stress Clustering for 16 and 32 thickness clusters. . . . 47
4.3.4 Error distribution for thickness and stress variation. . . . 51
4.3.5 MBB Beam tape width influence comparison . . . 56
4.3.6 Manufacturing weight and time results . . . 59

5 Conclusion 61

6 Future Recommendations 63
6.0.1 Clustering and Zone definition: . . . 63
6.0.2 Stress clustering and making zones uniform . . . 64
6.0.3 Optimization and conversion to manufacturing geometry . . . 66
6.0.4 Postprocessing . . . 66

A Stress Clustered Figures 71

B Stress Clustered Figures Finer mesh 72

C Error Distribution Graphs. 75
C.1 Error Distribution Graphs 50mm tape width. 75
C.2 Error Distribution Graphs 25mm tape width. 75

D Lamination Parameter Distribution Graphs for 25mm tape width. 92

List of Figures

2.1 Interior of industrial autoclave[25] . . . 14
2.2 Thermoplastic ATP schematic sketch[15] . . . 15
2.3 Objective function contour and constraint surfaces[22]. . . . 16
2.4 Topology optimized structure[23]. . . . 18
2.5 Process Illustration of projection method[23]. . . . 18
2.6 Illustration of generating equally spaced fiber paths(red lines) with EQS method and geometry boundary with blue lines[18] . . . 18
2.7 Vector field, initial vectors blue smoothed vector in green [11] . . . 19
2.8 Four stage ply shape and fiber path generation methodology[11] . . . 20
2.9 Schematic of variable thickness laminates[20] . . . 20
2.10 Horse shoe design problem[20] . . . 20

3.1 Methdology workflow. . . . 22
3.2 Altair Hyperworks topology and Free-size optimization[2]. . . . 23
3.3 Compliance of Topology and Free-size results[1]. . . . 23
3.4 Thickness clustering and laminate discretization. . . . 25
3.5 Stress clustering algorithm. . . . 27
3.6 Manufacturing mesh illustration for $0°$,$90°$ orientation. . . . 28
3.7 Mesh illustration for comparison of $0°$,$90°$ vs $\pm 45°$ orientation. . . . 29
3.8 Element overlap of manufacturing element(a,b) and four quadratic finite elements of varying amount of layers. . . . 29
3.9 Illustration of neighboring elements and layer reassignment. . . . 30
3.10 Illustration neighboring elements for $45°$ orientation. . . . 30
3.11 Manufacturing mesh illustration $0°$ orientation. . . . 31
3.12 Patching algorithm workflow. . . . 32
3.13 Miki's lamination diagram[26]. . . . 33

4.1 Cantilever plate illustration. . . . 36
4.2 Altair Hyperworks model of cantilever plate . . . 37
4.3 Free-size total thickness distribution of cantilever plate. . . . 37
4.4 Cantilever plate clustered into 4 zones based on total element thickness. . . . 38
4.5 Initial results clustered per orientation . . . 38
4.6 Cantilever plate clustered into 9 zones based on total element thickness. . . . 39
4.7 Cantilever plate 9 thickness zone and 3 allowed stress cluster per zone. . . . 39
4.8 Cantilever plate error distribution before optimization. . . . 40
4.9 Cantilever plate error distribution after optimization. . . . 41
4.10 MBB Beam load case, boundary conditions and dimension ratios[29]. . . . 42
4.11 Altair Hyperworks model of MBB Beam. . . . 43
4.12 Thickness distribution of MBB beam. . . . 43
4.13 Thickness distribution of $0°$ orientation. . . . 43
4.14 Thickness distribution of $\pm 45°$ orientation. . . . 43
4.15 Thickness distribution of $90°$orientation. . . . 44
4.16 Thickness clustering number of cluster 4. . . . 45
4.17 Close up Illustration of rogue elements. . . . 45
4.18 Thickness clustering number of cluster 16. . . . 46
4.19 Thickness clustering number of cluster 32. . . . 47
4.20 4 thickness clusters and 1 thickness clusters allowed. . . . 47
4.21 4 thickness clusters and 4 thickness clusters allowed. . . . 48
4.22 4 thickness clusters and 16 thickness clusters allowed. . . . 48

4.23 32 thickness clusters and 1 thickness clusters allowed. 48
4.24 16 thickness clusters and 1 thickness clusters allowed. 48
4.25 32 thickness clusters and 4 thickness clusters allowed. 49
4.26 32 thickness clusters and 16 thickness clusters allowed. 49
4.27 Stress clustered per orientation starting mesh vs finer mesh. 50
4.28 Error and standard deviation comparison for varying number of thickness and stress clusters for $50mm$tape. 51
4.29 Error distribution before GA optimization 4 thickness and 1 stress cluster 50mm tape. . 52
4.30 Error distribution after GA optimization 4 thickness and 1 stress cluster $50mm$ tape. . . 53
4.31 Error and standard deviation comparison for varying number of thickness and stress clusters for $25mm$ tape. 53
4.32 Finite element model lamination parameter distribution for V1 and V3 in 4 thickness clusters and 1 stress clusters allowed. 54
4.33 Patch-wise model lamination parameter distribution for V1 and V3 in 4 thickness clusters and 1 stress clusters allowed before optimization. 55
4.34 Patch-wise model lamination parameter distribution for V1 and V3 in 4 thickness clusters and 1 stress clusters allowed after optimization. 55
4.35 Tape width comparison for error and standard deviation before and after the optimization in the case of 16 thickness clusters. 57
4.36 Error distribution before GA application 4 thickness 16 stress cluster tape width 25mm. 57
4.37 Error distribution after GA application 4 thickness 16 stress cluster tape width 25mm. . . 58
4.38 Change in mass and manufacturing time 25mm tape width. 59
4.39 Change in mass and manufacturing time 50mm tape width. 60

6.1 The processing of data clustering by tri-level traditional k-means algorithm:(a) the data and initial cluster center used in the first-level cluster stage;(b) the result obtained in the first level cluster stage;(c) the result obtained in the second level cluster stage;(d) the initial clusters used in the final-level cluster stage; and (e) the result obtained in the final-level cluster stage [32]. 64
6.2 Orientation Illustration for zone inside the area of black rectangle. 65
6.3 Improved stacking sequence table with two ply-drops[19]. 67
6.4 Manufacturing mesh $\pm 45^{\circ}$ patches. 68

A.1 16 thickness clusters and 4 stress clusters allowed. 71
A.2 16 thickness clusters and 16 stress clusters allowed. 71

B.1 Caption 72
B.2 Thickness clustered 73
B.3 Stress clustered per orientation finer mesh 4 thickness 1 allowed stress. 73
B.4 Stress clustered per orientation finer mesh 4 thickness 16 allowed stress. 73
B.5 Stress clustered per orientation finer mesh 16 thickness 1 allowed stress. 73
B.6 Stress clustered per orientation finer mesh 16 thickness 16 allowed stress. 74
B.7 Stress clustered per orientation finer mesh 32 thickness 1 allowed stress. 74
B.8 Stress clustered per orientation finer mesh 32 thickness 4 allowed stress. 74
B.9 Stress clustered per orientation finer mesh 32 thickness 16 allowed stress. 74

C.1 Error distribution before GA optimization 4 thickness and 4 stress cluster 50mm tape. . 75
C.2 Error distribution after GA optimization 4 thickness and 4 stress cluster 50mm tape. . . . 76
C.3 Error distribution before GA optimization 4 thickness and 16 stress cluster 50mm tape. . 76
C.4 Error distribution after GA optimization 4 thickness and 16 stress cluster 50mm tape. . . 77
C.5 Error distribution before GA optimization 16 thickness and 1 stress cluster 50mm tape. . 77
C.6 Error distribution after GA optimization 16 thickness and 1 stress cluster 50mm tape. . . 78
C.7 Error distribution before GA optimization 16 thickness and 4 stress cluster 50mm tape. . 78
C.8 Error distribution after GA optimization 16 thickness and 4 stress cluster 50mm tape. . . 79
C.9 Error distribution before GA optimization 16 thickness and 16 stress cluster 50mm tape. 79
C.10 Error distribution after GA optimization 16 thickness and 16 stress cluster 50mm tape. . 80
C.11 Error distribution before GA optimization 32 thickness and 1 stress cluster 50mm tape. . 80

C.12 Error distribution after GA optimization 32 thickness and 1 stress cluster 50mm tape. . . 81
C.13 Error distribution before GA optimization 32 thickness and 4 stress cluster 50mm tape. . 81
C.14 Error distribution after GA optimization 32 thickness and 4 stress cluster 50mm tape. . . 82
C.15 Error distribution before GA optimization 32 thickness and 16 stress cluster 50mm tape. 82
C.16 Error distribution after GA optimization 32 thickness and 16 stress cluster 50mm tape. . 83
C.17 Error distribution before GA application 4 thickness 1 stress cluster tape width 25mm. . 83
C.18 Error distribution after GA application 4 thickness 1 stress cluster tape width 25mm. . . 84
C.19 Error distribution before GA application 4 thickness 4 stress cluster tape width 25mm. . 84
C.20 Error distribution after GA application 4 thickness 4 stress cluster tape width 25mm. . . 85
C.21 Error distribution before GA application 16 thickness 1 stress cluster tape width 25mm. 85
C.22 Error distribution after GA application 16 thickness 1 stress cluster tape width 25mm. . . 86
C.23 Error distribution before GA application 16 thickness 4 stress cluster tape width 25mm. 86
C.24 Error distribution after GA application 16 thickness 4 stress cluster tape width 25mm. . . 87
C.25 Error distribution before GA application 16 thickness 16 stress cluster tape width 25mm. 87
C.26 Error distribution after GA application 16 thickness 16 stress cluster tape width 25mm. . 88
C.27 Error distribution before GA application 32 thickness 1 stress cluster tape width 25mm. 88
C.28 Error distribution after GA application 32 thickness 1 stress cluster tape width 25mm. . . 89
C.29 Error distribution before GA application 32 thickness 4 stress cluster tape width 25mm. 89
C.30 Error distribution after GA application 32 thickness 4 stress cluster tape width 25mm. . . 90
C.31 Error distribution before GA application 32 thickness 16 stress cluster tape width 25mm. 90
C.32 Error distribution after GA application 32 thickness 16 stress cluster tape width 25mm. . 91

D.1 Finite element model lamination parameter distribution for V1 and V3 in 4 thickness clusters and 4 stress clusters allowed. 93
D.2 Patch-wise model lamination parameter distribution for V1 and V3 in 4 thickness clusters and 4 stress clusters allowed before optimization. 93
D.3 Patch-wise model lamination parameter distribution for V1 and V3 in 4 thickness clusters and 1 stress clusters allowed after optimization. 94
D.4 Finite element model lamination parameter distribution for V1 and V3 in 4 thickness clusters and 16 stress clusters allowed. 94
D.5 Patch-wise model lamination parameter distribution for V1 and V3 in 4 thickness clusters and 1 stress clusters allowed before optimization. 95
D.6 Patch-wise model lamination parameter distribution for V1 and V3 in 4 thickness clusters and 16 stress clusters allowed after optimization. 95
D.7 Finite element model lamination parameter distribution for V1 and V3 in 16 thickness clusters and 1 stress clusters allowed. 96
D.8 Patch-wise model lamination parameter distribution for V1 and V3 in 16 thickness clusters and 1 stress clusters allowed before optimization. 96
D.9 Patch-wise model lamination parameter distribution for V1 and V3 in 16 thickness clusters and 1 stress clusters allowed after optimization. 97
D.10 Finite element model lamination parameter distribution for V1 and V3 in 16 thickness clusters and 4 stress clusters allowed. 97
D.11 Patch-wise model lamination parameter distribution for V1 and V3 in 16 thickness clusters and 4 stress clusters allowed before optimization. 98
D.12 Patch-wise model lamination parameter distribution for V1 and V3 in 16 thickness clusters and 4 stress clusters allowed after optimization. 98
D.13 Finite element model lamination parameter distribution for V1 and V3 in 16 thickness clusters and 16 stress clusters allowed. 99
D.14 Patch-wise model lamination parameter distribution for V1 and V3 in 16 thickness clusters and 16 stress clusters allowed before optimization. 99
D.15 Patch-wise model lamination parameter distribution for V1 and V3 in 16 thickness clusters and 16 stress clusters allowed after optimization. 100
D.16 Finite element model lamination parameter distribution for V1 and V3 in 32 thickness clusters and 1 stress clusters allowed. 100
D.17 Patch-wise model lamination parameter distribution for V1 and V3 in 32 thickness clusters and 1 stress clusters allowed before optimization. 101

D.18 Patch-wise model lamination parameter distribution for V1 and V3 in 32 thickness clusters and 1 stress clusters allowed after optimization. 101
D.19 Finite element model lamination parameter distribution for V1 and V3 in 32 thickness clusters and 4 stress clusters allowed. 102
D.20 Patch-wise model lamination parameter distribution for V1 and V3 in 32 thickness clusters and 4 stress clusters allowed before optimization. 102
D.21 Patch-wise model lamination parameter distribution for V1 and V3 in 32 thickness clusters and 4 stress clusters allowed after optimization. 103
D.22 Finite element model lamination parameter distribution for V1 and V3 in 32 thickness clusters and 16 stress clusters allowed. 103
D.23 Patch-wise model lamination parameter distribution for V1 and V3 in 32 thickness clusters and 16 stress clusters allowed before optimization. 104
D.24 Patch-wise model lamination parameter distribution for V1 and V3 in 32 thickness clusters and 16 stress clusters allowed after optimization. 104

List of Tables

3.1 Genetic Algorithm parameters. 34

4.1 Material Values. 36
4.2 Simulation Parameters for Cantilever plate. 36
4.3 Cantilever plate initial optimization 40
4.4 Genetic String before and after optimization. 40
4.5 Simulation Parameters. 42
4.6 Test definitions. 44
4.7 Error Results with 50mm tape width. 52
4.8 Error Results with 25mm tape width. 56
4.9 Error Results with 10mm tape width. 57

Nomenclature

Abbreviations

Abbreviation	Definition
AFP	Automated Fiber Placement
ATP	Automate Tape Placement
VSL	Variable Stiffness Laminate
MBB	Messerschmitt-Bölkow-Blohm
EQS	Equally Spaced Metod
DD laminate	Double-Double laminate
UMLI	Uniform Multiple Laminates Interpolation
FEA	Finite Element Analysis
MAPDL	Mechanical Ansys Parametric Design Language
PyMAPDL	Python Mechanical Ansys Parametric Design Language
CDB	Constant DataBase
SMAPE	Symmetric Mean Absolute Percentage Error
GA	Genetic Algorithm

Symbols

Symbol	Definition	Unit
$\boldsymbol{u}$	Statefield	
ρ	Density	kg/m^3
V	Volume	m^3
C	Compliance	$\frac{m}{N}$
θ	local orientation	
K	Global Stiffness matrix	
$\boldsymbol{U}$	Global displacement vector	
τ_{xy}	Shear Stress	MPa
S_x	Normal Stress	MPa
S_y	Normal Stress	MPa
$\overline{\phi_i}$	Homogenized Angle	
φ_i	Principal Angle	
σ_i	Principal Stress	
cd_i	Deviation Metric	
w_{ij}	Overlap Weight Coefficient	
$A_{ij}^{Overlap}$	Overlap Area with Specific Finite Element	
A_j	Area of Manufacturing Mesh Element	
P_j	Number of Layers in manufacturing element	

Symbol	Definition	Unit
P_i	Number of layers in finite element mesh	
S	Transfer Sensitivity	
V1	Normalized Lamination Parameter	
V3	Normalized Lamination Parameter	
N_l	Number of layers	
tk	ply thickness of k-th ply in stacking order	
θ_k	orienation of k-th ply in a stacking order	
h	total laminate thickness	

1

Introduction

The aerospace industry faces increasing pressure to reduce its environmental impact in response to global warming and the urgent need for more sustainable transportation solutions. The development of technologies such as sustainable aviation fuel and advanced composite materials has emerged as a central pathway toward lowering emissions possibly by 14-15%[30]. Among these, weight reduction remains a straightforward and highly effective approach, as lighter aircraft directly translate to lower fuel consumption and reduced carbon emissions.

Composite materials, utilizing thermosets and thermoplastics as matrices, have therefore gained considerable attention within aerospace research and manufacturing. In recent years, thermoplastic composites in particular have been studied intensively due to their recyclability and their compatibility with advanced automated manufacturing processes such as automated fiber placement (AFP), automated tape placement (ATP), and welding[24]. These manufacturing advances enable higher production efficiency and open possibilities for innovative laminate designs that go beyond the conventional constant-thickness approach.

One such innovation is the use of variable stiffness laminates (VSLs), which allow fiber orientations and thickness distributions to vary across a structure. By tailoring stiffness to follow load paths, VSLs offer the potential to achieve strength improvement compared to constant thickness quasi-isotropic layup laminates[13]. However, despite this promise, the practical application of VSLs remains limited due to challenges in translating optimized designs into manufacturable geometries. For structures large in dimension such as galley insert panels using ATP can be more suitable. However, a design methodology is needed to be introduced, which takes into account manufacturing constraints.

In summary, VSLs are a promising towards weight savings due to stronger and stiffer designs compared to constant thickness laminates. However, the inclusion of the manufacturing constraints in terms of geometry limitation into a design methodology is difficult. This thesis aims to explore that and current state of the approaches to achieve will be discussed in the next section.

2

Literature review

2.1. Composites in the Aerospace industry

The first powered flight of the Wright brothers at 1903 sparked an unforeseen engineering development towards lightweight materials for aircraft. During the word wars the aviation industry went through rapid development in technology. The early airplanes were rudimentary constructed using mainly wood. The first metallic structure used in aero planes was developed in the first world war by Germany[27]. After the second word war the technological advancement in polymer and material technology allowed the introduction of composite materials. Composite materials show certain advantages over metallic structures. One of them is the design freedom to tailor the material stiffness for better lightweight structures and better weight to strength ratio. Furthermore, in the 21^{st} century global warming brought forward additional requirements for the aerospace industry. New emission goals in the aerospace industry encourages the development of new lightweight structures with innovative methods and materials.

Composite structures currently are constant thickness laminates based on a thermoset polymer matrix. The design of the uniform thickness laminate results in a constant stiffness design. The laminates are manufactured using traditional methods such as hand layup, vacuum resin infusion, which are well understood and used in the industry due to large amount of experience. Additional design requirements such as balanced and symmetric laminates allow the designer to avoid unwanted behavior under loading. However, new manufacturing methods allow the aerospace industry to design variable stiffness laminates. VSL are laminates where by varying the thickness or local orientation of fibers the overall distribution of stiffness or strength across the geometry varies [6]. Polymer matrices such as thermoplastics allow to further expand the possibilities of manufacturing. The use of thermoplastic polymer matrices allow the adoption of processes such as welding, tape laying and fiber placement as well as recycling of parts.

2.2. Manufacturing methods

Currently the aerospace industry heavily relies on traditional methods and thermoset polymer composites. The traditional methods such as autoclaves, which can be seen in figure 2.1 are costly to operate and substantial in energy consumption. Therefore the industry actively looks for more sustainable and energy efficient methods. ATP and laser assisted methods are an attractive alternative to traditional methods to manufacture thermoplastic composites[14]. In the rest of this section the basic differences between thermoset and thermoplastic polymers will be explained. Furthermore new and traditional manufacturing methods will be compared on several points such as precision, efficiency and production speed, cost and flexibility.

Thermoset polymers are formed from monomers with low viscosity and molecular weight through a chemical process called cross linking. The cross linking is driven by heat which is either the by product of a chemical process or externally supplied. The presence of cross links provide thermoset polymers excellent mechanical properties and thermal stability. However, the breakage of cross links is a complicated chemical process, which make thermoset polymer hard to recycle[16]. Thermoplastic polymers

Figure 2.1: Interior of industrial autoclave[25]

compared to thermoset polymer are formed without cross links from high molecular weight monomer chains. The lack of cross links makes the need of curing cycles unnecessary during manufacturing. However higher temperatures and pressure is necessary for shaping thermoplastic polymers [17].

Traditional manufacturing methods such as autoclaves, vacuum bag infusion and hand layup are the backbone of the aerospace industry. The heating cycles applied are costly and substantial in energy consumption[31]. Laser assisted methods such as automated tape placement(ATP) in figure 2.2 are a good alternative and a goal to achieve in situ-consolidation[5]. In ATP the prepreg laminas are heated by an external source such as a laser , the heat source melts the polymer to a sufficient flowability, which allows the molecular chains to diffuse under the applied pressure from the compaction roller[15]. During the ATP the material feed rate, laser heating power and scan speed allows for great precision and control due to robot mounted tooling. Traditional methods are effective at the production of large parts but struggle at intricate geometries and uniform consistent finish, so machining might be necessary as a last step.

The efficiency, production and cost is another major difference between modern methods such as AFP, ATP and traditional methods. For laser assisted methods the scalability for large products is a slow and expensive. Initial investment to equipment is high but the lower material waste, tooling cost and automation potential makes it attractive. Traditional methods on the other hand are more available for large scale production but long production cycles and material waste are the disadvantages[17].

The flexibility offered by laser assisted methods by compatibility with various materials and designs and minimal retooling are attractive to industry. Welding and surface treatments are possible to integrate into the manufacturing process in a single step, while minimizing excess material. Traditional methods on the other hand have tooling tailored for specific parts and substantial material waste. The use of autoclaves consumes a large amount of energy, which increases the economic footprint of traditional methods.

The differences in flexibility and control make laser assisted methods well suited for manufacturing thermoplastic composites. Furthermore AFP allows the possibility for steering the fibers over the geometry and to design variable stiffness laminates. The expansion of design flexibility requires more advanced design and optimization methods, which will be discussed in the next section.

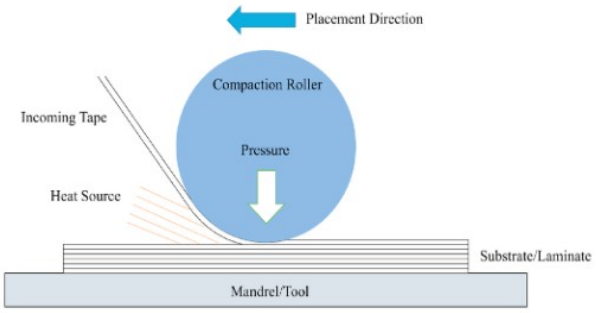

Figure 2.2: Thermoplastic ATP schematic sketch[15]

2.3. Optimization methods and Design for Manufacturing

2.3.1. Optimization methods

Over the last few decades engineering optimization has become an important topic for the industry and academic research. More efficient manufacturing methods and lighter structures are crucial to lower economic footprint of the aerospace industry. The basic terminology applied in the thesis has to be discussed first.

An optimization problem is, where the best optimal solution is obtained through methodical steps making use of mathematical methods or mimicking natural phenomenons. The optimal solution corresponds to a point of maximum or minimum of a certain function defined on the optimization problem.

In general the optimization methods can be categorized to be traditional methods or modern methods. Traditional methods make use of differential calculus for locating optimal points of the objective function. Differential calculus requires the optimal function to be differentiable and continuous to be applicable in the optimization problem. The traditional methods are diverse and applied in aerospace to various problems such as maximizing buckling loads . Modern methods on the other hand mimic natural phenomenons such as evolution, metal annealing or bird flock behavior. Compared to traditional methods modern methods do not use differential calculus in the solution process. Therefore modern methods are applicable to discrete functions as well. For structural optimization commercially available software Altair Optistruct makes use of traditional method called gradient based optimization method during topology and free-size optimization.

Further considerations are the existence of constraints. The constraints will limit the objective functions surface. For simple problems graphical methods can be used to sketch the objective function and search for the optimal solution. However multi variable problem can have complex three dimensional shapes and including the constraint surfaces calls for purely mathematical solutions. In figure 2.3 a simple contour graph of objective function values and few constraints can be seen. Optimization problems can be classified based on the nature of the design variables as well. The first category is search of an optimal value of certain design parameters to minimize a defined function while adhering to constraints. An example of the first category is the mass minimization of a beam under deflection constraints. Problems resembling the first category are static optimization problems. The second category, where the design variables are a function of a parameter and allowed to change over the geometry are called trajectory problems[22].

Further possibility to describe an optimization problem is the permissible values of the design problems. Depending on the nature of the problem if the design variables are allowed to take only discrete values the problem is an integer programming problem. On the other hand if the problem values are not limited to discrete values the problem is a real-valued programming.

Modern Methods introduced earlier mimic natural systems. The natural systems vary from genetic algorithms, simulated metal annealing to ant colony behavior. Since, the methods do not use differential calculus the algorithm only needs the objective function values to work. Furthermore, the algorithms have a higher probability to avoid the problem of stopping at a local minimum. In engineering optimization problems for practical applications include a large number of design variables with mixed continuous-discrete variables and nonconvex design spaces.

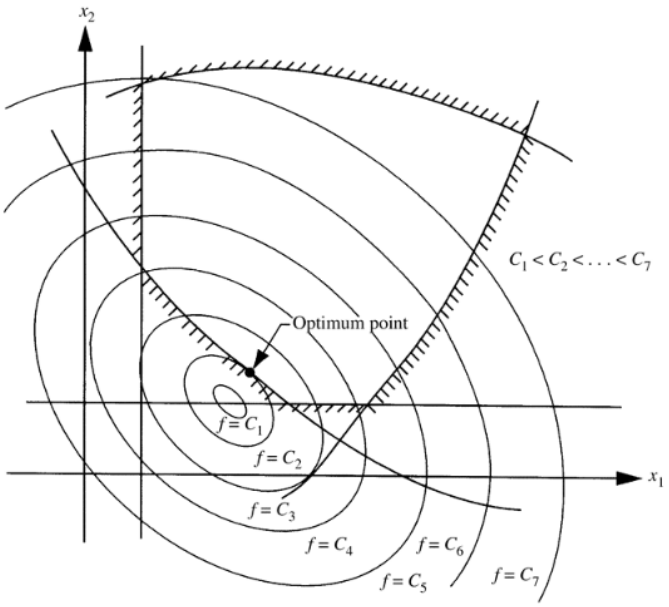

Figure 2.3: Objective function contour and constraint surfaces[22].

Genetic algorithms(GA) have been popular due to high probability of finding the global optimum. The working principle of genetic algorithms is based on Darwin's theory survival of the fittest. The GA differs from traditional algorithms on multiple aspects. First the start design point is not singular, but multiple population points are used at the start of the procedure . The size of the population is estimated based on the number of design variables n to be twice or four times larger. The GA method is derivative free and uses only the objective function values. The design variable are represented in a binary form string. The fitness is represented by the value of the objective function. The GA arrives to a suitable solution by using three aspects of evolution reproduction, cross over and mutation. Reproduction is the selection of suitable designs from the initial population to form a mating pool. The process to choose the best fitness value strings is probabilistic. The probabilistic solution ensures more copies of high fitness in the mating pool. At the reproduction stage no new strings are added ensuring survival of the fittest. Crossover is the step to generate new strings by exchanging information among randomly chosen strings of the mating pool. In the string the site of optimal crossover for information is not known. The uncertainty of lower fitness string occurring after crossover might occur due to the random location of information exchange, but the lower fitness strings will die out. Mutation operation changes a binary string value to the opposite value at a random location. The probability of mutation can be further defined as well. The purpose of mutation is to generate new string in the neighborhood of current string, to safeguard the health of the genetic string against important information loss and maintain diversity of the population. During the optimization process in every generation the fitness values of the population is compared and the highest fitness value correspond to the best candidate solution. Due to the probabilistic nature genetic algorithms have possibility to explore larger part of the design space and avoid early convergence into a feasible solution instead reaching the global optimal solution.

Another modern method capable of finding optimal solution is particle swarm optimization(PSO). PSO is behavior based algorithm compared to evolution based algorithm GAs. The algorithm mimics the dynamics of a bird flocks or how bee hives behave for searching for "food" similar to finding a global maximum or minimum value of the objective function. The behavior of the swarm has three rules. The first rule is that the animals in the flock keep sufficient distance from each other. The second rule is that every animal follows the average direction of other birds. The last rule is the flock tries to fit an average position between each other with no wide gaps overall in the flock.

The search for the optimal solution considers three considerations. First consideration is that if an animal in the swarm locates a promising solution the location of the solution is instantly transmitted to the rest of the flock. The second consideration is that the flock will head toward to the optimal location but not on a direct route. The last consideration is the every part of the swarm is independent thinking

like a single animal and has a past memory. The basic PSO has drawbacks and many different versions can be applied. A modification of PSO is the gray-wolf whale hunting algorithm, where if an optimal solution is found the swarm will surround the optimal location and an animal from the flock will detach. The detached animal will circle around the area of optimal solution trying to find a better location. In the case of a better location found the swarm will head towards a better solution. However, PSO algorithms in general are more suitable to handle continuous optimization problems[9].

For the aerospace industry the optimization problems corporate many components of an aircraft. The main focus of the thesis is structural optimization. A common method applied in the aerospace industry is topology optimization. Topology optimization first was applied on simple truss like structures such as bridges. Later towards the end of the 20^{th} century Bendsøe and Kikuchi pioneered the earliest form of topology optimization method. In 1989 Bendsøe developed the Solid Isotropic Material with Penalization(SIMP) method for topology optimization[29]. Generally in topology optimization the goal is to find a density distribution, where the objective function f is minimized over the whole domain Ω. The topology optimization problem can be simply described by equation 2.1:

$$
\begin{aligned}
&\text{min :} \\
&\quad f = f(\boldsymbol{u}(\rho), \rho) = \int_{\Omega} f_l(\boldsymbol{u}(\rho), \rho) dV \\
&\text{Objective :} \\
&\quad V = \int_{\Omega} \rho(x) dx \\
&\quad C(\rho) = \sum_{e=1}^{N} \rho_e [u_e]^T [K] [u_e] \\
&\quad \text{where} \\
&\quad \rho(x) = 0 \text{ or } 1, \forall x \in \Omega
\end{aligned}
\tag{2.1}
$$

,where objective function f is evaluated locally f_l and integrated over the whole domain and the state-field is $\boldsymbol{u}$. The objective function usually aim to minimize volume(V) or compliance(C) of the structure. The minimization is accomplished by varying each element's density between the value of 0 or 1. However, in equation 2.1 the main assumption is that the material behavior is isotropic. Multi-material topology optimization and anisotropic topology optimization is also possible. For composite material additionally to the density of the elements as a design variable the orientation can be introduced. Equation 2.1 the compliance formulation has to be modified to equation 2.2.

$$
\begin{aligned}
C(\rho, \theta) &= \frac{1}{2} \boldsymbol{U}^T(\rho, \theta) \boldsymbol{K}(\rho, \theta) \boldsymbol{U}(\rho, \theta) \\
\boldsymbol{K}_e &= \int_{\Omega} \boldsymbol{B}_e^T \boldsymbol{D}_e \boldsymbol{B}_e d\Omega
\end{aligned}
\tag{2.2}
$$

,where $\boldsymbol{\rho}$ and $\boldsymbol{\theta}$ are design variables representing the pseudo densities and local orientation of the materials, $\boldsymbol{K}$ and $\boldsymbol{U}$ are the global stiffness matrix and displacement vector, $\boldsymbol{K_e}$ is the element stiffness matrix [23]. Due to the element wise orientation optimization the resulting structure is not only topologically optimized but variable stiffness as well. A resulting example of such optimization can be seen in figure 2.4. The local fiber orientation varies greatly during AFP some geometrical constrain need to be taken into account. In the next subsection 2.3.2 some methods will be shown, which process and take manufacturing constraints into account.

2.3.2. Design for Manufacturing

In the previous subsection 2.3.1 topology optimization has been shown for generating designs. In this subsection some methodologies will be shown that process and/or generate designs while taking manufacturing constraints in to account. Continuing from the previous subsection in figure 2.4 it can be seen that the resulting local fiber orientation is not suitable for production straight away due to large variance in between local fiber orientation. The result has to be further processed towards AFP manufacturing process. To process towards AFP two methods are applicable namely projection method and equally-spaced method(EQS). In the projection method the local orientation field is used to generate a

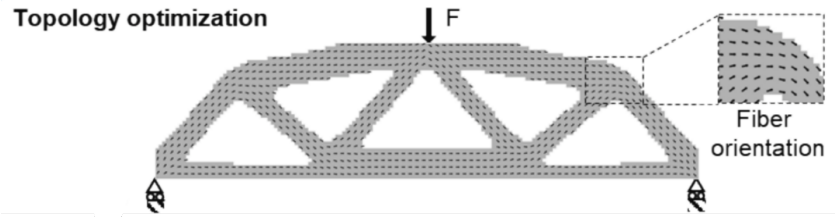

Figure 2.4: Topology optimized structure[23].

scalar field for the orientation distribution. The scaler field can be further processed into a tool path with a wave function. In figure 2.5 the steps of projection method are illustrated. The second method EQS creates a continuous fiber path by generating control points at equal spaced points and connecting the points with a smooth fiber path. The spacing of the control points is dependent on the geometry's inner voids. In figure 2.6 EQS method is illustrated. Comparing the projection method and EQS, projection method has a main advantage by solely relying on standardized vector field input completely eliminating constraint imposed by local geometry[23].

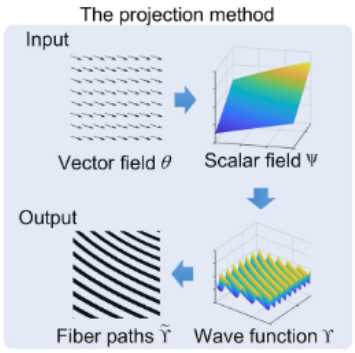

Figure 2.5: Process Illustration of projection method[23].

Further possibilities for composite optimization and multi-material optimization is the adoption of Double-Double laminates(DD laminates). DD laminates were proposed by Tsai and feature two orientations in a balanced stacking order. The balanced stacking order results at the end of an optimization process in a better homogenized bending properties compared to quad laminates only featuring orientations of $0°$,$\pm 45°$ and $90°$[7]. Furthermore, DD laminates allow to uniform multiple laminates interpolation(UMLI) methodology for topology optimization. UMLI is a multiphase material topology optimization method where the stiffness of the material is interpolated during the optimization. A key advantage of the UMLI method is that the number of design variables do not increase per element. The optimization interpolates the ABD matrix of the element from the predefined angle combinations of $\pm$ angle combinations for the DD laminates.

For aerospace structures not only the angle can be optimized for the variable stiffness structures but

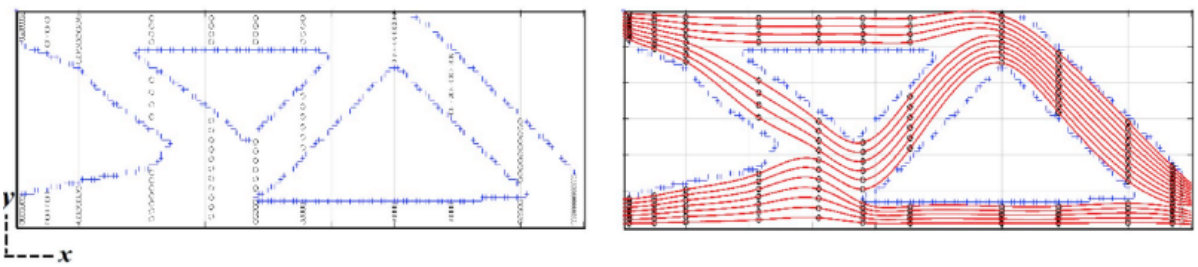

Figure 2.6: Illustration of generating equally spaced fiber paths(red lines) with EQS method and geometry boundary with blue lines[18]

ply shape as well. The possible ply shapes are generated based on preliminary finite element analysis(FEA). Commercially available software is capable of generating VSL laminates, but the generated laminate due to ply-drops loses performance. To overcome the performance loss a clustering algorithm can be applied. The clustering algorithm based on a function value divides the geometry into zones with k-means algorithm. For effective processing the input parameters have to be smoothed. Smoothing of the data set is necessary due to the hight variability of the input. In figure 2.7 a vector field can be seen where a Laplacian smoothing is applied.

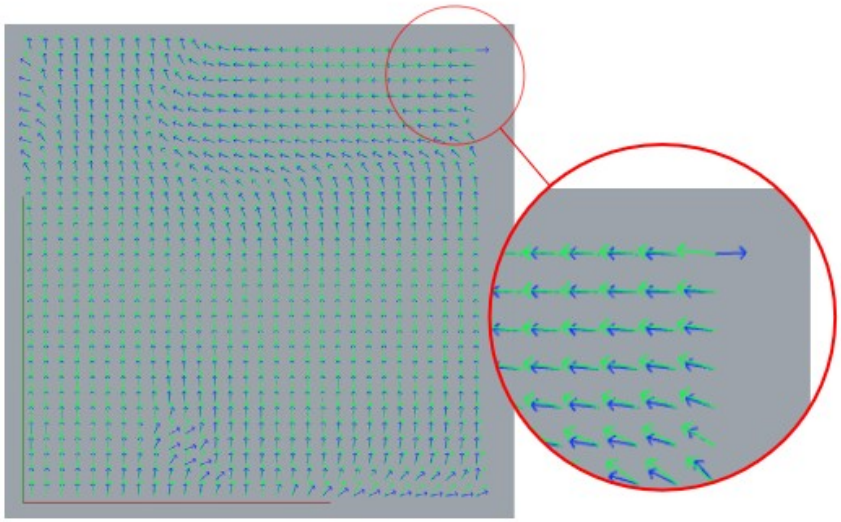

Figure 2.7: Vector field, initial vectors blue smoothed vector in green [11]

Normalization is further applied on the data points for faster processing with k-means algorithm. The k-means algorithm is an iterative algorithm dividing the given data set into number of non-overlapping clusters in a way of minimal variance inside the cluster between the data points[11]. In figure 2.8 a four stage process can be seen towards automatic manufacturing process. After the clusters are generated a vector based path finding algorithm constructs the reference curve taking constraints into account. For non-straight clusters reference path generation is applied. Due to fiber steering overlaps and other manufacturing defects can occur, therefore offset method is used for optimal fiber path. The final result of the algorithm is figure2.8(d), where on a ply level a mix unidirectional and steered layup can be seen.

So far optimization methods, ply shape planning and DD laminates have been shown. To generate variable stiffness laminate a thickness variation can be used. The variable stiffness can be achieved by dropping plies in the stacking order in the geometry. For the ply dropping algorithm are capable of producing single or multi-peak laminates. In figure 2.9 a schematic can be seen of single and multi-peak laminates. The multi-peak laminates are generated through an algorithm making use of SST tables. The algorithm takes variable thickness design and divides the geometry into small regions based on a buckling factor estimation. The smaller regions are estimated as simply supported plates and a genetic algorithm is applied to generate the stacking order[20]. The algorithm is applied on the horse shoe design problem. In figure 2.10 the design problem can be seen with the defined loading conditions. The algorithm takes the smaller predefined regions and optimize it for multi-peak design. The performance of the algorithm compared to other stacking sequence algorithms is considerably better. However, the regions shapes are not considered part of the problem. For variable stiffness design a gap in current research is towards straight fiber variable stiffness laminates. In the next section a novel method is proposed for design of variable stiffness laminates aiming for automated manufacturing processes.

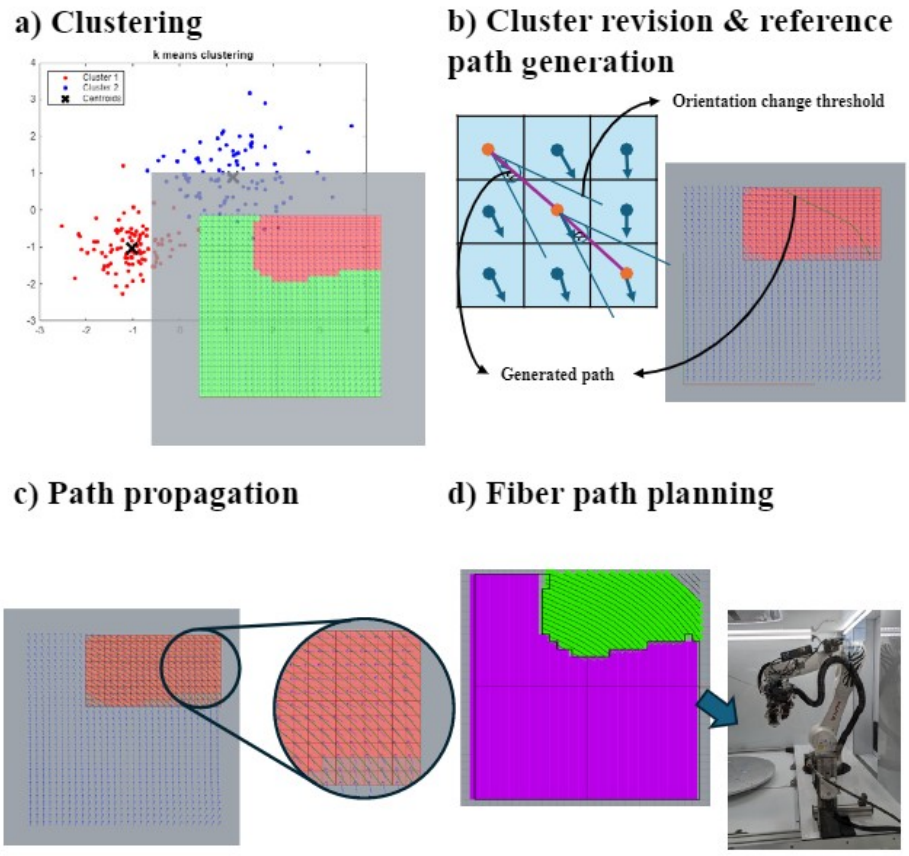

Figure 2.8: Four stage ply shape and fiber path generation methodology[11]

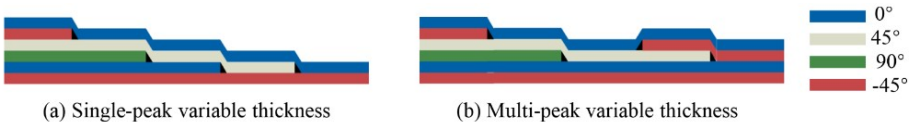

Figure 2.9: Schematic of variable thickness laminates[20]

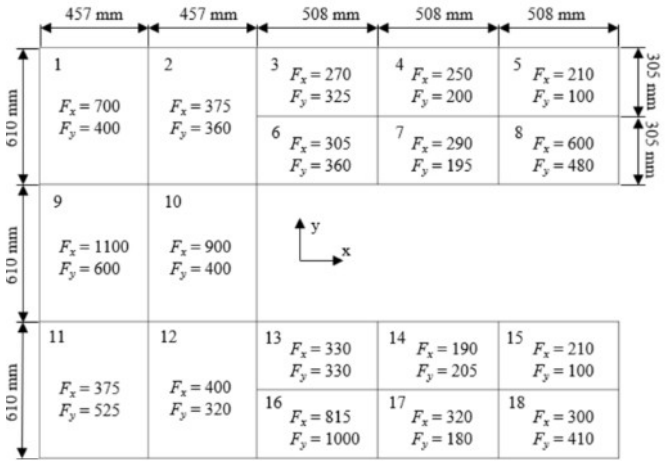

Figure 2.10: Horse shoe design problem[20]

2.4. Research Objective and research questions

This thesis aims to deliver a start to end design methodology for variable thickness laminate designs. There is a need from the industrial side of aerospace for lighter structures, however fiber steering is complex and costly to adopt on a large scale. Furthermore, interior structures are not primary load carrying of an aircraft but still contribute to fuel costs due to unexplored optimization possibilities. The methodology aims to fill the gap by laying the foundation to translating optimized results into a manufacturing geometry for straight fiber variable thickness laminates. The translation to manufacturing geometry simplifies the complexity of the design by using patch-wise definition with less information to describe the same model. However, the conversion changes the model information, therefore the patch wise definition is optimized via a genetic algorithm to match the input before the conversion to the manufacturing geometry. The main objective of the thesis is:

> The objective of this research is to develop a methodology ensuring manufacturability and suitability for automated methods by using an optimized variable thickness design processed through an algorithm to generate a patch divided straight fiber variable thickness laminate.

- How to systematically define zones on the geometry based on provided input parameters from a free-size optimization?
- Which algorithms can be used for optimization of the design ensuring automated manufacturing processes can be applied?
- What is the performance of the developed algorithm applied on a beam?
- What is the future development path for full scale application on aerospace structures of the methodology?

3

Methodology

In this chapter, a methodology is shown aiming to full-fill the research objective. The proposed methodology builds upon the stages introduced in Section 2, namely free-size optimization, two-level clustering, patch definition, and optimization through a genetic algorithm. Each of these stages contributes to progressively refining the laminate design, guiding it from an initial conceptual configuration toward a manufacturable geometry that satisfies both performance and production requirements. The complete methodology is illustrated in Figure 3.1.

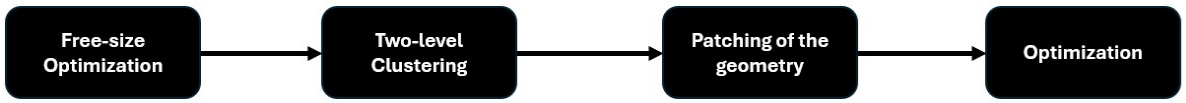

Figure 3.1: Methdology workflow.

The central aim of the workflow is to translate the results of free-size optimization into a design that can be realized in manufacturing. The process begins with a problem definition, which may involve components from the aerospace industry such as a composite lavatory panel, lug, or beam. During free-size optimization, the designer specifies requirements such as allowable failure index, laminate thickness, and stacking sequence, while typically using compliance or mass minimization as the optimization objective of the optimization.

Following this stage, clustering algorithms are applied to group finite elements into zones. The purpose of clustering is to achieve a more homogeneous thickness distribution across the structure, while also reducing local variability. The number of clusters has a direct impact on both mechanical performance and manufacturability, and the outcome of this step is a zone-based finite element model with updated element information.

The methodology then proceeds with the patch definition stage, in which the finite element model is translated into a geometry that can be directly used in manufacturing. To achieve this, custom-developed algorithms generate a manufacturing mesh and determine the number of layers based on user-specified parameters such as tape width and minimum placement length. The output is a patch-wise representation of the structure that includes information on segment locations, dimensions, and the number of layers assigned to each orientation ($0°$, $\pm 45°$, and $90°$).

The final stage involves optimization using a genetic algorithm, which aims to minimize the mismatch in stacking sequences between the patch-wise definition and the clustered finite element model. By reducing this error, the patch-wise model definition aims to reproduce the weight and in-plane stiffness distribution of the clustered model with high fidelity. In the following sections, each stage of the methodology will be discussed in detail.

3.1. Free-size Optimization

The first stage in this process is the free-size optimization, which will be discussed in detail here. Free-size optimization is an approach conceptually related to topology optimization and is implemented in the commercially available software package Altair HyperWorks. In topology optimization, the optimization procedure discretely varies the thickness of each finite element between predefined values, resulting in a geometry that is either at a minimum or maximum thickness for each element. The minimum of the interval can be changed as a setting. Free-size optimization, by contrast, permits continuous variation of the element thickness within a user-defined range. This continuous variation can produce a smoothly varying thickness distribution across the design domain, which can lead to more structurally efficient solutions. In figure 3.2 an example of applying topology and free-size optimization can be seen on a cantilever plate. In sub-figure 3.2(a) the definition of cantilever plate can be seen with the left side edge being fully constrained in all degrees of freedom and a point load applied on the right side edge. In sub-figure 3.2(b) the resulting thickness distribution can be seen for topology and free-size optimization, where for thickness distribution the color red corresponds to maximum and blue for minimum thickness. In sub-figure 3.2(b) the topology optimized results in a truss like design, while the free-size results is smoother variable thickness design.

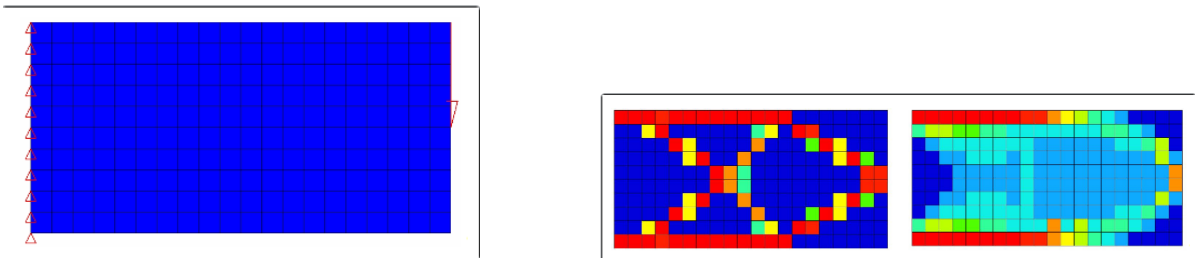

((a)) Cantilever plate.

((b)) Topology(left) vs Free-size optimization(right).

Figure 3.2: Altair Hyperworks topology and Free-size optimization[2].

In figure 3.3 a compliance comparison can be seen for topology and free-size optimized result.

Figure 3.3: Compliance of Topology and Free-size results[1].

A further advantage of using Altair HyperWorks for free-size optimization is that it produces an output containing a spatially varying stacking configuration over the geometry. However, it is important to note that this output does not correspond to a discrete laminate stacking sequence; rather, both the stacking configuration and total element thickness vary continuously on an element-by-element basis. Therefore indirectly providing a design with varying stacking order.Consequently, while the free-size optimization provides a useful preliminary design iteration, the resulting configuration requires further postprocessing. The further processing entails of manually dividing zones and running iterative studies on the zone division, the iterative studies take up a large amount of time.

Despite these limitations, free-size optimization serves as an effective starting point in the design workflow. It is capable of accommodating multiple design variables, objectives, and constraints, including

displacement limits, stress constraints, and failure criteria. The optimized results can be directly exported in the Ansys MAPDL CDB file format, enabling straightforward import into PyMAPDL for subsequent stages of analysis and optimization. During the Ansys conversion the model is defined in Shell 181 elements[28]. This interoperability facilitates integration into a broader automated design pipeline, ensuring that the free-size optimization stage can be seamlessly connected with later stages of the workflow.

3.2. Two level clustering

The imported CDB file must satisfy a set of predefined assumptions to ensure that the developed code can process the data correctly. These assumptions primarily concern the organization and completeness of the model data, which is extracted from the CDB file and stored as a Python-based data structure for subsequent processing.The main assumption is the exported finite elements shape. The subsequent algorithms assume quadratic constant edge length finite elements. Within the two-level clustering procedure, the first stage focuses on thickness clustering, followed by stress-based clustering. The thickness clustering is carried out using a k-means clustering algorithm. This algorithm identifies the elements whose thickness value is closest to the mean of the cluster and iteratively assigns elements to clusters. In this study, the number of thickness clusters is not fixed to a single value but is instead varied within a predefined range in order to investigate its influence on the final results. As discussed previously, the thickness distribution obtained from the free-size optimization does not correspond to a discretized laminate stacking sequence. Therefore, clustering serves as an intermediate step toward discretization. The process of grouping the continuous thickness field into discrete categories, followed by the definition of corresponding laminate layups, is illustrated in Figure 3.4. In figure 3.4 the processing steps to discretize can be seen from the free-size results. The left side illustrates the thickness over the geometry and one element as an example. The middle corresponds to the zone division example in which the design is divided into zones with red crosses illustrating the zone centers. The right side illustrates the discretized laminate stacking order. This transformation is essential for bridging the gap between the free-size optimization output and a suitable composite laminate configuration for manufacturing.The number of layers in the stacking order is defined by equation 3.1, the number of layers is rounded up to the nearest integer.

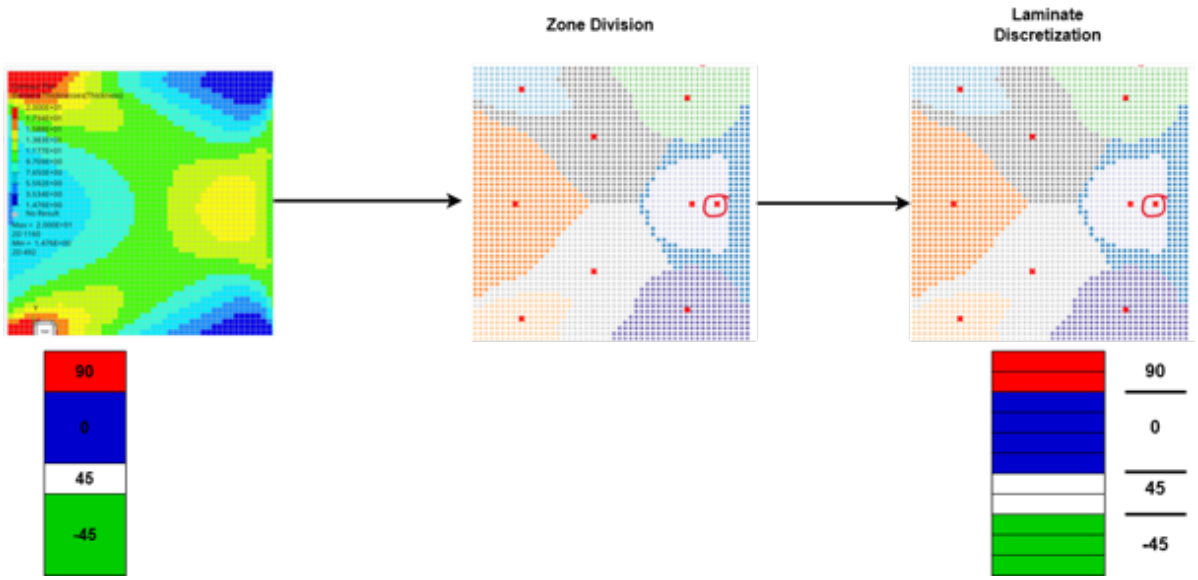

Figure 3.4: Thickness clustering and laminate discretization.

$$number\ of\ layers = \frac{\text{free-size thickness}}{ply\ thickness} \tag{3.1}$$

Since the thickness clustering groups elements based solely on their thickness values, the resulting clusters may still contain elements with varying layup characteristics. To enhance the uniformity of the elements within each thickness cluster, a subsequent stress clustering step is performed. The overall procedure of the stress clustering algorithm is illustrated in Figure 3.5. The first step involves calculating the homogenized principal stress angle for each cluster in principal direction 1 and 2 namely in plane, as defined in Equation 3.3. In cases where multiple stress clusters exist within a single thickness cluster, this homogenized angle is computed individually for each stress cluster.Using the homogenized angle as a reference, the algorithm calculates the angle deviation of each element relative to this mean

orientation. The orientation of the principal stresses are determined in equation 3.2:

$$2\varphi = \frac{2\tau_{xy}}{S_x - S_y} \tag{3.2}$$

,where φ is the principal angle, τ_{xy} element shear stress, S_x and S_y are the normal stresses on an element level. The principal angle is used in equation 3.3 and equation 3.4. This deviation is then compared to a user-defined allowable angle deviation threshold. The number of stress clusters is incrementally increased until every stress cluster exhibits an angle deviation below the specified limit or until a maximum predefined number of clusters is reached. For each cluster, the dominant angle is selected based on minimizing the angle deviation, as detailed in Equation 3.4. A low value of the clustering deviation metric cd_i indicates that the elements within the cluster align well with one of the principal directions. The direction 1 or 2 is chosen based on which $cd_{_1}$ or cd_2 takes a smaller value. For the rest of division based on stress the direction dominance is kept the same. Meaning if direction 1 is chosen then further division principal stress 1 values are used. Then accordingly, the clustering algorithm selects the elements with the highest stress from the cluster in this direction as a representative of the cluster.

This stress clustering approach is conceptually based on the local reinforcement algorithm presented by Berges et al. [4], which aims to identify and reinforce critical regions within the laminate by grouping elements according to their stress orientations. By combining thickness and stress clustering, the methodology ensures that clusters are not only similar in thickness but also exhibit consistent stress characteristics, which is essential for defining effective and manufacturable patch geometries.

$$\overline{\phi_i} = \frac{1}{\sum |\sigma_i|} \cdot \sum \varphi_i \cdot |\sigma_i| \tag{3.3}$$

,where $\overline{\phi_i}$ the homogenized angle is the mean of principal angles φ_i. σ_i are the principal stresses in their respective clusters.

$$c_{d,i} = \sqrt{\sum (\varphi_i - \overline{\phi_i})^2 \cdot \frac{|\sigma_i|}{\sum |\sigma_i|}} \tag{3.4}$$

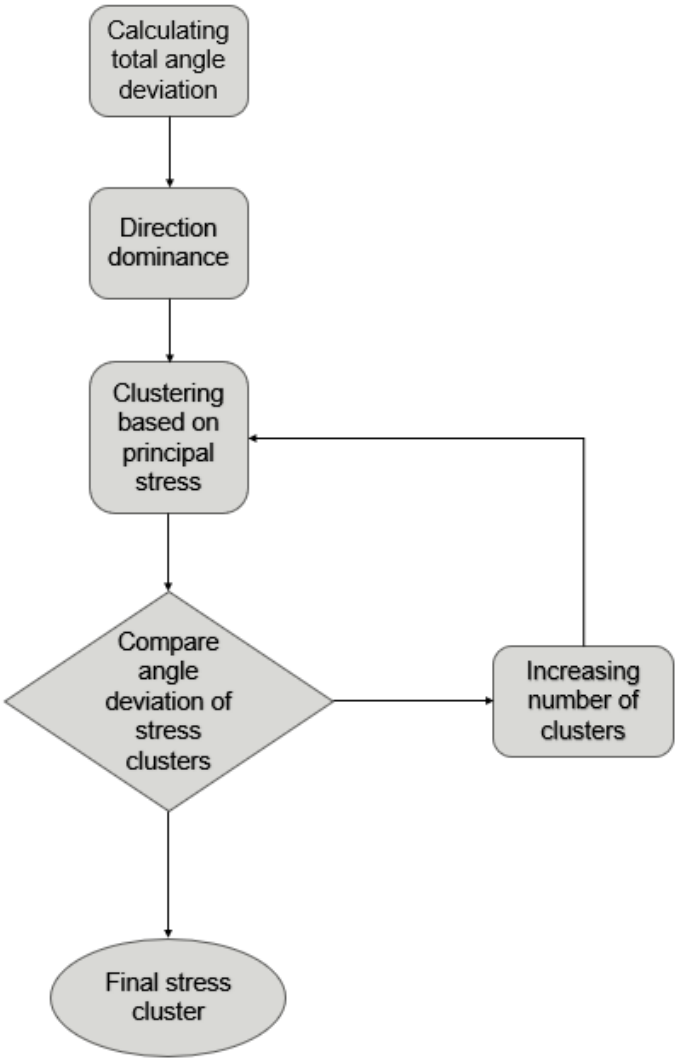

Figure 3.5: Stress clustering algorithm.

3.3. Patching Algorithm

The postprocessed results obtained from the free-size optimization are not directly suitable for manufacturing due to the presence of large variations in thickness across the geometry. While the two-level clustering approach, comprising thickness and stress clustering, serves to homogenize the finite elements and reduce these variations, further transformation of the geometry is necessary to produce a design that can be reliably and efficiently manufactured using automated processes.

3.3.1. Manufacturing mesh generation

The initial step in adapting the optimized geometry for manufacturing involves the generation of a manufacturing mesh. The input geometry is provided as an STL file, which is then discretized into a set of elements and segments based on the manufacturing constraint geometry. These constraints include the tape width and the minimum allowable placement length, which dictate the granularity and layout of the manufacturing mesh. The manufacturing mesh is composed of right-angled triangular elements. Figure 3.6 depicts one an example of manufacturing mesh for $0°, 90°$ orientation. In the manufacturing geometry as segment is defined as a continuous collection of elements upon which a single tape layer can be deposited during the tape laying process. The segment for $0°$ and $90°$ The dimensions of each element—its width and height—are directly derived from the tape width and the minimum placement length, respectively, ensuring compatibility with the physical capabilities and limitations of the tape laying equipment. Since the segment have to be deposited in a diagonal direction for $\pm 45°$ orientation.

Therefore manufacturing mesh differs in the triangular element configuration in figure 6.2 the manufacturing mesh with few elements is illustrated for $0°$,$90°$ and the $\pm 45°$ orientation.

It is important to note that the manufacturing mesh varies depending on the tape orientation used. For orientations $\pm 45°$ the tape width and minimum placement length must be carefully matched during the mesh generation process to maintain consistency in the geometry. The manufacturing mesh is orientation specific. A self-developed algorithm allows the user to define other angles as well, however for angles other than $0°, \pm 45°, 90°$ further work is necessary. This orientation-specific meshing is crucial to accurately capturing the manufacturing geometry constraints and ensuring that the tape layers can be laid down according to orientations.

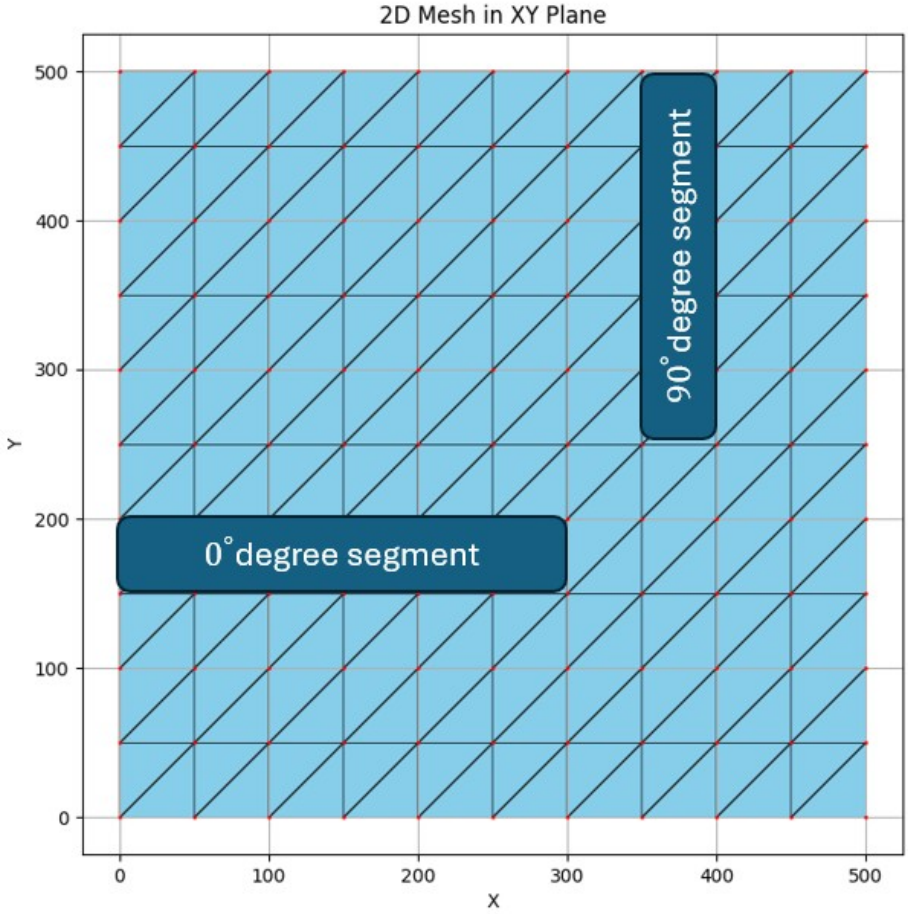

Figure 3.6: Manufacturing mesh illustration for $0°$,$90°$ orientation.

The element sizes in the finite element mesh and the manufacturing mesh differ, necessitating the implementation of a layer assignment function to accurately transfer design information between these meshes. This layer assignment function operates by calculating weighted contributions based on the overlapping areas between the finite elements and the manufacturing mesh's triangular elements. Specifically, the function uses area-based weighting coefficients, as defined in Equation 3.5, to determine the effective contribution of each finite element toward the layer count of the manufacturing mesh elements. The total number of layers assigned to each triangular element in the manufacturing mesh is then computed according to Equation 3.6, which aggregates these weighted contributions. Furthermore, if the user of the code requires a transfer sensitivity can be calculated to gather information about the transfer sensitivity shown in equation 3.7. In the further analysis this metric was not used due to the use of normalized lamination parameters, which will be used in later section 3.4. In figure 3.8 an illustration can be seen for the overlap between the manufacturing mesh and finite element mesh. In the illustration the manufacturing mesh is represented with two elements a and b. The finite elements are represented with four element $1, 2, 3, 4$ with assigned number of layers $10, 12, 15$ and 13. In equation

Figure 3.7: Mesh illustration for comparison of $0°$,$90°$ vs $\pm 45°$ orientation.

3.8 an example calculation can be seen representing the case in figure 3.8. In the example calculation element 1 has 75% coverage and element 2 has a 25% resulting in an approximate of 11 layers for element a in the manufacturing mesh. It is apparent that the example is oversimplified but illustrates the idea of the method to assign the number of layers to a manufacturing mesh's elements.

Following this initial layer assignment, a secondary filtering algorithm is applied. This algorithm iterates through neighboring triangular elements within the manufacturing mesh and adjusts their assigned layer numbers by assigning the maximum value found among adjacent elements to both elements in the pair. In figure 3.9 the neighboring elements are illustrated for manufacturing mesh of $0°, 90°$ orientation. For the orientations of $\pm 45°$ orientation an illustration can be seen in figure 3.10. This step ensures the manufacturing mesh elements numbers are consistent for neighbours, which is essential for manufacturability and reliable tape laying. The filtering process thus enforces a conservative layer assignment that respects manufacturing constraints, preventing potential issues such as a mismatch between the neighboring elements number of layers in manufacturing mesh.'

$$w_{ij} = \frac{A_{ij}^{Overlap}}{A_j} \tag{3.5}$$

, where w_{ij} is overlap weight coefficient.$A_{ij}^{overlap}$ are the overlap area with a specific finite element and A_j are the area of the manufacturing mesh.

$$P_j = \sum w_{ij} \cdot P_i \tag{3.6}$$

,where P_j is the number of layers in the manufacturing mesh element, P_i are the number of layers in the finite element mesh.

$$S = \sum w_{ij} |P_i - P_j| \tag{3.7}$$

,where S is the transfer sensitivity.

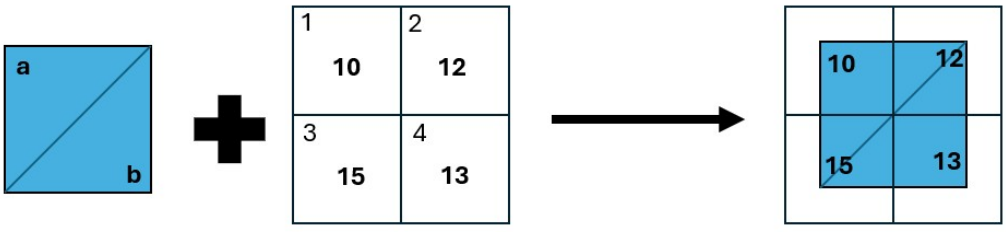

Figure 3.8: Element overlap of manufacturing element(a,b) and four quadratic finite elements of varying amount of layers.

$$\begin{aligned} &\text{Element a} : 10 \cdot 0.75 + 15 \cdot 0.25 = 11 \\ &\text{Element b} : 12 \cdot 0.40 + 13 \cdot 0.60 = 13 \end{aligned} \tag{3.8}$$

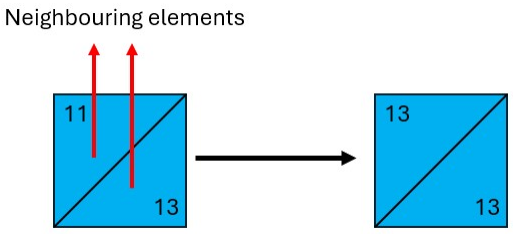

Figure 3.9: Illustration of neighboring elements and layer reassignment.

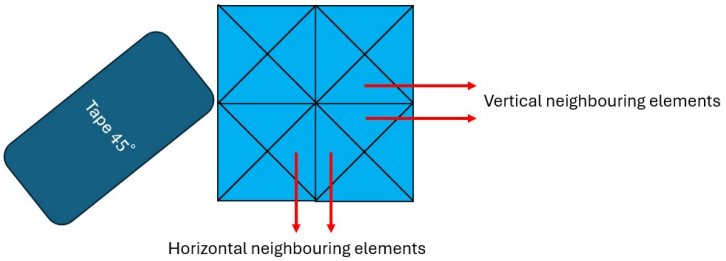

Figure 3.10: Illustration neighboring elements for $45°$ orientation.

In figure 3.11 a manufacturing mesh is shown. Similar manufacturing mesh can be generated for the varying designs. The example shows here is with a coarse tape width of 50mm.

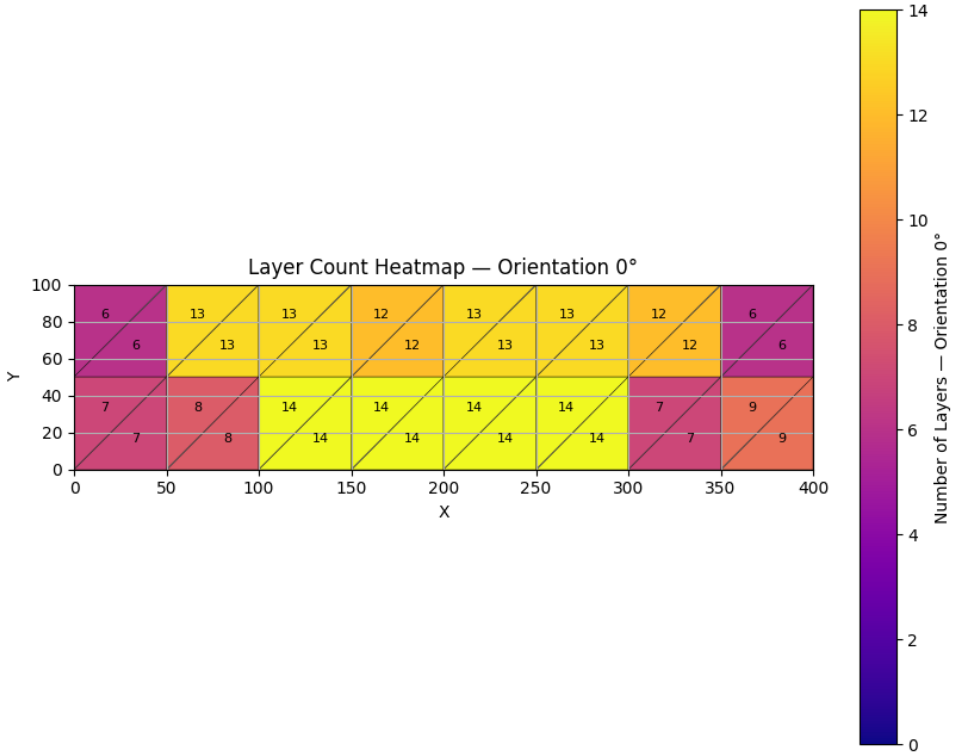

Figure 3.11: Manufacturing mesh illustration 0° orientation.

3.3.2. Patch generation

Following the generation of the manufacturing mesh, the number of resulting elements can vary significantly depending on the tape laying dimensions and geometric complexity. Given that each element can contain multiple orientations, the volume of model information becomes substantial. Directly optimizing thousands of elements and their orientations using a genetic algorithm would be computationally prohibitive and inefficient. To address this challenge, a patching algorithm has been developed to reduce the model complexity while preserving essential design features and information.

The patching algorithm operates by handling each fiber orientation independently. For each orientation, a dedicated patch library is constructed, which encapsulates key geometric and design parameters for each patch. Specifically, the patch library stores the center coordinates (Cx,Cy), width w, and length l of each patch. Additionally, the number of layers and the corresponding fiber orientation associated with each patch are recorded. This structured representation enables the reduction of the model's dimensionality by grouping elements into larger, uniform regions—referred to as patches—thereby simplifying the optimization problem.

The overall workflow of the patching algorithm is illustrated in Figure 3.12. By employing this patch-based description, the model can be efficiently represented with significantly fewer variables, making it more tractable for genetic algorithm optimization while maintaining fidelity to the original manufacturing constraints and design intent. Based on the patch library, the genetic string for the genetic algorithm

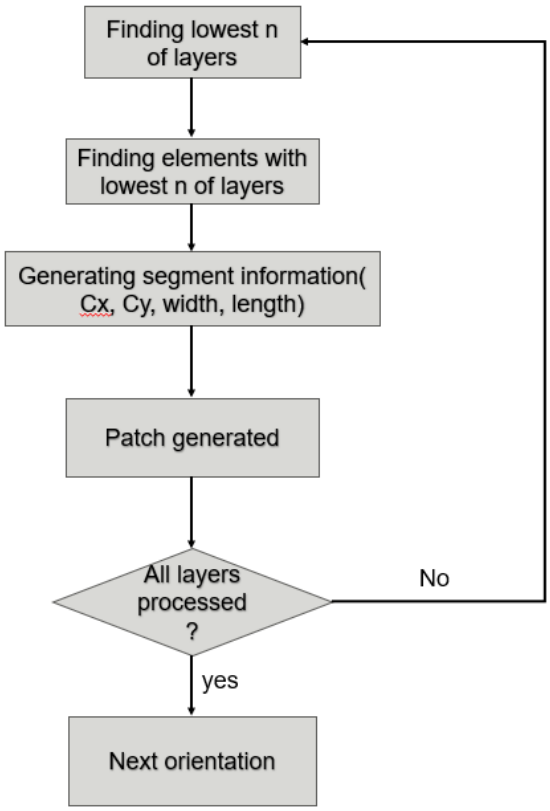

Figure 3.12: Patching algorithm workflow.

(GA) can be constructed. Each entry in the genetic string corresponds to the number of layers assigned to a specific patch within the model. During the optimization process, variations in the genetic string effectively modify the number of layers for each patch, thereby altering the overall stacking sequence and laminate configuration of the design. This representation enables the GA to explore a wide range of laminate designs by adjusting the layer distribution at the patch level, rather than at the level of individual elements, significantly reducing the complexity of the optimization problem.

3.4. Optimization Employing a genetic algorithm

The fitness function employed within the genetic algorithm is formulated to evaluate the mismatch error between the target lamination parameters and those of the current design iteration. By minimizing this mismatch, the GA seeks to produce laminate configurations that closely align with the desired mechanical and manufacturing requirements similar to the design input, ensuring optimal structural performance, while adhering to manufacturing constraints. In a symmetric and balanced stacking sequence, out of the four normalized lamination parameters (V_1, V_2, V_3, V_4) only two parameters,V_1 and V_3, are non-zero [26]. These parameters are defined as follows:

$$V_1 = \frac{1}{h}\sum_{k=1}^{N_l} t_k \cos(2\theta_k) \tag{3.9}$$

$$V_3 = \frac{1}{h}\sum_{k=1}^{N_l} t_k \cos(4\theta_k) \tag{3.10}$$

where $N_l$represents the total number of layers, $t_k$is the thickness of the k-th ply, θ_k denotes the ply orientation, and h is the total laminate thickness. These normalized lamination parameters typically range between -1 and 1. Figure 3.13 illustrates the feasible values of the lamination parameters depending on the stacking sequence. For the scope of this thesis layups of consisting four orientations($0°$,$\pm 45°$,$90°$) will be use mainly. The genetic algorithm is initially tested with orientations consisting only $0°$ and $90°$ orientation. The lamination parameter calculation requires a stacking order. The finite element model's stacking order is easily retrieved through PyMAPDL. However, the patch-wise definition of the model requires a self-written stacking order retrieval function. The function to build the stacking order constructs a segment element map. The segment element map contains information about the specific finite elements that the segment overlaps. For thesis it was assumed that the finite elements center coordinate is used for the construction of the segment overlap.

The genetic algorithm's fitness function is based on the calculation of an error metric quantifying the deviation of the current design's lamination parameters from the target values. This error is computed using the Symmetric Mean Absolute Percentage Error (SMAPE), whose formulation is given in Equation 3.11. SMAPE is evaluated for each element individually, and the resulting errors are averaged over the entire design domain to yield a global fitness score used in the optimization process.

The choice of SMAPE over the more conventional Mean Absolute Percentage Error (MAPE) is motivated by its improved numerical stability, particularly near zero values of lamination parameters. As observed in Figure 3.13, certain quasi-isotropic layups can yield V_1 and/or V_3 values close to zero. In such cases, MAPE may produce disproportionately large error percentages, approaching infinity, even for minimal differences involving only one or two plies. SMAPE avoids this issue by symmetrizing the percentage error calculation, resulting in a more robust and reliable measure of lamination parameter mismatch during the optimization.

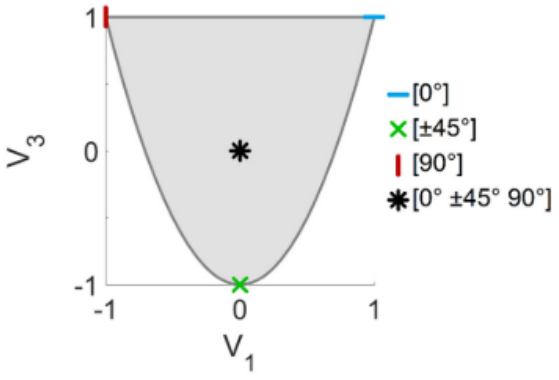

Figure 3.13: Miki's lamination diagram[26].

Table 3.1: Genetic Algorithm parameters.

Genetic algorithm parameters	
Parent Selection Method	Tournament
Cross Over Method	Scattered
Mutation Method	Random mutation
Range of values	0-50

$$SMAPE\% = \frac{|\text{expected} - \text{given}|}{(|\text{expected}| + |\text{given}|)/2} \cdot 100 \tag{3.11}$$

During the genetic algorithm (GA) optimization, the patching information evolves with each generation within the population. For every individual in the population, the lamination parameters are computed for both the finite element mesh and the manufacturing mesh. The Symmetric Mean Absolute Percentage Error (SMAPE) is then calculated for each lamination parameter and averaged across all elements. Once these errors are obtained for all individuals, their overall average and standard deviation are computed to characterize the population's performance.

The fitness function used to evaluate each candidate solution is expressed in Equation 3.12. Notably, this function is formulated as a maximization problem. Although optimization tasks are traditionally framed as minimization problems, the Python genetic algorithm library utilized in this thesis, PyGAD [21], requires fitness functions to be maximized. This convention necessitates the inversion or transformation of the error metric accordingly. Furthermore, in equation 3.12 the desired output represents a user-defined value. The goal of the desired output is to set a value such that the fitness function could have earlier convergence. As an example the optimization problem could lead to an average error of 0%, but the desired output of 10% could lead to an earlier convergence.

Several GA parameter settings employed in this work are summarized in Table 3.1. The discrete nature of the design variables—specifically, the integer values corresponding to the number of layers per patch—makes the genetic algorithm particularly well suited for this optimization problem. Throughout each generation, the GA evaluates the lamination parameter mismatch error for every element in both the finite element and manufacturing meshes, averaging these errors to obtain a global metric. The optimization process, therefore, effectively minimizes the average lamination parameter error across the entire geometry, guiding the search toward laminate designs that meet both performance and manufacturability criteria.

$$\text{Fitness} = \frac{1}{1 + |\text{Avg. error} - \text{desired output}|} \cdot 100 \tag{3.12}$$

4

Results

In this chapter, the results of applying the proposed methodology to a cantilever plate and a Messerschmitt-Bölkow-Blohm(MBB) beam are presented and discussed in detail. The analysis begins with an examination of thickness and stress clustering, focusing on how variations in the number of clusters affect the results. The performance of the clustering algorithm is evaluated based on its ability to group elements according to their thickness and stress characteristics.

For the stress clustering, additional attention is given to evaluating how well the underlying assumptions translate into practical design parameters, such as the determination of the number of layers, and how effectively the resulting clusters capture the primary load paths within the structure.

Finally, the performance of the genetic algorithm is assessed by examining changes in both the average values and the standard deviations of the results, comparing outcomes before and after the application of the algorithm to determine its impact on the clustering quality and overall optimization.

4.1. Test cases and free-size optimization input

The algorithm workflow, along with the capability of the genetic algorithm to reduce the mismatch error relative to the target lamination parameters using a geometry defined by manufacturing constraints will be validated through a representative test case. The selected cases are the cantilever plate and the MBB beam, a well-known benchmark problem in structural optimization. Traditionally a composite plate would be not loaded as shown in figure 4.10. The case is shown to generate a model with varying thickness and additional parameter such as buckling problems are not taken into accounts. The MBB beam case study shown in the thesis will be containing four orientations($0°$,$\pm 45°$,$90°$). Additionally, an initial result of square plate will be shown containing of only $0°$ and 90 orientation, which was made at the earlier stages of the thesis as initial demonstration of the thesis methodology.

Throughout the report, the material properties of a unidirectional tape, as specified in Table 4.1, will be consistently used. The free-size optimization models generated in Altair Hyperworks and their corresponding results serve to exemplify the input data and conditions for the proposed design methodology. While alternative free-size optimization results may be generated for other industrial applications, the fundamental workflow and procedural steps of the design methodology remain consistent and applicable across different cases.

Table 4.1: Material Values.

Material constant	Value
E_1	127700[MPa]
E_2	7400[MPa]
G_{12}	6900[MPa]
ρ	1.8t/mm^3
X_t	1717[MPa]
X_c	1200[MPa]
Y_t	30[MPa]
Y_c	216[MPa]
S	33[MPa]

4.2. Initial Test Results

The goal of the initial results is to demonstrate the initial clustering based on total thickness and the stress based clustering. Furthermore, the robustness of the optimization will be shown for the initial results cantilever plate. The initial model is a $500by500mm$ cantilever plate fully constrained left edge and a downwards load applied along the right edge. The cantilever plate is illustrated in figure 4.1. The material data is the same as the one shown in table 4.1 and the simulation parameters can be seen in table 4.2. In the initial cantilever plate the only orientation present are $0°$ and $90°$ degrees in a balanced stacking order with the same amount of $0°$ and $90°$. During the optimization process since only two orientations are present only one lamination parameter was used for the error calculation. In figure 4.2 the Altair Hyperworks model can be seen. As previously mentioned the left side edge is fully constrained and a $5000N$ load is applied on the right edge. In figure 4.3 the element thickness distribution can be seen for the cantilever plate as a result from free-size optimization. The individual thickness distribution for orientation of $0°$ and $90°$ are not shown, because the orientation are set to be balanced therefore the overall distribution does not change only in values.

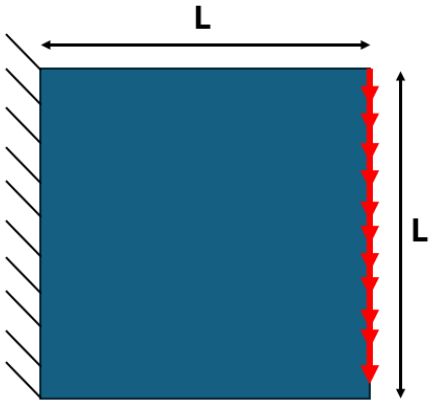

Figure 4.1: Cantilever plate illustration.

Table 4.2: Simulation Parameters for Cantilever plate.

Simulation parameters	Value
Force	5000[N]
Ply thickness free-size optimization	5[mm]
Volume fraction constrain	0.6
Failure index constraint	1

In figure 4.4 the clustered plate can be seen based on total element thicknesses. The design has been

Figure 4.2: Altair Hyperworks model of cantilever plate

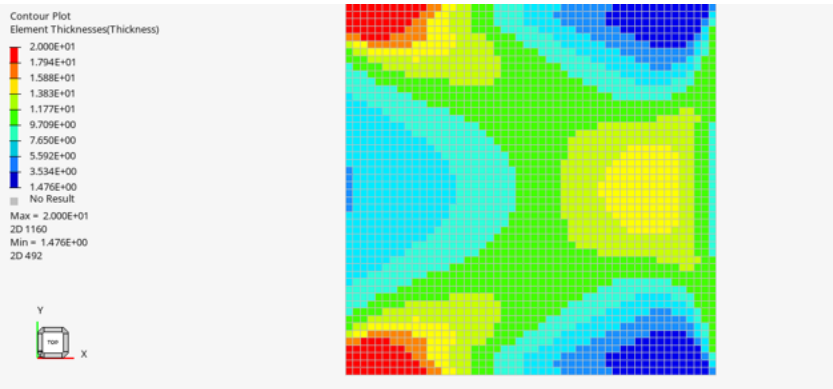

Figure 4.3: Free-size total thickness distribution of cantilever plate.

clustered in 4 zones. First in figure 4.4 it can be observed that a horizontal symmetry is conserved similarly to free-size result in figure 4.3. Furthermore, in figure 4.5 the stress clustered layer distribution can be seen per orientation. The horizontal symmetry still holds. After the initial results it was concluded that the next step in the optimization is the increase in number of thickness and stress clusters.

In figure 4.6 the number of thickness clusters has been increased to 9. Similarly to figure 4.4 the zone division holds the horizontal symmetry. Further in figure 4.7 it can be observed that with allowing 3 stress cluster per thickness cluster the symmetry is broken. In subsection 4.3.2 a similar loss of symmetry occurs. In the thickness clustering the division is based on total element thickness. In figure 4.4 the thickness distribution shows variance but larger areas with similar thicknesses are present. Data with large variance can show complications in the use of the clustering algorithm in poor zone shapes for the division. However, in figure 4.4 and figure 4.6 for the initial zone division the clustering algorithm performs quite well. The loss of symmetry more likely stems from the stress clustering algorithm. In the stress clustering the principal direction are calculated by equation 3.2, which makes use of stress outputs in a global coordinate system. The use of principal angle in a local coordinate system could lead to the symmetry loss since the local and global coordinate system can be miss-aligned. However, in MAPDL the stress outputs S_x,S_y and S_{xy} by default are in the global coordinate system for shell element 181[28]. Therefore the miss-match between a local and global coordinate system is unlikely to cause the loss of symmetry. During the stress clustering algorithm the dominating principal direction is chosen based on the deviation metric cd_i. The dominating principal direction once is decided is

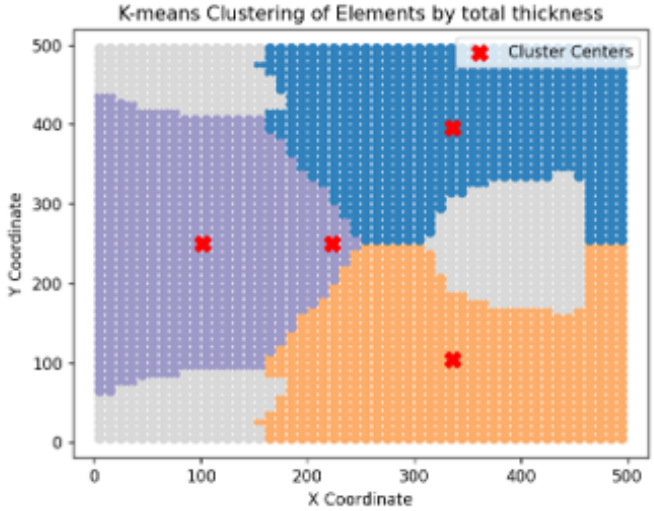

Figure 4.4: Cantilever plate clustered into 4 zones based on total element thickness.

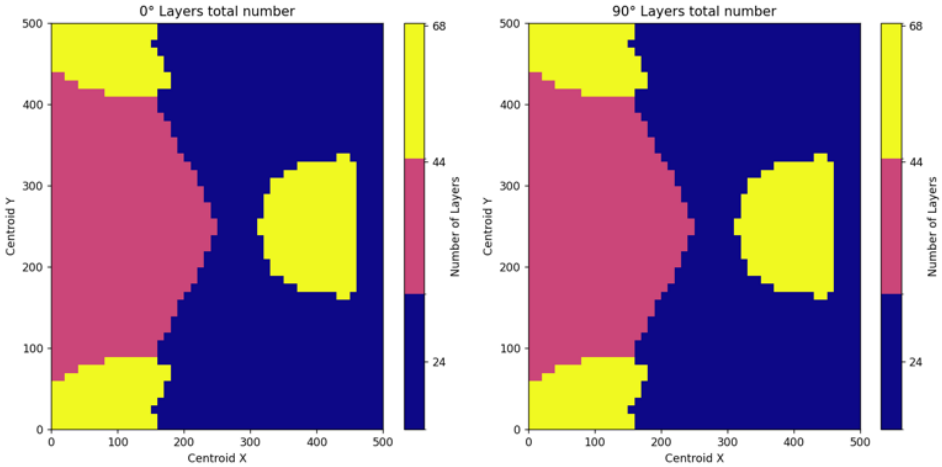

Figure 4.5: Initial results clustered per orientation

kept during for the rest of the zone division. During the further zone division the direction dominance could change, since in larger thickness zone the elements' alignment might not correspond to just one direction once more zones are introduced. This could lead to loss of symmetry in the zone division. The improvement of this stress clustering algorithm is a difficult problem and out of the scope of this thesis and recommended for future work.

The next step in the methodology is the application of the genetic algorithm on the patch-wise definition of the geometry. For the initial results the cantilever plate the layup contains balanced stacking order of the $0°$ and $90°$ orientation. To test the genetic algorithm separately the free-size result was translated directly into a manufacturing geometry with a tape width of $20mm$ without clustering. The genetic string contains the initial information for both $0°$ and $90°$ patches. Therefore change in the genetic string entry would change information for both orientation patches.

In table 4.3 the initial error and standard deviation can be seen for the cantilever plate before and after optimization. The decrease in error is quite low meaning the initial manufacturing geometry was quite close to the finite element model. Furthermore, in figure 4.8 and figure 4.9 the error distribution can be seen before and after the optimization. The highlighted elements with light blue border are the elements corresponding to values of outside of one standard deviation. The error values are comparable on the low side, because due to the $0°$ and $90°$ balanced stacking order. Furthermore, the tape width and the

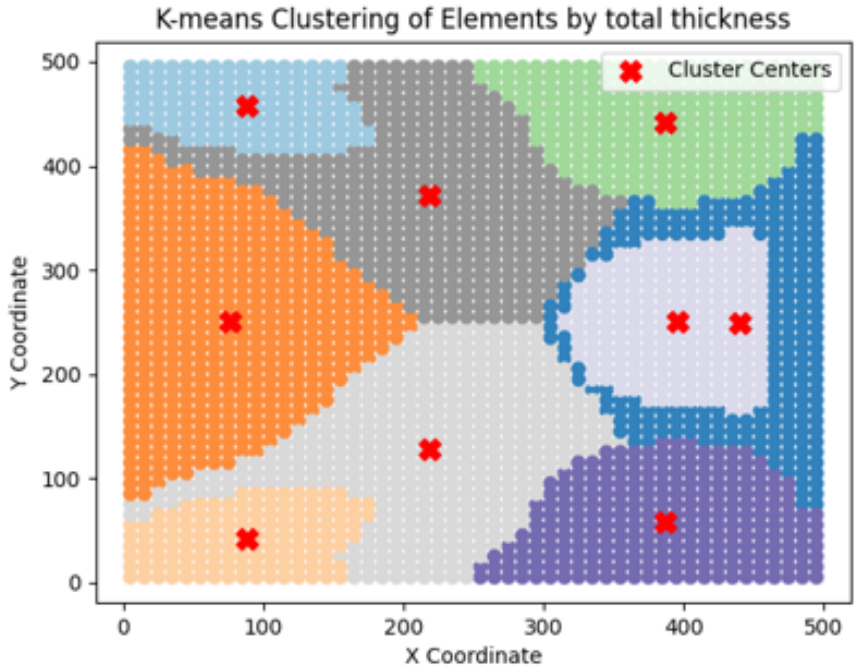

Figure 4.6: Cantilever plate clustered into 9 zones based on total element thickness.

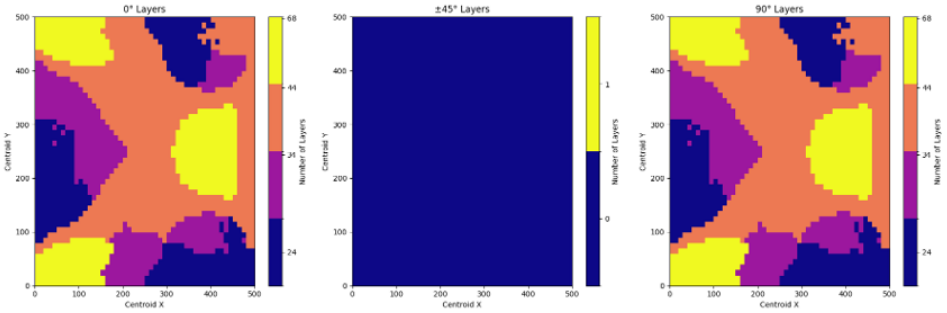

Figure 4.7: Cantilever plate 9 thickness zone and 3 allowed stress cluster per zone.

lower variation in thickness allowed the tape width allowed the layer assignment function to follow the initial design well. After optimization the error decreases meaning the optimization is successful in terms of trying to match the input of the genetic algorithm. For the change in thickness the performance of the genetic algorithm can be evaluated based on the genetic string values. In table 4.4 the genetic strings can be seen before and after the application of the optimization. After optimization the resulting genetic string shows the some of the patches containing one plies are added to some of the existing patches. This indicates that during the optimization due the patch generating algorithm the genetic algorithm effectively reassign the patches, while resulting in patch definition that closer to the input. Based on this initial results the decision was made to increase the complexity of the problem by including further orientations. In the next section the MBB beam will be used, where the methodology is further tested with varying clustering definitions and tape widths.

Table 4.3: Cantilever plate initial optimization

Configuration	**Error and Standard deviation before GA**	**Error and Standard deviation after GA**
Cantilever plate	error 7.17% std 10.98	error 7.05% std 11.64

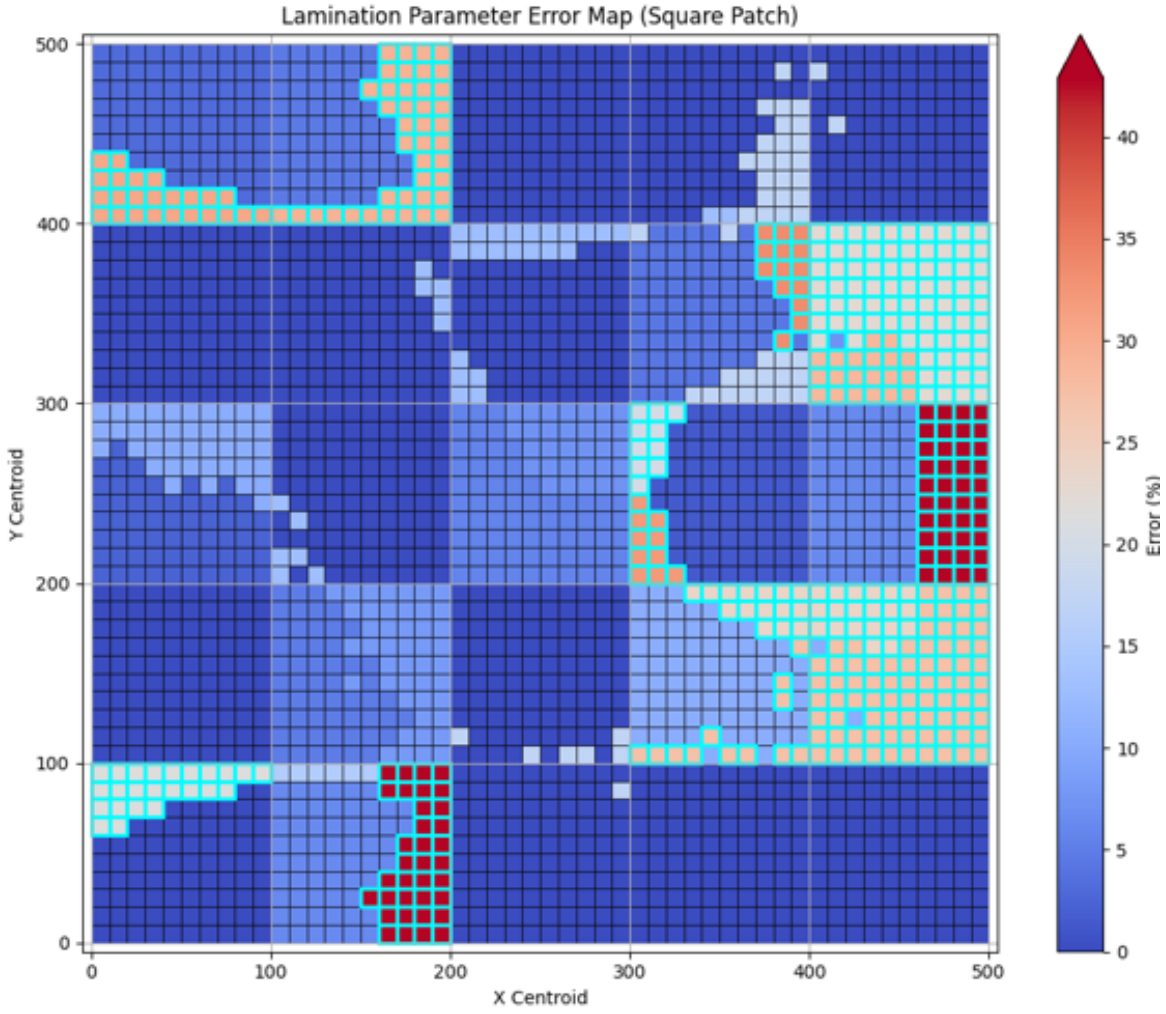

Figure 4.8: Cantilever plate error distribution before optimization.

Table 4.4: Genetic String before and after optimization.

	Genetic String
Before optimization	[12 5 2 1 1 1 2 6 1 1 1 1]
After optimization	[12 5 1 0 1 5 2 8 0 0 0 0]

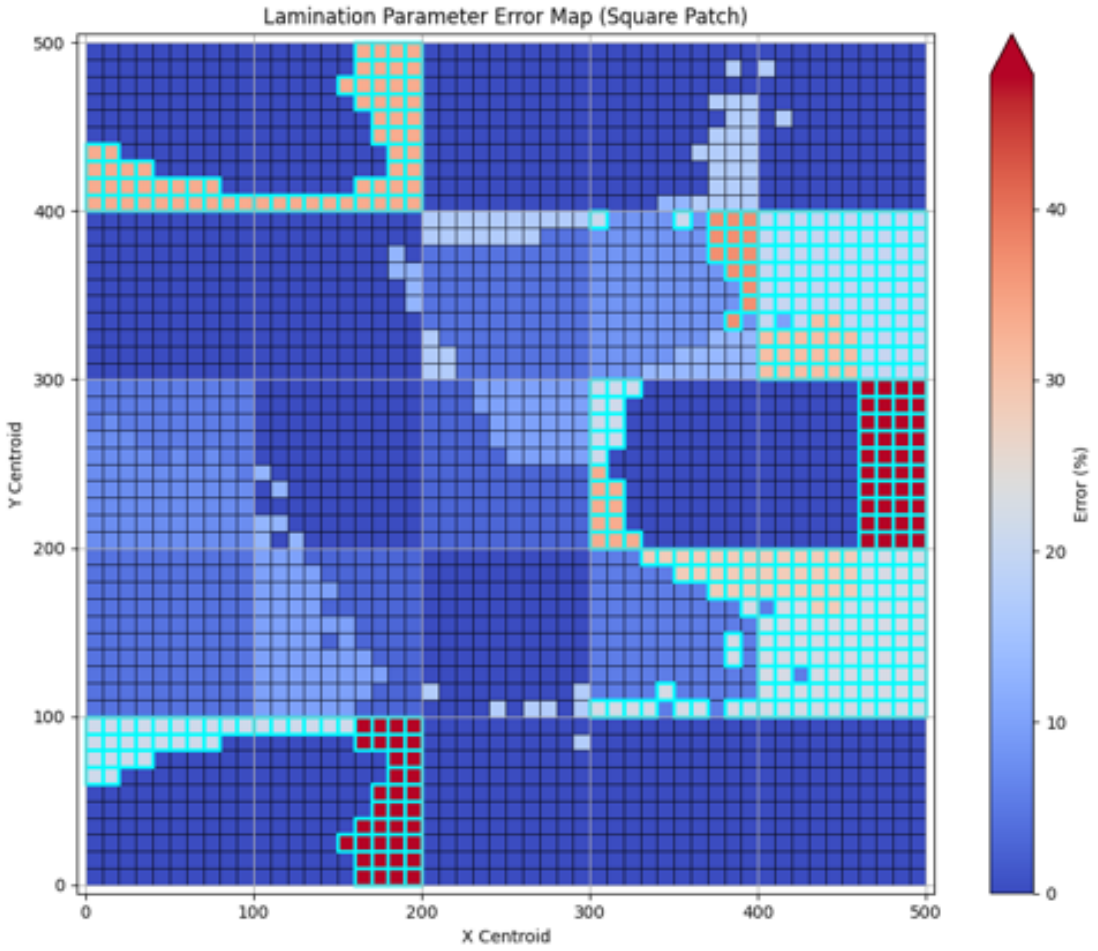

Figure 4.9: Cantilever plate error distribution after optimization.

4.3. MBB Beam

In figure 4.10 an MBB Beam illustration can be seen, where the L correspond to the length and in the thesis will be $L = 100mm$. The model was generated in Altair Hyperworks and optimized in free-size optimization using Optistruct. The input and simulation parameters can be seen in figure 4.10 and table 4.5. The ply thickness input corresponds to the starting thickness at the start of the optimization. A further simulation parameter not shown in table 4.5 is the minimum allowable density . The minimum allowable density by default is set to be 10% of the starting ply thickness. For the generation of the free-size result the minimum allowable density is set to be 10^{-4}.The resulting total thickness distribution can be seen in figure 4.12. The thickness varies between of a maximum thickness of $16mm$ and minimum of $3.4 \cdot 10^{-}3mm$. In figure 4.12 the maximum thickness is assigned to certain areas. Better free-size results, where the maximum thickness does not occur are possible to generate. However, due to time limitation and small relevance to the over goal of the thesis smaller time were spent on the generation of the free-size results. In the case of this thesis the maximum thickness is assigned to the top and bottom edge of the beam. In figure 4.13 the thickness distribution for one $0°$ orientation ply can be seen. The thickness distribution shows the upper and bottom edge has the maximum thickness assigned. The upper edge of the beam is under tension loading, while the bottom edge is under compression. Therefore, the assignment of maximum thickness in the upper and bottom edge of $0°$ orientation is sensible. In figure 4.14 the thickness distribution can be seen for $\pm 45°$ orientation can be seen. The maximum values occur on the top and bottom edge similarly to figure 4.13. Further areas of maximum of the $\pm 45°$ orientation correspond to areas where the load path connects force application location to the corners. In figure 4.15 the thickness distribution the maximum thickness areas correspond to the same areas as for $0°$ orientation. Following the free-size optimization, as previously described, the results are exported as an ANSYS CDB file. This file is then imported into the Python environment for further processing. Upon import, the design is discretized and subjected to both thickness and stress clustering algorithms.

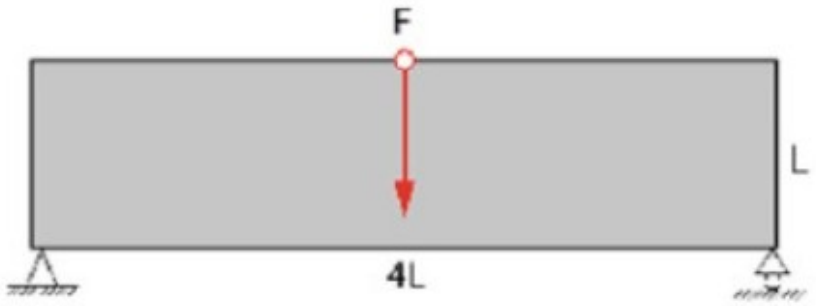

Figure 4.10: MBB Beam load case, boundary conditions and dimension ratios[29].

Table 4.5: Simulation Parameters.

Simulation parameters	**Value**
Force	5000[N]
Ply thickness free-size optimization	2[mm]
Volume fraction constrain	0.6
Failure index constraint	1

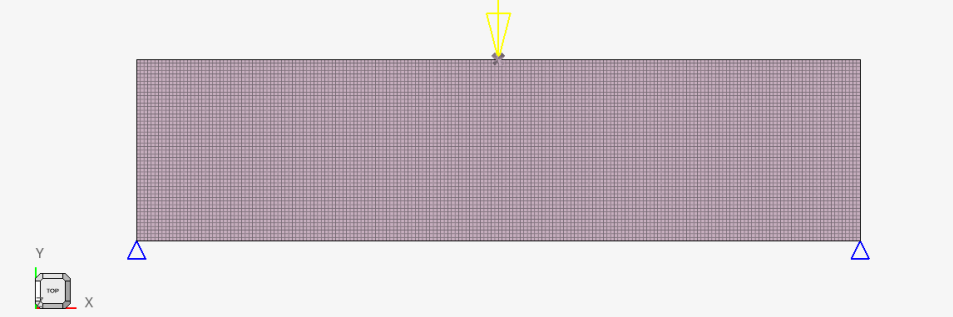

Figure 4.11: Altair Hyperworks model of MBB Beam.

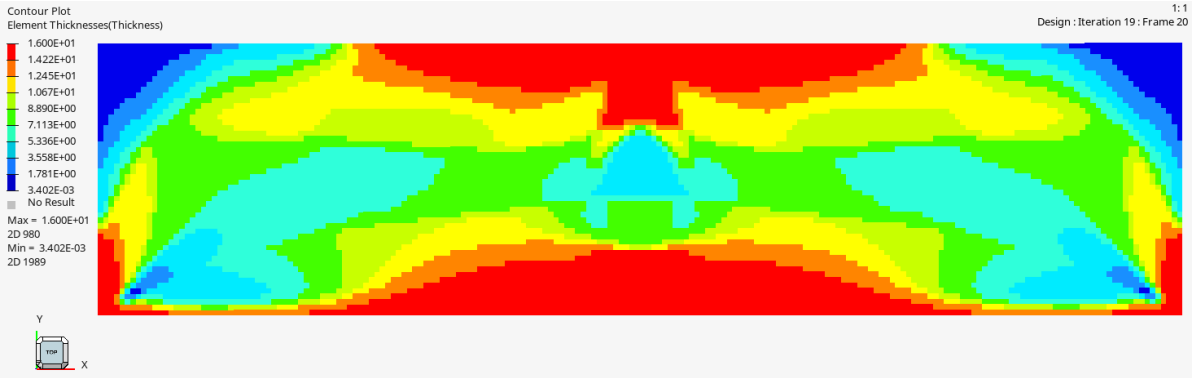

Figure 4.12: Thickness distribution of MBB beam.

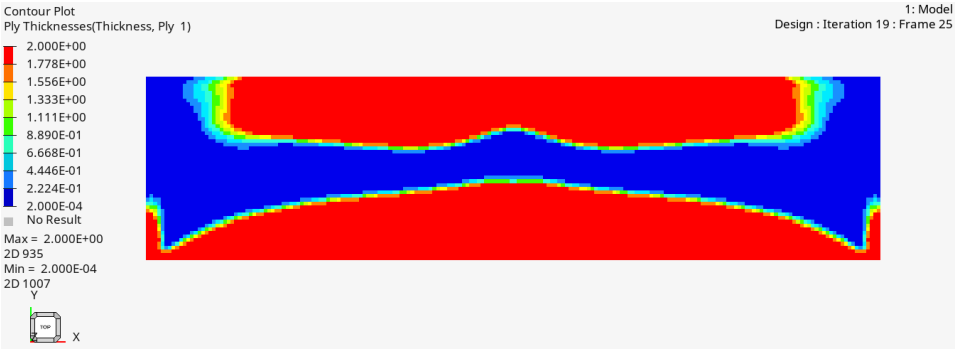

Figure 4.13: Thickness distribution of 0° orientation.

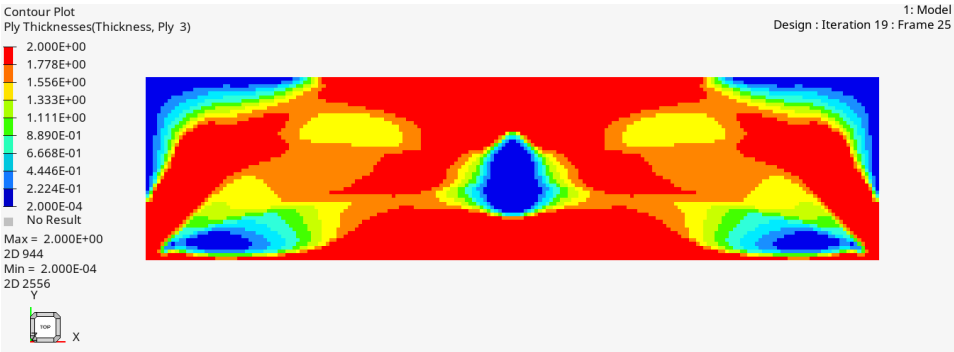

Figure 4.14: Thickness distribution of $\pm 45^\circ$ orientation.

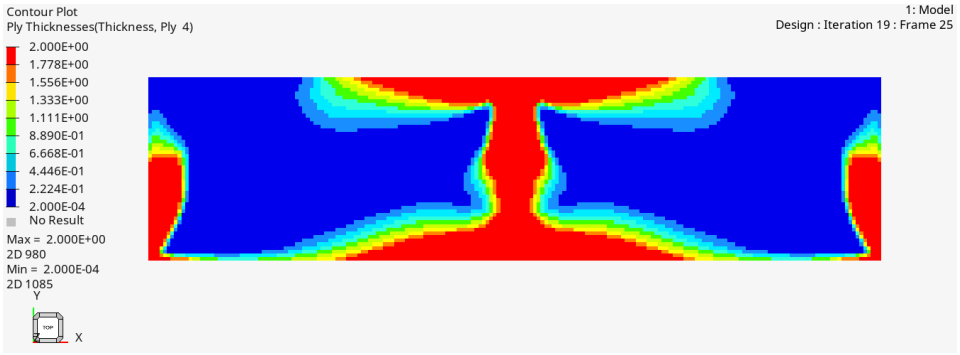

Figure 4.15: Thickness distribution of $90°$ orientation.

4.3.1. Test Plan

In the thesis the MBB Beam will test three parameters. The influence of the number of thickness and stress clusters and change of manufacturing parameters. The manufacturing parameters are the tape width used to define the manufacturing mesh. In table 4.6 the test plan can be seen. Furthermore, two additional tests are run. First, a run with finer finite element mesh, which has been determined necessary based on the initial results in the MBB clustering section.

Table 4.6: Test definitions.

Beam	**MBB Beam**
Number of thickness clusters	[4,16,32]
Number of allowed stress clusters	[1,4,16]
tape width[mm]	[50,25]
Finer finite element mesh with small tapewidth	10000 elements, 10mm tape width

4.3.2. MBB Beam Thickness and Stress Clustering Variation

In this section the results will be shown for varying number of thickness and allowed stress clusters. The goal of varying the number of clusters to see performance of clustering based on total element thickness. Furthermore, in the initial result the loss of symmetry has been shown. The MBB beam contains four orientation($0°$,$\pm 45°$,$90°$) compared to the initial results of two orientations($0°$,$90°$). The addition of further orientation makes the design more complex, therefore the clustering study is necessary for the main topic of this subsection.

Thickness clustering

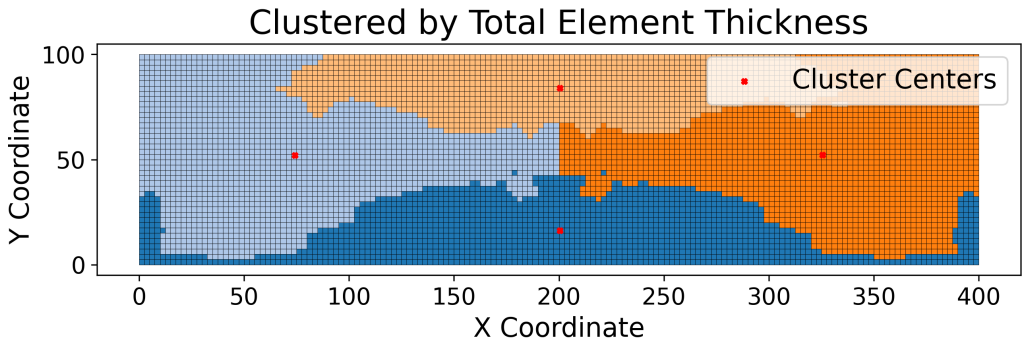

Figure 4.16: Thickness clustering number of cluster 4.

The thickness clustering uses K-means clustering algorithm, which makes use of the LLoyd clustering default setting. The number of thickness clusters are set to be $4, 16$ and 32. Figure 4.16 presents the results of the thickness clustering. When compared to the overall thickness distribution, the clustering algorithm with four clusters effectively captures the symmetry observed in the thickness distribution obtained from the free-size optimization. Despite this overall agreement, certain elements do not align closely with their assigned clusters. These elements, which will hereafter be referred to as rogue elements, appear separated from the main body of their respective clusters. Their occurrence can be attributed to the intrinsic characteristics of the thickness distribution. A close up illustration of rogue element can be seen in figure 4.17, where the rogue elements can be seen in the circle not connected to the green cluster.

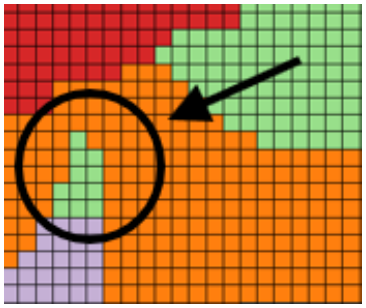

Figure 4.17: Close up Illustration of rogue elements.

As shown in Figure 4.12, some regions exhibit notably low thickness values, while the distribution as a whole demonstrates substantial variability. Highly variable data pattern is characteristic of anisotropic data distributions [12], where the data does not conform to uniform variance in all directions. This anisotropy influences the clustering results and contributes to the presence of rogue elements. Addressing these effects would require further refinement of the clustering methodology, which forms a key component of the planned future development of this study.

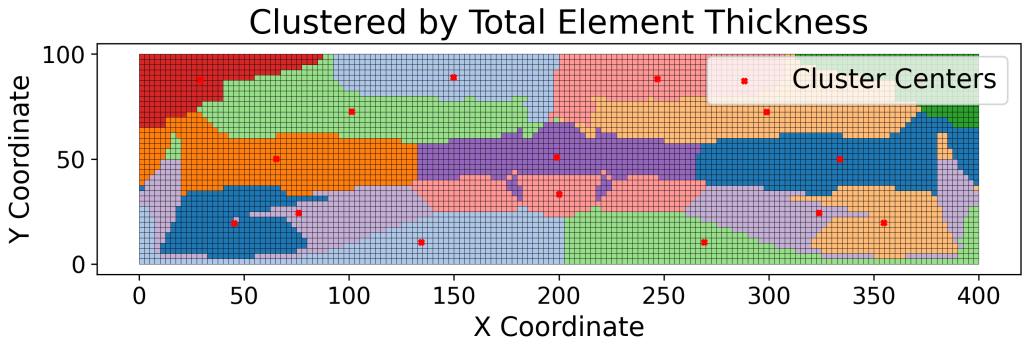

Figure 4.18: Thickness clustering number of cluster 16.

Figure 4.18 illustrates the clustering results for the case with 16 clusters. The overall symmetry of the model is maintained; however, the issue of rogue elements persists. In this configuration, a greater number of elements deviate noticeably from their respective clusters, making the presence of rogue elements more pronounced compared to the four-cluster case.

In contrast, Figure 4.19 shows the clustering results for 32 clusters. While challenges related to cluster division remain evident, the number of rogue elements is less pronounced than in the 16-cluster case, suggesting a partial improvement in cluster cohesion as the number of clusters increases. Further, comparing figure 4.16, figure 4.18 and figure 4.19 it can be seen that with the increasing number of clusters the symmetry compared to the free-size results introduced at the start of the results section is lost.

Stress Clustering for 4 thickness clusters.
For the stress clustering, the number of allowed clusters is varied between 1, 4, and 16. The primary objective of stress clustering is to achieve a more uniform distribution within the thickness clusters by accounting for stress variations.

Figure 4.20 shows the stress clustering results per ply orientation for the case with a single allowed stress cluster. For the 0 and 90 orientations, the thickest regions are correctly identified compared to figure 4.13, figure 4.15 and assigned in critical areas, ensuring adequate reinforcement where it is most needed. However, for the 45 orientation, the limited number of stress clusters prevents the algorithm from accurately following the thickness distribution seen in figure 4.14. As a result, the necessary number of layers cannot be effectively assigned to crucial locations, leading to suboptimal representation of the stress distribution in this orientation.

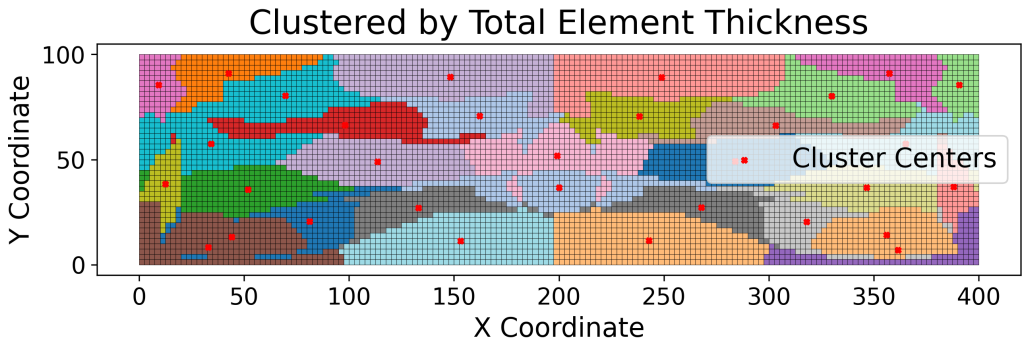

Figure 4.19: Thickness clustering number of cluster 32.

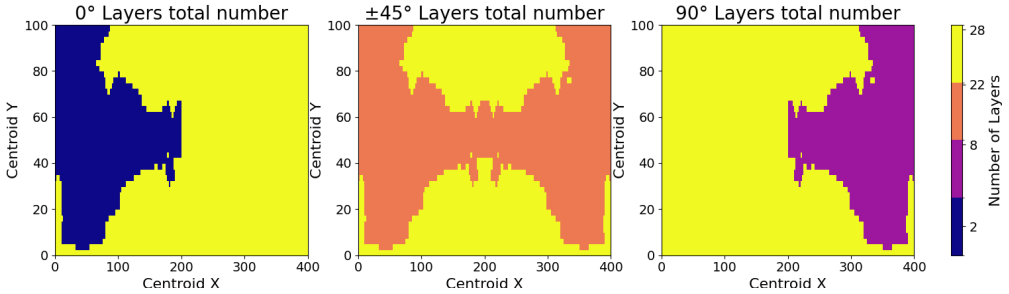

Figure 4.20: 4 thickness clusters and 1 thickness clusters allowed.

In figure 4.21 the 4 stress clusters allowed per orientation. In the case of 0 degree orientation the lower left corner the layer assignment assign a low number of 0 layers. Furthermore, $90°$ degree orientation the layer assignment the middle section have less layers, which compared to the original free-size result shows mismatch. The $\pm 45°$ orientations show minimal improvement, however the load path shows a diagonal direction from the middle section of the plate to the bottom corners noticeable in figure 4.14.

In figure 4.22 the 16 stress clusters allowed per orientation can be seen. Firstly it can be observed that the symmetry for all of the orientation are lost compared to the thickness clustering results. Furthermore, the rogue elements are still present due to clustering. The rogue elements in figure 4.22 can be identified the by singular different color elements in the middle of another section.

4.3.3. Stress Clustering for 16 and 32 thickness clusters.

The result for 16 and 32 thickness cluster will be discussed together. In figure 4.23 the 32 thickness cluster and 1 allowed stress cluster case can be seen. The results for 16 thickness clusters and 1 stress cluster can be seen in figure 4.24. Comparing the two figures 4.23 and 4.24 it can be seen that for 1 allowed stress cluster the resulting layer distribution will be different. However, comparing later clustered design the resulting distribution after clustering converges to a similar result at higher number of stress clusters. This can be seen in figure 4.25 and figure 4.26.

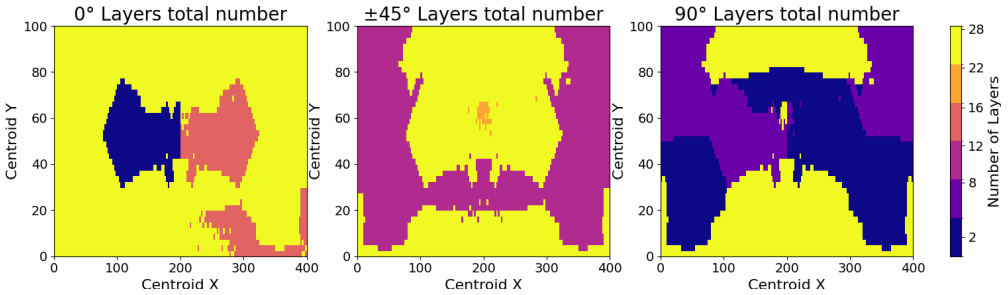

Figure 4.21: 4 thickness clusters and 4 thickness clusters allowed.

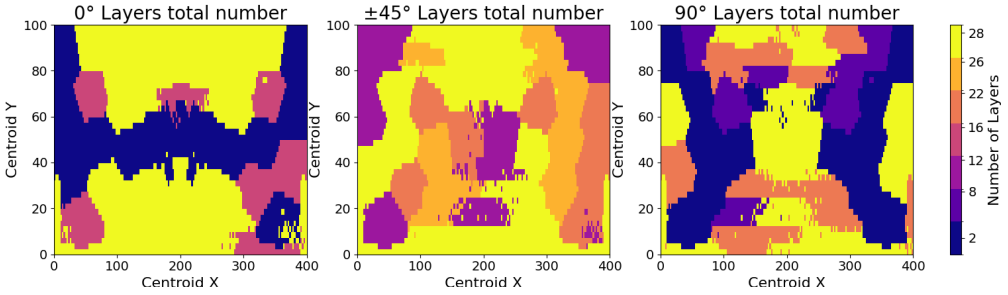

Figure 4.22: 4 thickness clusters and 16 thickness clusters allowed.

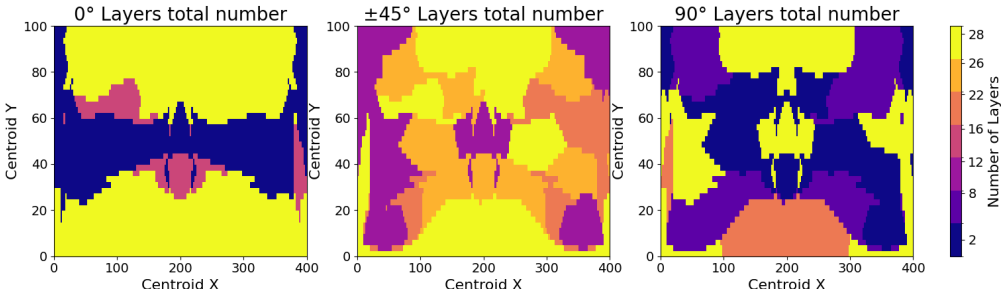

Figure 4.23: 32 thickness clusters and 1 thickness clusters allowed.

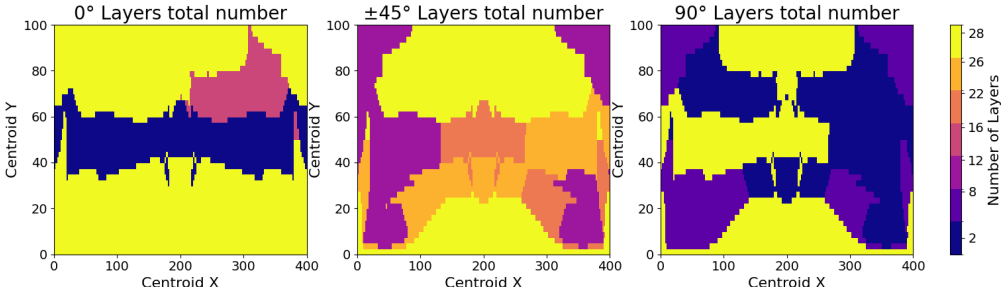

Figure 4.24: 16 thickness clusters and 1 thickness clusters allowed.

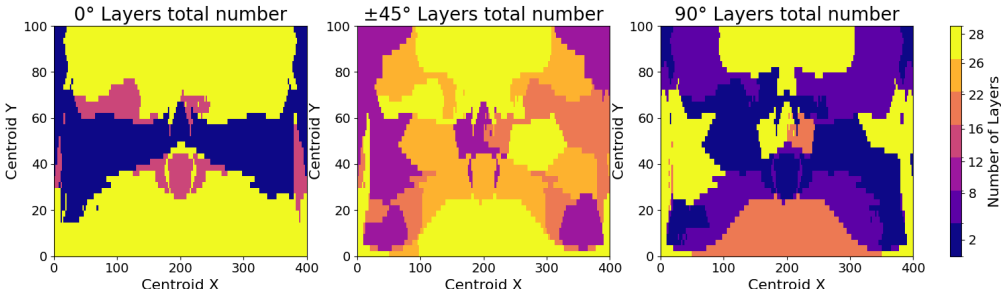

Figure 4.25: 32 thickness clusters and 4 thickness clusters allowed.

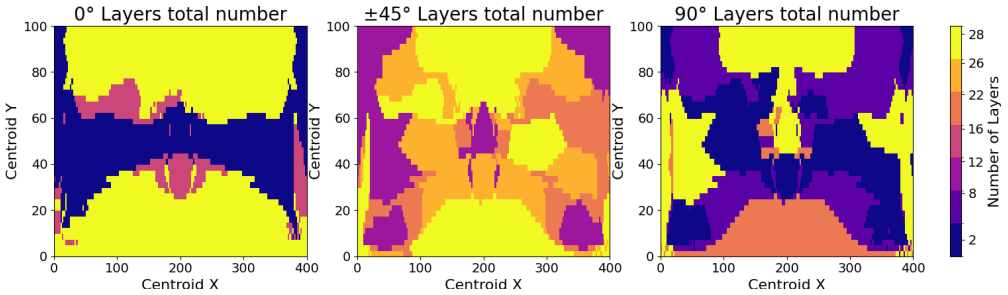

Figure 4.26: 32 thickness clusters and 16 thickness clusters allowed.

Stress Clustering 10000 elements.

In the previous subsection the presented results are with finite element mesh of 5000 elements. The number of element was chosen after a convergence study of free-size optimization. However, after analyzing the initial results and the presented problems such as the rogue elements and difficulty of the stress clustering algorithm to follow the load path a finite element mesh with increased number of elements has been generated. The finer finite element model has a total 10000 quadratic elements. In figure 4.27 the case for 4 thickness and 4 allowed stress clusters can be seen. The rogue elements do not disappear, which indicates that simply increasing the number of elements does not help for better division of thickness clusters. As previously mentioned the anisotropic distribution indicates that more research is necessary and additional refinement for the stress clustering algorithm. The loss of symmetry that has been shown previously also occurs in the case of finer mesh. Meaning a simple refinement of mesh does not result in the stress clustering algorithm performing better. The assumption of the choice of dominating direction and therefore choosing the elements for the clusters needs revision for future research especially regarding taking into account the anisotropic layup of the elements.

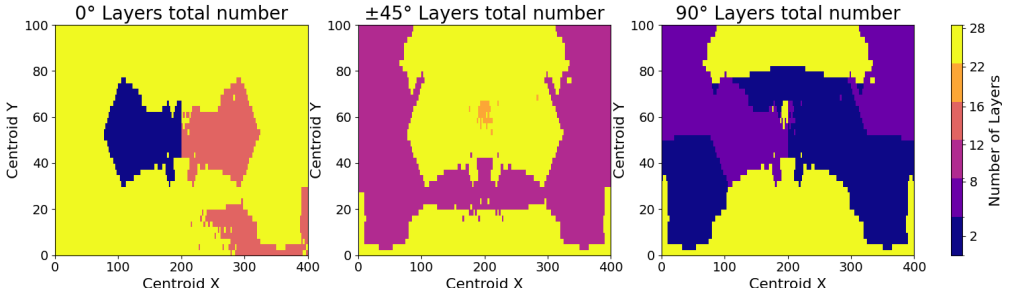

((a)) Stress clustered per orientation 4 thickness 4 allowed stress.

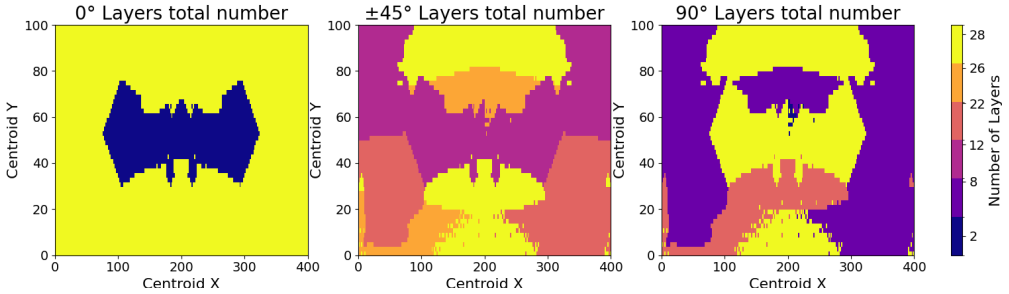

((b)) Stress clustered per orientation finer mesh 4 thickness 4 allowed stress.

Figure 4.27: Stress clustered per orientation starting mesh vs finer mesh.

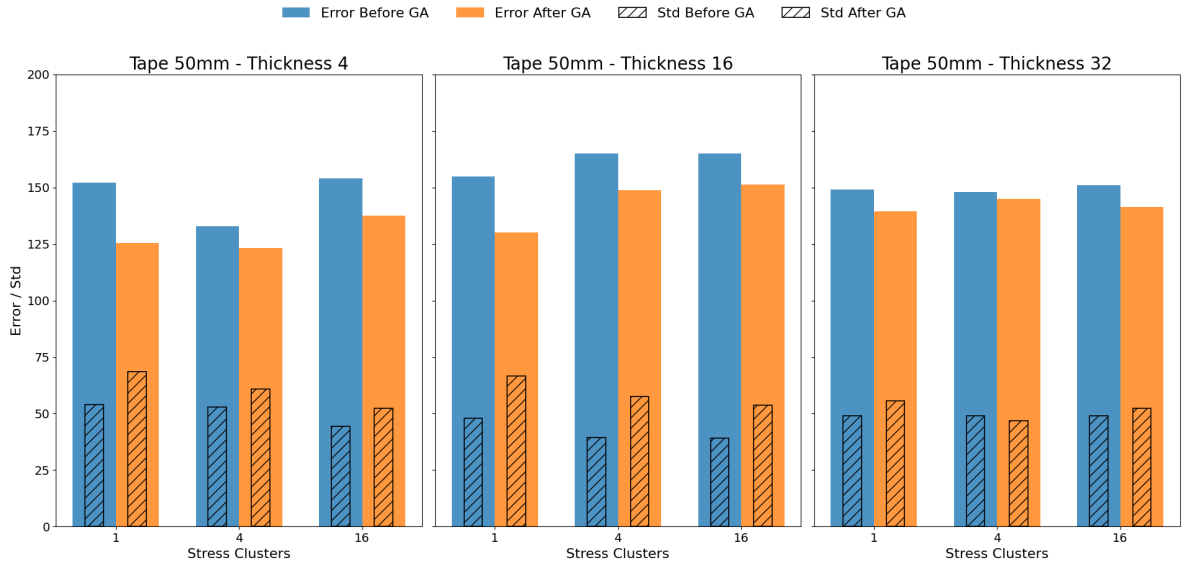

Figure 4.28: Error and standard deviation comparison for varying number of thickness and stress clusters for $50mm$tape.

4.3.4. Error distribution for thickness and stress variation.

In this section, the results of applying the genetic algorithm to the thickness and stress cluster test cases are presented. The evaluation focuses on how effectively the algorithm reduces error, how clustering influences the outcomes, and how manufacturing constraints—specifically tape width—affect the results. The primary metrics for comparison are the reduction in average error, the change in standard deviation and the variation in the number of elements exhibiting maximum error.

The first set of test cases considers a 50 mm tape width, with variations in thickness and stress clustering, as summarized in Table 4.7. The high value of error distribution does not mean that the elements are a 100% meaning the stacking order as an example has double the amount of layers. In the error calculation method $SMAPE$ the denominator has $\frac{1}{2}$ fraction in the formula that changes the overall scale to $0 - 200\%$

Before the application of the genetic algorithm, it is observed that the overall error mismatch increases slightly with an increasing number of clusters. This minimal increase can be attributed to the relatively large 50 mm tape width, which limits the resolution of the manufacturing process and thereby constrains the potential for significant improvement through clustering alone. However, in the case of four thickness clusters combined with four allowed stress clusters, the initial error is noticeably smaller compared to the other 50 mm test cases. This can be explained by the alignment between the clustered design and the manufacturing mesh at this particular configuration, which allows for a better match between design intent and manufacturing geometry. However in the case of 32 thickness clusters the error is lower than 16 thickness clusters. The change in error can be seen in figure 4.28. In figure 4.28 the error and standard deviations can be seen before and after the optimization has been applied.Furthermore, figure 4.28 contains information regarding different thickness and stress clustering number as well. The number thickness cluster can be on the top of the sub-figures and the number of allowed stress clusters on the bottom axis in sub-figures. In figure 4.28 it can be seen that for most cases the overall standard deviation increases, which is due to an increase in the number of larger error elements. Furthermore, the overall error after the genetic algorithm has been applied shows a decrease.

After applying the genetic algorithm, the error percentage for all 50 mm cases is successfully reduced. Nevertheless, this improvement is accompanied by an overall increase in the standard deviation, due the reduction of high error elements and increase in low error elements. To illustrate how the distribution of error changes, two representative examples are presented in the following discussion.

Table 4.7: Error Results with 50mm tape width.

Configuration	Error and Standard deviation before GA	Error and Standard deviation after GA
4 thickness 1 stress cluster	error:152% std:53.88	error:125.59% std:68.67
4 thickness 4 stress cluster	error:133% std:52.98	error:123.24% std:60.73
4 thickness 16 stress cluster	error:154% std:44.4	error:137.53% std:52.36
16 thickness 1 stress cluster	error:155% std:48.04	error:130.02% std:66.75
16 thickness 4 stress cluster	error:165% std:39.39	error:148.83% std:57.64
16 thickness 16 stress cluster	error:165% std:39.01	error:151.35% std:53.75
32 thickness 1 stress cluster	error:149% std:48.94	error:139.48% std:55.52
32 thickness 4 stress cluster	error:148% std:49.14	error:145.02% std:46.71
32 thickness 16 stress cluster	error:150.99% std:48.98	error:141.38% std:52.35

In figure 4.29 and figure 4.30 the 4 thickness cluster and 1 stress clustered allowed can be seen. The first thing to observe is the reduction in the amount of high error elements. Throughout all cases the trend of reducing error is recurring for element numbers. Due to the large tape width dimension the resolution of manufacturing is quite small and for all orientations it can not follow the clustered dimension that well. Furthermore, it can be observed that in the error graph the shape of light blue elements, which are outside the standard deviation correspond to the high error elements and the shape correspond to the out line of the stress clustered elements. In figure 4.29 and figure 4.20 it can be observed that the middle section of the beam and the high error elements are the same.

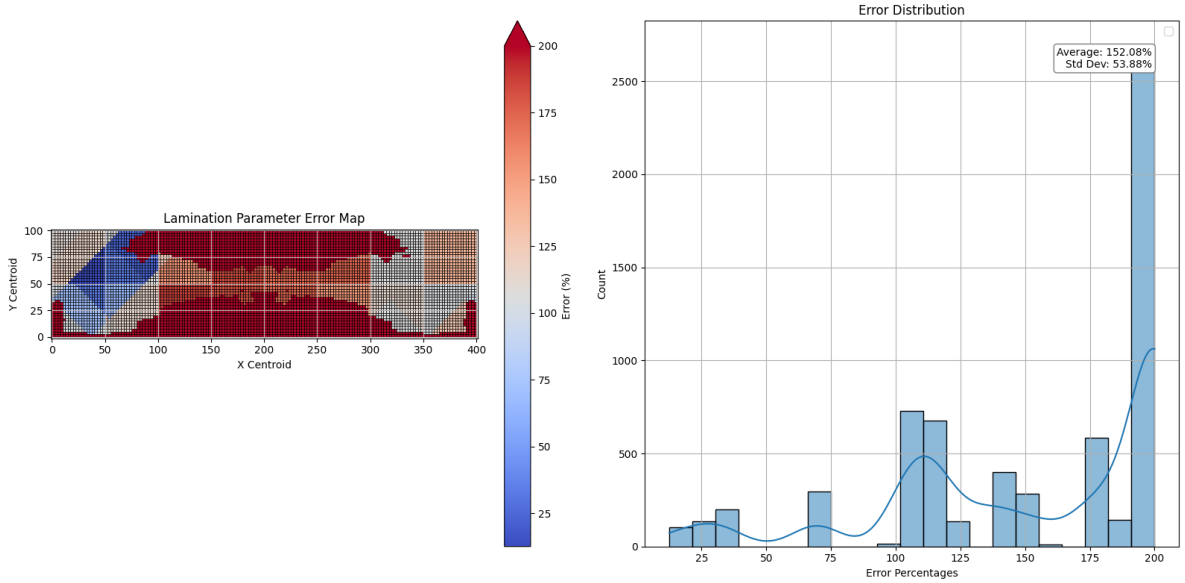

Figure 4.29: Error distribution before GA optimization 4 thickness and 1 stress cluster 50mm tape.

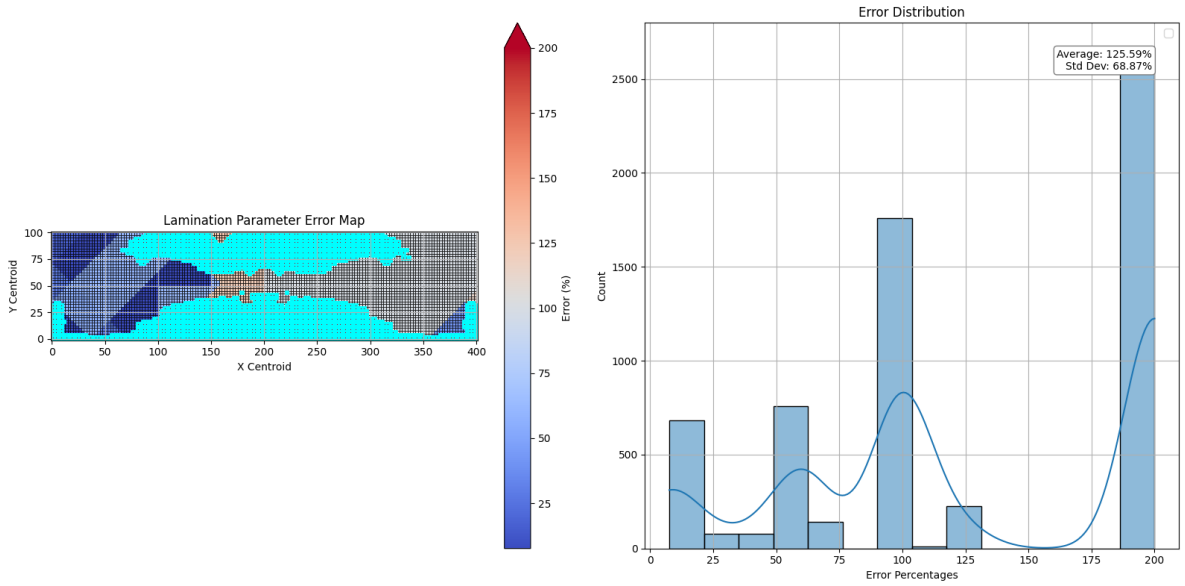

Figure 4.30: Error distribution after GA optimization 4 thickness and 1 stress cluster $50mm$ tape.

The thickness cluster and stress cluster variation was also performed for $25mm$ tape width. The previously mentioned change in error distribution, where the distribution changes in an favorably can be observed for the $25mm$ case as well. Therefore, the figure can be seen in appendix C. However, table 4.8 shows the resulting error and standard deviation. Figure 4.31 shows the error and standard deviation for different cluster configurations. The results show that the final error similarly to the 50mm case occurs at the lowest cluster numbers. Furthermore, the standard deviation increases less for the 25mm after the genetic algorithm. One thing to note comparing figure 4.28 and figure 4.31 that the starting and final error for some cases such as the 16 are close to the 32 thickness clusters at higher number of allowed stress clusters. The closeness of the result can be explained with the similar number of final number of clusters at the end of the clustering.

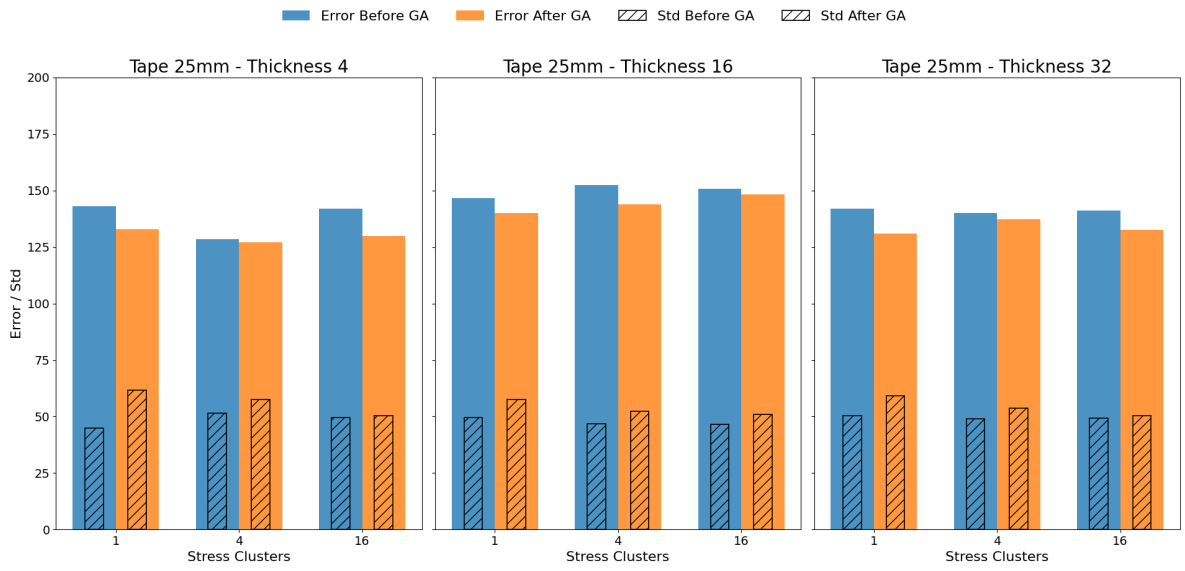

Figure 4.31: Error and standard deviation comparison for varying number of thickness and stress clusters for $25mm$ tape.

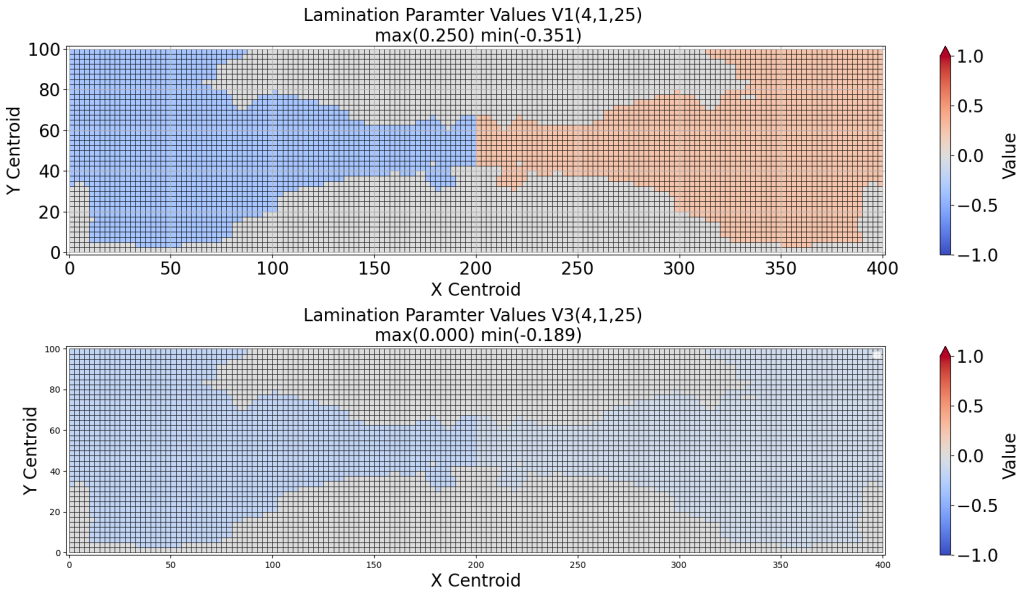

Figure 4.32: Finite element model lamination parameter distribution for V1 and V3 in 4 thickness clusters and 1 stress clusters allowed.

Previously it was shown that there is a large parts of element, where the error is high. Compared to the initial results, where the error was much lower. The main difference between the MBB beam and the initial results are the inclusion of $\pm 45^{\circ}$ orientation patches. In figure 4.32 the finite element lamination parameter distribution can be seen for 4 thickness clusters and 1 allowed stress cluster. The lamination parameter distribution graphs were only generated for the 25 mm tape width cases. The conversion to the manufacturing geometry a similar graph can be created, the model has a patch distribution called patch-wise model. In figure 4.33 the patch-wise's model lamination parameter distribution can be seen before optimization. The figure furthermore shows the minimum and maximum values of the lamination parameters under the sub-figure title. In figure 4.33 the maximum values is 1, which indicates that some of the locations do not contain $\pm 45^{\circ}$. The lack of $\pm 45^{\circ}$ indicates that one of the self-written functions need revision namely the stacking order retrieval function. The retrieval function checks the patch overlap with finite element model and based on overlap builds a stacking order for comparison with the finite element's stacking order. For a small amount of elements less than 10% of the total number elements the stacking order function does not correctly retrieve the $\pm 45^{\circ}$ showing the complexity of including them in the patch-wise model. Therefore, for future work the stacking order retrieval model needs revision. The retrieval function is one of the reasons for the high error. A further complexity for the high error element is that after the optimization some of the $\pm 45^{\circ}$ patches get deleted. in figure 4.34 the lamination distribution can be seen after genetic algorithm optimization. Due to some of the $\pm 45^{\circ}$ patches are deleted during the optimization, which can be seen some regions changing on V3 lamination parameter. However certain areas for lamination parameters V3 the optimizer adds more layers to the patches resulting in better match in the stacking order. The mentioned behavior of changing the layer number for the $\pm 45^{\circ}$ orientation during the optimization is observed for all cases. The rest of the lamination parameter distribution can be seen in the appendix D.

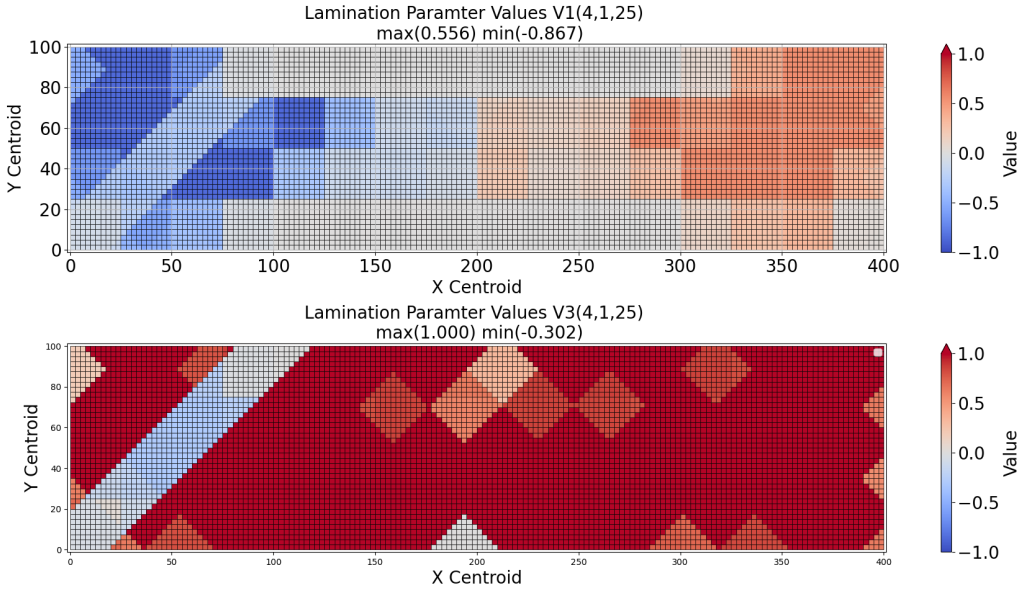

Figure 4.33: Patch-wise model lamination parameter distribution for V1 and V3 in 4 thickness clusters and 1 stress clusters allowed before optimization.

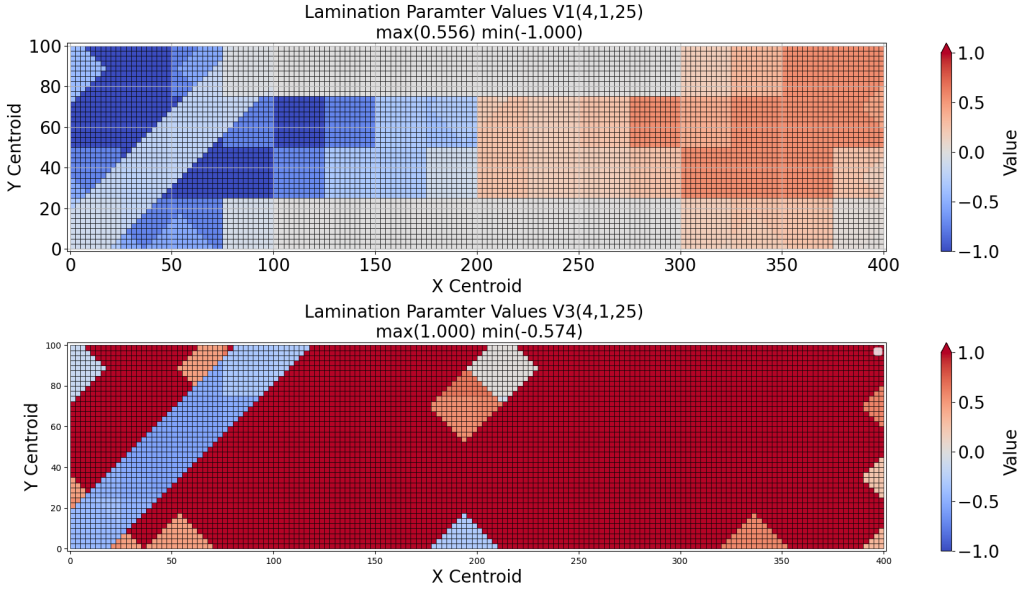

Figure 4.34: Patch-wise model lamination parameter distribution for V1 and V3 in 4 thickness clusters and 1 stress clusters allowed after optimization.

Table 4.8: Error Results with 25mm tape width.

Configuration	Error and Standard deviation before GA	Error and Standard deviation after GA
4 thickness 1 stress cluster	error:143% std:44.8	error:133% std:61.67
4 thickness 4 stress cluster	error:128.42% std:51.64	error:127.07% std:57.64
4 thickness 16 stress cluster	error:141.9% std:51.04	error:129.86% std:50.39
16 thickness 1 stress cluster	error:146.59% std:49.57	error:140% std:57.45
16 thickness 4 stress cluster	error:152.36% std:46.84	error:143.92% std:52.24
16 thickness 16 stress cluster	error:150.74% std:46.6	error:148.2% std:50.89
32 thickness 1 stress cluster	error:142% std:50.32	error:130.87% std:59.24
32 thickness 4 stress cluster	error:140% std:48.98	error:137.19% std:53.79
32 thickness 16 stress cluster	error:141.04.99% std:49.24	error:132.94% std:50.278

4.3.5. MBB Beam tape width influence comparison

In this section the different tape geometries and the performance of the genetic algorithm will be evaluated. First the 25mm tape width will be shown with the similar test cases as the thickness and stress clustering variation. Secondly a comparison will be shown with 50mm and 10mm show case to summarize the findings and overall performance of the genetic algorithm on the patch wise definition and optimization.

In table 4.8 the results of the genetic algorithm optimization using 25mm tape width are shown. The first thing to observe that the error percentage before the optimization using a genetic algorithm is lower for the 50mm tape width cases. The change in tape width results in a decrease of starting error of approximately 10% across all configurations. Furthermore, after applying the genetic algorithm the final resulting error percentages of the design are lower then 50mm case. In the case 50mm the resulting error percentage after the GA application has shown that for larger cluster number the GA could not lower the error percentage significantly. However, in the case of 25mm for larger cluster numbers the recovery percentage does not show the same behavior. The standard deviation for 25mm after GA application show similar behaviour to the 50mm tape width. However, in the case 25mm the error distribution show more change. In figure 4.36 and 4.37 the error distribution can be seen for 4 thickness and 16 allowed stress cluster with 25mm tape width.In table 4.9 the resulting errors with the use of 10 mm tape width can be seen. The smaller tape compared to larger sizes such as 25 and 50 produces a smaller error. The smaller is expected due to the conversion producing a higher resolution geometry.

Figure 4.35 shows a comparison of tape widths of 10, 25, and 50 mm, illustrating both the error and standard deviation. The errors before optimization are highlighted with a thicker border line. Based on these results, one conclusion is that smaller tape widths lead to a closer match with the input. Furthermore, the error after optimization varies with tape width, reaching a minimum at the 10 mm tape. In the case of the 10 mm tape, the standard deviation is the only instance where it does not increase significantly, likely due to the finer resolution provided by the smaller tape width.

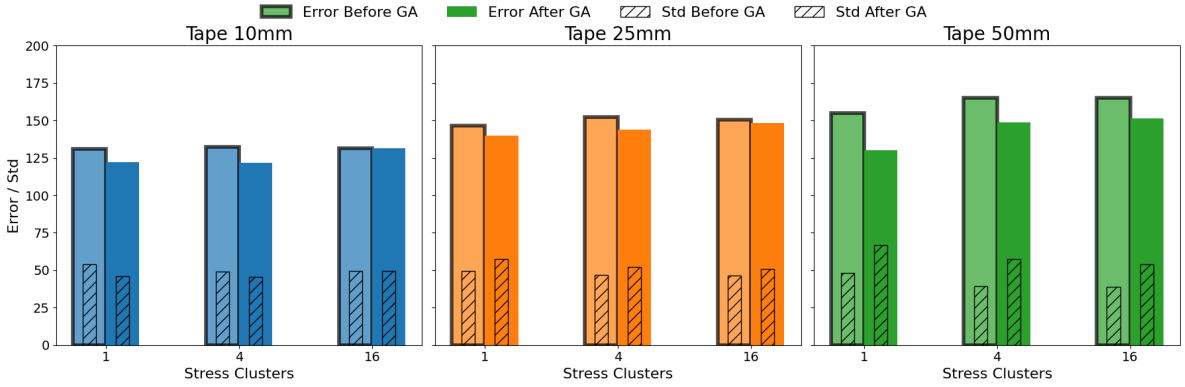

Figure 4.35: Tape width comparison for error and standard deviation before and after the optimization in the case of 16 thickness clusters.

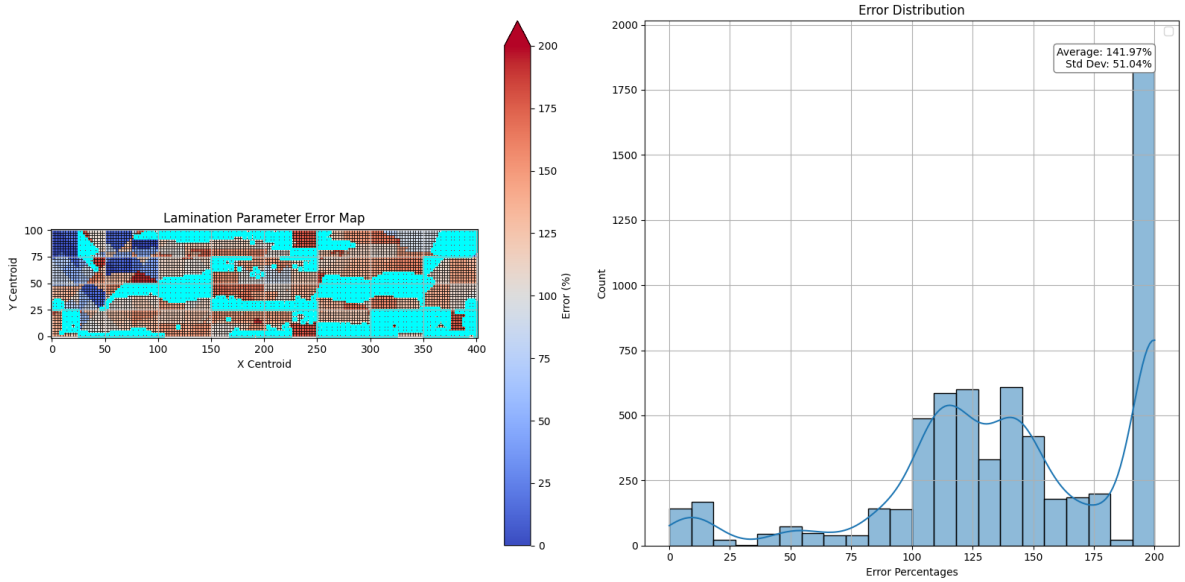

Figure 4.36: Error distribution before GA application 4 thickness 16 stress cluster tape width 25mm.

Table 4.9: Error Results with 10mm tape width.

Configuration	**Error and Standard deviation before GA**	**Error and Standard deviation after GA**
16 thickness and 1 stress cluster	error 131% std 53.39	error 122% std 46.08
16 thickness and 4 stress cluster	error 132.37% std 49.24	error 121.61% std 45.44
16 thickness and 16 stress cluster	error 131.36% std 49.52	error 131.36% std 49.52

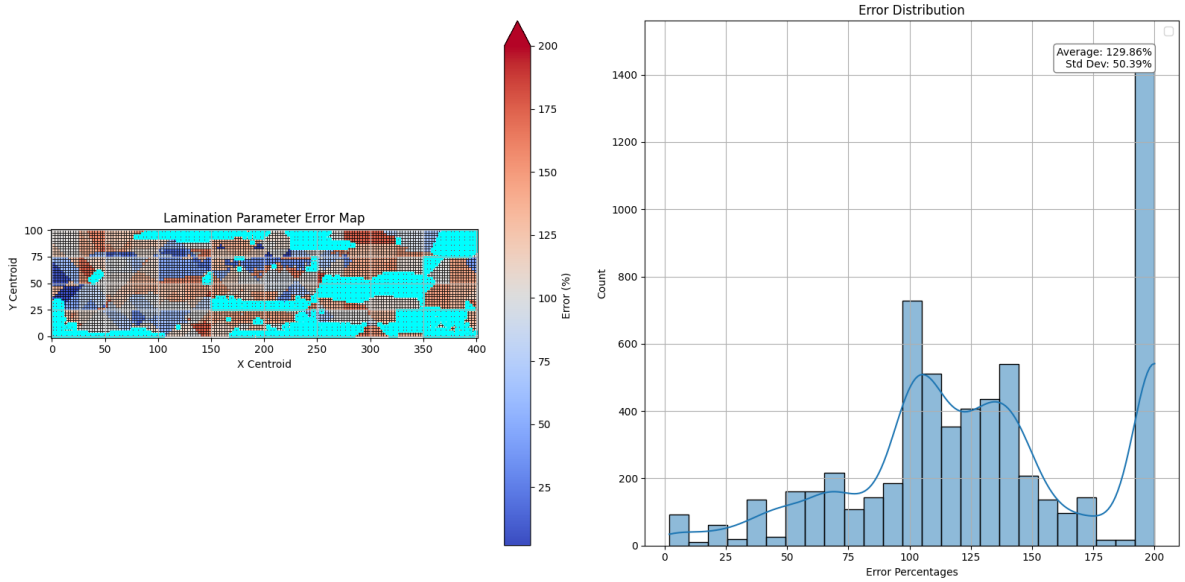

Figure 4.37: Error distribution after GA application 4 thickness 16 stress cluster tape width 25mm.

4.3.6. Manufacturing weight and time results

In this section the optimized and input patch wise geometries are compared. The manufacturing time is simply estimated in equation 4.1.

$$\textbf{Manufacturing time} = \frac{\textbf{Print Length}}{\textbf{Print Speed}} \tag{4.1}$$

, where **Print Length** is the sum all segments length that needs to be printed and **Print Speed** is the tape laying specified. The manufacturing weight is defined in equation 4.2.

$$\textbf{Manufacturing Weight} = \sum \textbf{Segment Volumes} \cdot \textbf{Ply Density} \tag{4.2}$$

Since, the resulting thickness increases significantly due the poor performance of the genetic algorithm the resulting manufacturing time and weight changes significantly as well. The resulting weight change and manufacturing time can be seen in figure 4.38.

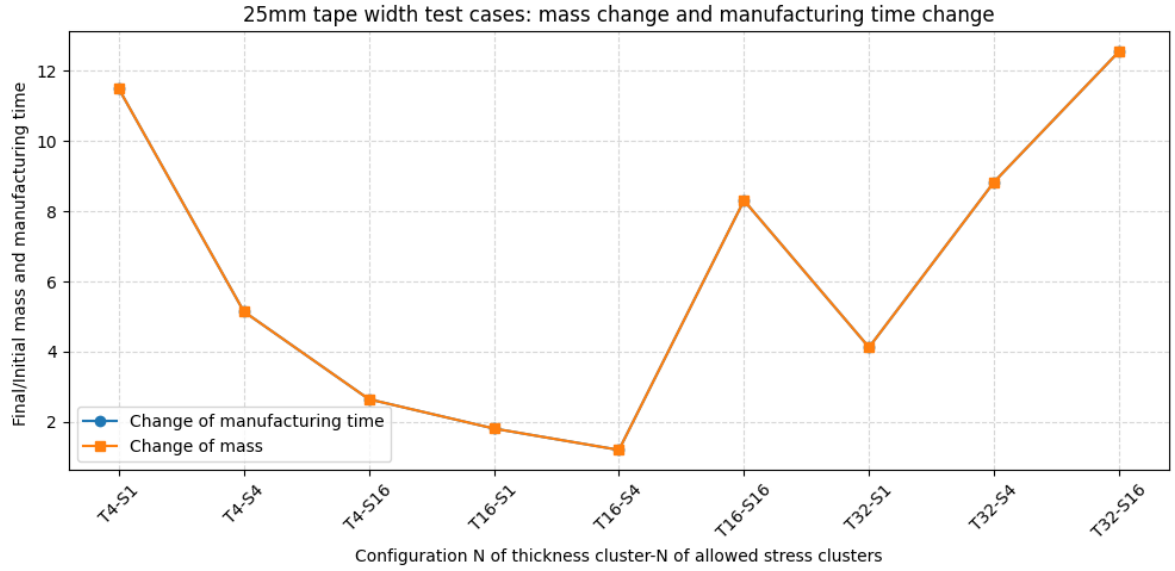

Figure 4.38: Change in mass and manufacturing time 25mm tape width.

In figure 4.38, where the horizontal edge shows the different configuration of the test cases. As an example $T16-S1$ corresponds to the test case of 16 thickness clusters and 1 allowed stress cluster. The vertical axis shows $\frac{Final}{Initial}$ mass. In figure 4.38 it can be seen that the change in mass and manufacturing time is similar in magnitude and substantial in change. Since, the change of mass and manufacturing time is correlated the number of segment the change in both parameters overlap in the graph similarly in figure 4.39. In figure 4.39 the change of manufacturing time and mass can be seen for 50mm cases. Comparing the cases for 25 and 50 mm it can be seen that the results vary large depending on the geometry definition from thickness and stress clusters. The variation validates the assumption that the genetic algorithm is struggling to converge to solution, which is close to the original input in terms of weight.

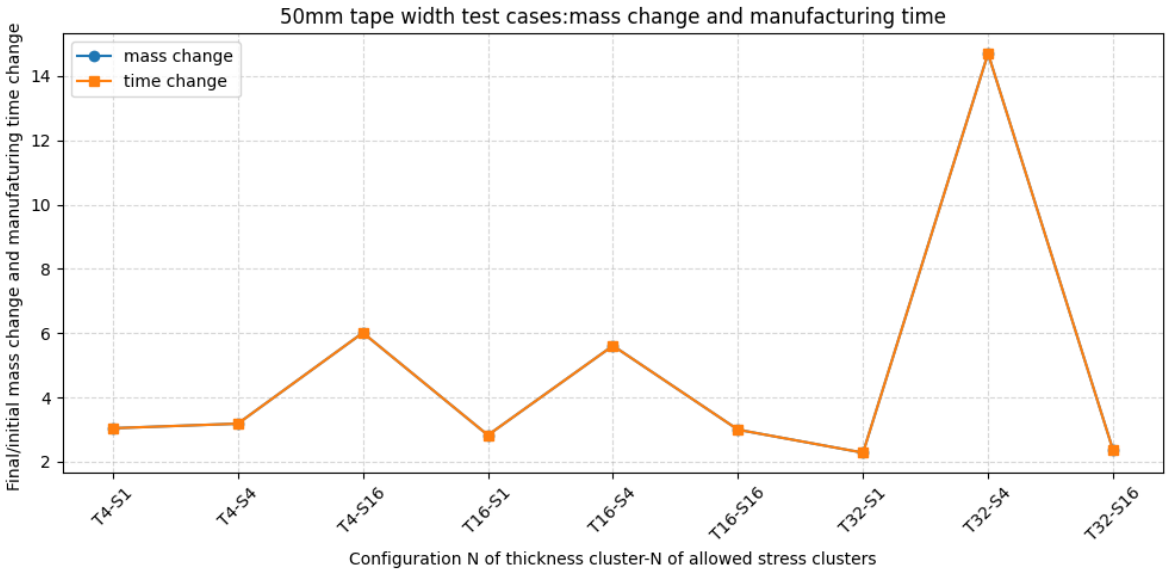

Figure 4.39: Change in mass and manufacturing time 50mm tape width.

The final error indicates success of the optimization method using patch wise definition using a genetic algorithm as the optimization method as well as using the lamination parameters in the error and fitness function. However, the final weight indicates that the genetic algorithm converges to a wrong solution. There are three reasons for the observed behavior in the optimization. The first reason is the use of lamination parameter in the error calculation. The lamination parameters are normalized to the total thickness during the calculation in equation 3.9 and equation 3.10. The use of normalized lamination parameters causes the optimization process to no penalize heavy designs. The lack of penalization in the error and fitness function do not filter out designs such as the ones shown in the staking order illustration 4.3. The stacking orders shown would show minimal difference in terms of error during the optimization process, however the resulting thickness could be even double after the genetic algorithm optimization.

$$\begin{aligned} \text{Staking order 1 in finite element model} &= [0/90/+45/-45]_s \\ \text{Stacking order 2 result after optimization} &= [0_2/90_2/45_2/-45_2]_s \end{aligned} \tag{4.3}$$

The second reason for the optimization towards a wrong optimization is the lack of large enough population. All test cases were ran with a population size of 50, which paired with a genetic string of 30 length could be enough. However genetic algorithm with small population could converge towards a solution which satisfies the fitness but overall is meaningless in reality. However the small population size should be not the case. In the initial stages of the methodology development only $0°$ and $90°$ orientation were used. The resulting designs after the genetic algorithm has been applied were a solution lighter than the input patch wise design. The observation of the difference between the quasi isotropic and orthotropic layup brings forwards the last reason for the behavior of the genetic algorithm.

The third reason is the patch wise definition of the geometry. For the manufacturing mesh and the patch wise model only containing orientation $0°$ and $90°$ orientation definition is uniform in terms of elements. Since the manufacturing only differs on the segment definition due to the orientation difference. However, the addition $\pm 45°$ orientations increases the complexity and without introducing additional complexity to the optimization process the converged results is not realistic and too heavy to be a viable option.

Methods and steps to mitigate explore validation processes for the convergence of the optimization method is discussed in more detail in a later future recommendations chapter 6.

5

Conclusion

This chapter provides the overall research findings of the thesis. The goal of the thesis was to deliver a start to end automatic design methodology for variable thickness laminates. The aerospace industry is on the hunt for new lighter structures making use of innovative design and materials. Interior products of aeroplanes, such as seating galley inserts lavatory panels are not primary load carrying structures. Traditionally aerospace structure are made of constant thickness laminates. VSL laminates allow to tailor the stiffness of product as well as decrease the overall weight. Modern manufacturing methods for thermoplastic composites such as ATP and AFP allow to make use of the benefits of VSL laminates. The traditional design methodology even using Altair Hyperworks requires manual input from an experienced designer. Therefore the aim of the thesis is to deliver and automatic design methodology and interpret the drawback and possible improvement points. For a reminder the research objective and research question are shown once more:

> The objective of this research is to develop a methodology ensuring manufacturability and suitability for automated methods by using an optimized variable thickness design processed through an algorithm to generate a patch divided straight fiber variable thickness laminate.

- How to systematically define zones on the geometry based on provided input parameters from a free-size optimization?
- Which algorithms can be used for optimization of the design ensuring automated manufacturing processes can be applied?
- What is the performance of the developed algorithm applied on a beam?
- What is the future development path for full scale application on aerospace structures of the methodology?

Research Objective and Research Question 1

The thesis has shown a four step methodology capable of translating an optimized design taking into account manufacturing geometry for automated tape laying. Firstly, the methodology shows a systematic way to define zones and make the zone uniform based on principal stresses. The initial zone definition uses a k-means clustering algorithm and shows initial promise. However the large variability over the whole geometry of the total element thickness causes the clustering algorithm to lose symmetry compared the free-size optimized result. The second level clustering based on principal stresses assign further zone division to the thickness clustered design and shows a similar behavior to the thickness clustering. In conclusion the two-level clustering shows promise in terms of automatically define zones and assign element to the zone to produce a more homogeneous design. However, during the clustering the final thickness shows the loss of symmetry compared to a symmetrical output from free-size optimization. The loss of symmetry is most likely causality of a setting in the clustering algorithm. Further research is needed to fully explore the capabilities and drawbacks of the clustering algorithms applied for the two-level clustering due to the complexity of the choosing elements.

Research Question 2&3
For the optimization of the patches a genetic algorithm was chosen due to the capability to handle discrete variables. In the optimization process the genetic algorithm changes the layer information of the patches, which take up discrete values. The algorithm shows promise in terms of minimizing error. However, investigation of the result in terms of final weight showed a large increase of multiple folds. The final weight increase is due to the use SMAPE method and the normalized lamination parameters. This does not indicate that the application of genetic algorithm is not suitable. The variability of number clusters and tape width dimension has shown that the genetic algorithm performs better with less intricate design in terms of thickness variation and complexity of the design problem. Further refinement is needed in the application optimization problem.

Research Question 4
The application of the methodology has been shown on an MBB beam. The thesis succeeded of delivering a self-developed algorithm capable of taking an optimized design and translating it into geometry suitable for automated process. However, at sub-steps areas has been identified for further development. At particular the future development can be categorized into pre-manufacturing geometry and post conversion to manufacturing geometry. The pre-manufacturing geometry need to focus on better zone division and improving the zone uniform in terms of layup. The post conversion in the development path has been shown method to use different model information to use during the optimization such as the use of A matrix. A more detailed explanation for research question can be in chapter 6.

In conclusion the thesis successfully laid down the foundation for the methodology to translate a free-size result. The results of thesis furthermore shows areas, where improvement is necessary for future research to scale the methodology for full scale use.

6

Future Recommendations

In this section, the prospective development path of the methodology is outlined. The aim is to identify key areas that offer significant potential for further investigation and refinement, thereby establishing a foundation for future research. These areas include zone and clustering definition, stress clustering and zone element unionizing, patch conversion and optimization, and post-processing with the introduction of additional manufacturing constraints.

The first area focuses on improving the definition of zones by developing more robust criteria based on the total thickness distribution, with the goal of enhancing both the accuracy and the structural relevance of the clustering.

The second area addresses potential enhancements to stress clustering, including alternative approaches for achieving more uniform zones and strategies for merging elements within zones to improve continuity and manufacturability.

The third area involves possible modifications to the optimization process itself, as well as the integration of new features that could expand the design space and improve the quality of the resulting patches.

Finally, the last area explores future steps in post-processing, with an emphasis on incorporating additional manufacturing constraints and developing tools to translate the optimized geometry into manufacturable components that account for real-world parameters and the practical limitations of automated manufacturing methods.

6.0.1. Clustering and Zone definition:

In the previous section, it was shown that the applied clustering algorithm has difficulty in defining zones, as evidenced by the presence of rogue elements. One potential approach to enhance the performance of the k-means clustering algorithm is the use of a multi-level clustering strategy. This necessity arises from the fact that factors such as data shape, spatial distribution of data points, and value similarity can negatively impact clustering performance [32].

The concept of tri-level clustering compared to general clustering differs in terms of clustering definition. In general clustering the data grouping happens in a single step. The thesis used general clustering done in a single step. Tri-level clustering on the other hand performs the division in multiple steps. In figure 6.1 the multiple step approach can be seen for tri-level clustering. The data is into general zones after,which the clustering algorithm further refines the zone by clustering only inside the parent cluster. Figure 6.1 illustrates this through sub-figure (a, b, c). In the thesis during the initial zone division based on total element thickness rogue elements were present. By using tri-level clustering better zone division should be possible for more refined initial thickness zones.

However, in the context of zone thickness definition, the closeness of data point values may still contribute to the persistence of rogue elements, even under a multi-level scheme. For this reason, an alternative improvement could be the use of a bi-layer k-means algorithm, which may provide a better

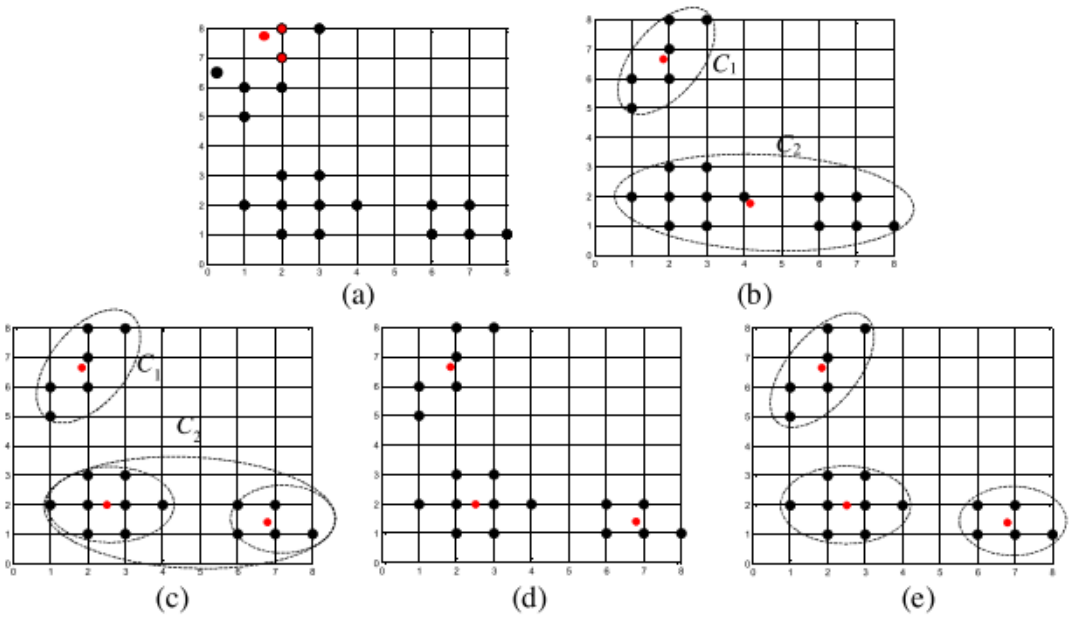

Figure 6.1: The processing of data clustering by tri-level traditional k-means algorithm:(a) the data and initial cluster center used in the first-level cluster stage;(b) the result obtained in the first level cluster stage;(c) the result obtained in the second level cluster stage;(d) the initial clusters used in the final-level cluster stage; and (e) the result obtained in the final-level cluster stage [32].

balance between accuracy and computational efficiency while addressing the limitations of standard clustering in regions with minimal value variation. The biggest benefit of the bi-layer algorithm is the ability to deal with noisy data and outliers, which can be common during the zone definitions.

6.0.2. Stress clustering and making zones uniform

During the methodology it has been shown that while the stress clustering algorithm produces a more uniform thickness distribution. The main assumption of the clustering and methodology lead to a design not following the primary loading path in the most optimal way. Another approach that is worth investigating is directly going from the thickness to defining stacking or per zone to make them uniform. The method uses the fact that free-size optimization provides per cluster element wise information. Per cluster it is then possible to extract distribution of orientation based on that distribution an average can be taken and used for the cluster as the new stacking order to make it uniform. In figure 6.2 an illustration can be seen for orientation distribution for an element, in a case without any balance requirements. Additionally the cluster is represented by the black triangle. The approach for taking the element information could rather focus on the zone shape optimization and aim for dividing the geometry into uniform thickness zone. The zone shape would directly influence, which elements belong to the zone and the final orientation distribution.

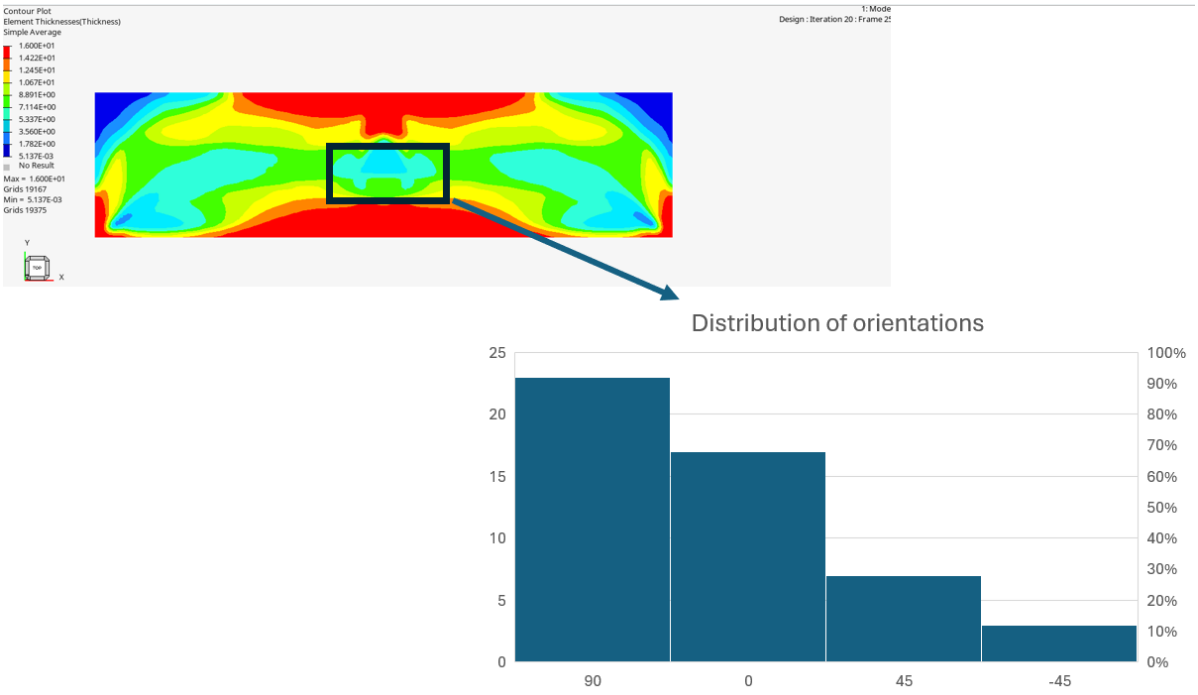

Figure 6.2: Orientation Illustration for zone inside the area of black rectangle.

6.0.3. Optimization and conversion to manufacturing geometry

In its current form, the implemented genetic algorithm operates by modifying only the number of layers within each defined patch. While this approach allows for a reduction in the discrepancy between the intended structural design and the geometry required for manufacturing, the extent of this error reduction remains limited by the simplicity of the method. A substantial improvement in performance could be achieved by increasing the complexity of the optimization procedure, particularly by enabling changes not only in the thickness distribution but also in the spatial arrangement of the segments. In the present formulation, the positions of the segments remain fixed throughout the optimization process. Introducing the ability to relocate these segments, either through translation or reorientation, would allow the algorithm to achieve a closer correspondence between the optimized laminate configuration and the target structural behavior, thereby reducing the residual error.

A further enhancement could be realized by introducing a conceptual separation of the laminate into a base patch and a set of strengthening patches. The base patch would form the fundamental laminate structure and could be manufactured using more efficient, large-scale processes, providing the essential stiffness and strength required for the component. The strengthening patches, by contrast, would be applied selectively in regions where additional reinforcement is necessary. In the context of the genetic algorithm, these strengthening patches could be treated in a manner analogous to the current methodology, with their placement, orientation, and thickness distribution forming the principal design variables. Such a separation would reduce the number of variables in the genetic string, making it possible to incorporate segment relocation without increasing the genetic string length to an impractical degree.

This distinction between base and strengthening patches would also yield benefits from a manufacturing perspective. Since the base laminate would not require precise placement by tape laying, it could be produced more rapidly and cost-effectively. The strengthening patches, requiring greater precision, could then be applied in a subsequent stage of manufacturing. For certain aircraft panel structures, this approach would enable multiple products to share an identical base design, with only the strengthening patches varying according to specific structural demands. For example, in lavatory panels, a common base laminate could be used across the fleet, with reinforcement applied only in regions subjected to higher loads. Similarly, in galley inserts where cabin attendant seating is integrated, strengthening patches could be positioned in the load-bearing regions to provide the additional structural support required by certification standards. In both cases, the combination of increased optimization flexibility and manufacturing efficiency could lead to more versatile and cost-effective design solutions.

Another solution for the conversion and optimization is separating the orientation patches. In the current methodology all of the orientations are under one model during optimization due to the use of lamination parameters. The patches can be separated to just their own orientation. The separated method will need to use other parameters for the optimization process. In the manufacturing mesh generation the number of layers are assigned based on intersection areas according to equation 3.5. Based on this intersection area model an error can be calculated, which shows the patches error number of layers mismatch for the finite element mesh. The same patch wise definition can be used further in the optimization process, however instead of joining the patches are optimized independently.

A further possible improvement to the application of genetic algorithm is using the ABD matrix. During the thesis the main focus was on the in-place parameters therefore the use of A matrix should suffice enough. Due to time limitation the full application of this option was not possible to generate all results, but the option is adapted into the code. The use of A would eliminate the problem of the error calculation for the fitness functions. The use of normalized lamination parameters meant that the error calculation would have to divide values close to 0. Furthermore, the normalization did not show large errors even though two stacking order during comparison could have double the amount layers.

6.0.4. Postprocessing

The current optimization results are not subjected to additional postprocessing steps that account for manufacturing effects beyond the initial geometric constraints. The focus of the present work has been confined primarily to in-plane properties, with out-of-plane bending performance left outside the scope of the investigation. However, for a complete structural design process, both in-plane and bending behavior must be considered, particularly as the latter has a strong influence on stability and buckling

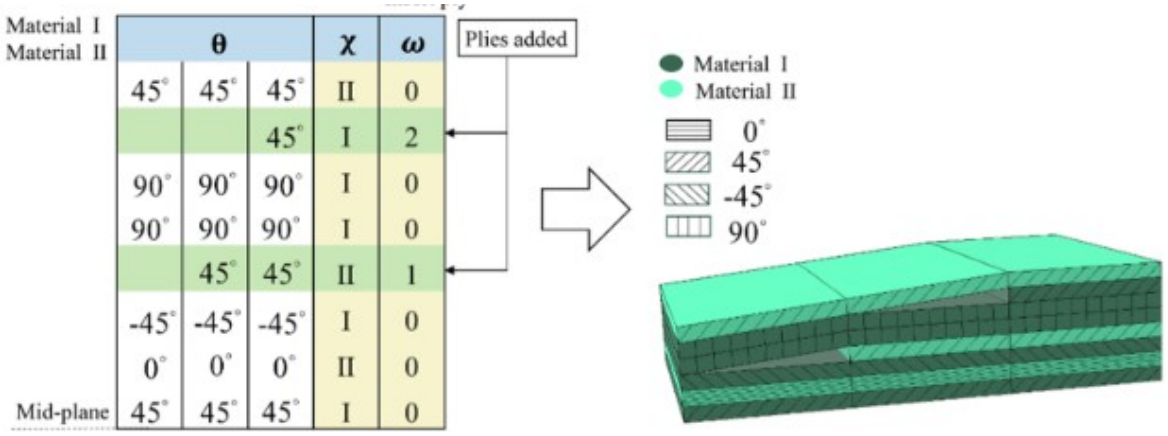

Figure 6.3: Improved stacking sequence table with two ply-drops[19].

resistance. The bending stiffness is governed by the D-component of the laminate ABD matrix, which is sensitive to the stacking sequence of the plies. This implies that an optimized in-plane configuration may still require adjustment to ensure sufficient resistance to out-of-plane loads.

An effective approach to incorporating bending performance considerations would be the use of stacking sequence table (SSt) optimization methods applied after the initial geometry-based optimization stage. In this framework, the manufacturing geometry serves as a sub-panel division, within which the stacking sequence can be refined to improve bending stiffness and buckling performance. Classical SST optimization problems, such as the so-called horseshoe configuration shown in Figure 2.10, illustrate how certain stacking arrangements can lead to undesirable stiffness anisotropy. An improved SST method, as illustrated in Figure 6.3, could be adopted to incorporate ply-drops directly into the stacking definition. This extension would allow the optimization process to target critical buckling factor improvement, as discussed in recent studies [19], while remaining compatible with manufacturing constraints.

A particular challenge lies in adapting the SSt-derived stacking sequences to manufacturing patch definitions, especially for $\pm 45°$ patches, which must conform to the geometric limitations of the manufacturing mesh, as shown in Figure 6.4. Achieving compatibility between the stacking table optimization and the patch-based manufacturing geometry is essential, as it ensures that the theoretical improvements in structural performance remain physically realisable. By integrating these postprocessing steps into the workflow, the methodology could advance from purely in-plane optimization to a more holistic laminate design process, ultimately producing configurations that are both structurally optimal and fully manufacturable. The second area of improvement in post processing is the inclusion of manufacturing defects. During AFP the material is in-situ consolidated. Since the material cools down the presence of gaps and overlaps will change and shrink. Some closure can occur due to this shrinkage and change the gaps and overlaps[3]. Models are available to predict the final gap and overlap location the influence on the mechanical performance can be predicted by defect layer method[8]. The adoption of defect layer method and prediction of gaps of overlap due to manufacturing would take the method proposed further towards full scale start to end method.

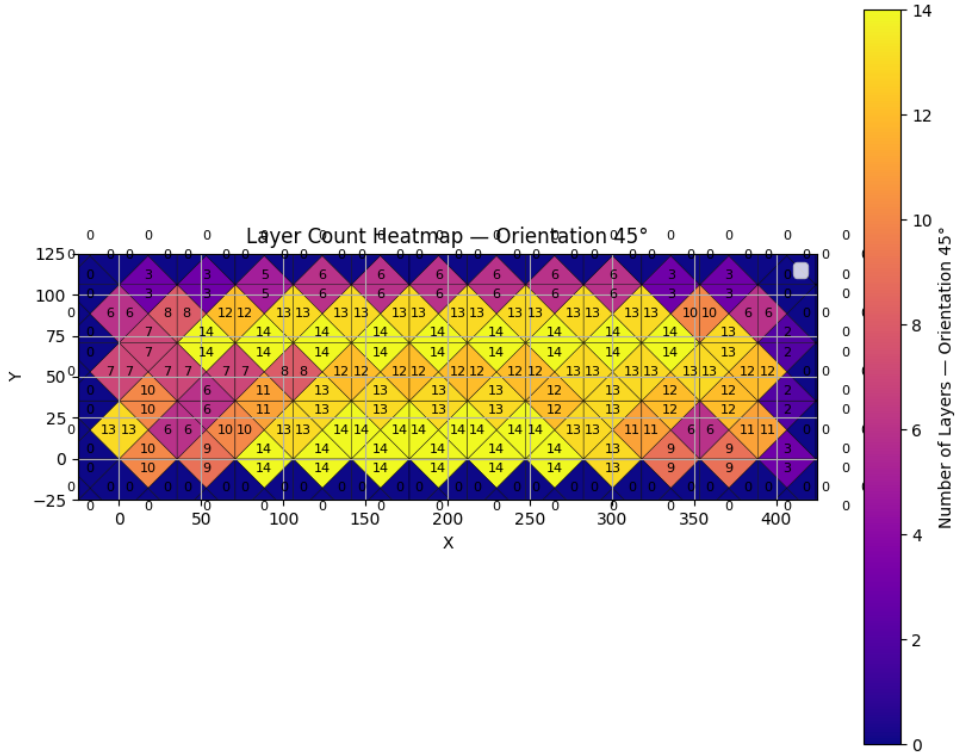

Figure 6.4: Manufacturing mesh $\pm 45^\circ$ patches.

Bibliography

[1] Altair Optistruct. *Composite Topology and Free-size Optimization*. URL: https://help.altair.com/hwsolvers/os/topics/solvers/os/composite_topology_free_size_opt_r.htm.

[2] Altair Optistruct. *Free-size Optimization*. URL: https://2021.help.altair.com/2021/hwsolvers/os/topics/solvers/os/free_size_optimization_intro_r.htm.

[3] Jonathan P.H. Belnoue et al. "Understanding and predicting defect formation in automated fibre placement pre-preg laminates". In: *Composites Part A: Applied Science and Manufacturing* 102 (Nov. 2017), pp. 196–206. ISSN: 1359835X. DOI: 10.1016/j.compositesa.2017.08.008.

[4] Julius Moritz Berges et al. "Methodology for the concept design of locally reinforced composites". In: *Applied Sciences (Switzerland)* 11.16 (Aug. 2021). ISSN: 20763417. DOI: 10.3390/app11167246.

[5] A. J. Comer et al. "Mechanical characterisation of carbon fibre-PEEK manufactured by laser-assisted automated-tape-placement and autoclave". In: *Composites Part A: Applied Science and Manufacturing* 69 (Feb. 2015), pp. 10–20. ISSN: 1359835X. DOI: 10.1016/j.compositesa.2014.10.003.

[6] O. Falcó et al. "Variable-stiffness composite panels: Defect tolerance under in-plane tensile loading". In: *Composites Part A: Applied Science and Manufacturing* 63 (2014), pp. 21–31. ISSN: 1359835X. DOI: 10.1016/j.compositesa.2014.03.022.

[7] Pingchu Fang et al. "Uniform multiple laminates interpolation model and design method for double–double laminates based on multi-material topology optimization". In: *Computer Methods in Applied Mechanics and Engineering* 433 (Jan. 2025). ISSN: 00457825. DOI: 10.1016/j.cma.2024.117492.

[8] Kazem Fayazbakhsh et al. "Defect layer method to capture effect of gaps and overlaps in variable stiffness laminates made by Automated Fiber Placement". In: *Composite Structures* 97 (Mar. 2013), pp. 245–251. ISSN: 02638223. DOI: 10.1016/j.compstruct.2012.10.031.

[9] José García-Nieto and Enrique Alba. "Hybrid PSO6 for hard continuous optimization". In: *Soft Computing* 19.7 (July 2015), pp. 1843–1861. ISSN: 14337479. DOI: 10.1007/s00500-014-1368-8.

[10] Jens Hinrichsen and Cesa Bautista. "The Challenge of Reducing both Airframe Weight and Manufacturing Cost". In: *Air &Space Europe* 3 (2001).

[11] Raphael Höfer et al. "Advanced Ply Shape Generation in Composite Material Layup Using FEA-derived Fiber Information". In: *Procedia CIRP* 131 (2025), pp. 26–31. ISSN: 22128271. DOI: 10.1016/j.procir.2024.09.007. URL: https://linkinghub.elsevier.com/retrieve/pii/S2212827125000514.

[12] *K-Means assumptions*. URL: https://scikit-learn.org/stable/auto_examples/cluster/plot_kmeans_assumptions.html#sphx-glr-auto-examples-cluster-plot-kmeans-assumptions-py.

[13] A. Khani et al. "Design of variable stiffness panels for maximum strength using lamination parameters". In: *Composites Part B: Engineering* 42.3 (Apr. 2011), pp. 546–552. ISSN: 13598368. DOI: 10.1016/j.compositesb.2010.11.005.

[14] Ronald Krueger and Andrew Bergan. *Advances in Thermoplastic Composites Over Three Decades-A Literature Review*. Tech. rep. 2024. URL: http://www.sti.nasa.gov.

[15] Xin Liu et al. "Isothermal crystallisation ATP process for thermoplastic composites with semi-crystalline matrices using automated tape placement machine". In: *Composites Part B: Engineering* 227 (Dec. 2021). ISSN: 13598368. DOI: 10.1016/j.compositesb.2021.109381.

[16] R. Morales Ibarra. “Recycling of thermosets and their composites”. In: *Thermosets: Structure, Properties, and Applications: Second Edition*. Elsevier, 2018, pp. 639–666. ISBN: 9780081010211. DOI: 10.1016/B978-0-08-101021-1.00020-4.

[17] Seyedeh Fatemeh Nabavi and Hamid Dalir. *A review on laser-assisted manufacturing process of thermoset composites: A review of fundamentals, processes, scientific modelling, challenges and prospective*. Feb. 2025. DOI: 10.1016/j.optlastec.2024.111713.

[18] Vasileios S. Papapetrou, Chitrang Patel, and Ali Y. Tamijani. “Stiffness-based optimization framework for the topology and fiber paths of continuous fiber composites”. In: *Composites Part B: Engineering* 183 (Feb. 2020). ISSN: 13598368. DOI: 10.1016/j.compositesb.2019.107681.

[19] Xiang Peng et al. “Optimization design of stacking sequence and material distribution for variable thickness hybrid composite structure based on improved stacking sequence table”. In: *Composite Structures* 307 (Mar. 2023). ISSN: 02638223. DOI: 10.1016/j.compstruct.2022.116641.

[20] Xiang Peng et al. “Stacking sequence optimization of variable thickness composite laminated plate based on multi-peak stacking sequence table”. In: *Composite Structures* 356 (Feb. 2025). ISSN: 02638223. DOI: 10.1016/j.compstruct.2025.118886.

[21] *PyGAD*. URL: https://pygad.readthedocs.io/en/latest/index.html#.

[22] Singiresu S Rao. *Engineering Optimization-Theory and Practice*. 5th. 2020.

[23] Huilin Ren et al. “Performance and manufacturability co-driven process planning for topology-optimized structures fabricated by continuous fiber-reinforced polymer additive manufacturing”. In: *Composites Part A: Applied Science and Manufacturing* 192 (May 2025). ISSN: 1359835X. DOI: 10.1016/j.compositesa.2025.108813.

[24] *Revolutionizing Aircraft Materials and Processes*. Springer International Publishing, 2020, pp. 87–114. DOI: 10.1007/978-3-030-35346-9.

[25] Mohammad Amin Roohi et al. “Safe optimization with grey-box information: Application to composites autoclave processing improvement on the fly”. In: *Composites Part C: Open Access* 16 (Mar. 2025). ISSN: 26666820. DOI: 10.1016/j.jcomc.2025.100560.

[26] Gokhan Serhat and Ipek Basdogan. “Multi-objective optimization of composite plates using lamination parameters”. In: *Materials and Design* 180 (Oct. 2019). ISSN: 18734197. DOI: 10.1016/j.matdes.2019.107904.

[27] Farah Syazwani Shahar et al. “History and future of aerospace materials”. In: *Aerospace Materials: Novel Technologies and Practical Applications*. Elsevier, Jan. 2025. Chap. 2, pp. 41–60. ISBN: 9780443221187. DOI: 10.1016/B978-0-443-22118-7.00002-6.

[28] *Shell 181 Ansys APDL documentation*. URL: https://ansyshelp.ansys.com/public/account/secured?returnurl=/Views/Secured/corp/v242/en/ans_elem/Hlp_E_SHELL181.html.

[29] Bence Szederkenyi, Norbert Krisztian Kovacs, and Tibor Czigany. *A comprehensive review of fiber-reinforced topology optimization for advanced polymer composites produced by automated manufacturing*. Jan. 2024. DOI: 10.1016/j.aiepr.2024.05.002.

[30] Andrew J. Timmis et al. “Environmental impact assessment of aviation emission reduction through the implementation of composite materials”. In: *International Journal of Life Cycle Assessment* 20.2 (Feb. 2015), pp. 233–243. ISSN: 16147502. DOI: 10.1007/s11367-014-0824-0.

[31] Robert A. Witik et al. “Economic and environmental assessment of alternative production methods for composite aircraft components”. In: *Journal of Cleaner Production* 29-30 (July 2012), pp. 91–102. ISSN: 09596526. DOI: 10.1016/j.jclepro.2012.02.028.

[32] Shyr Shen Yu et al. “Two improved k-means algorithms”. In: *Applied Soft Computing Journal* 68 (July 2018), pp. 747–755. ISSN: 15684946. DOI: 10.1016/j.asoc.2017.08.032.

A

Stress Clustered Figures

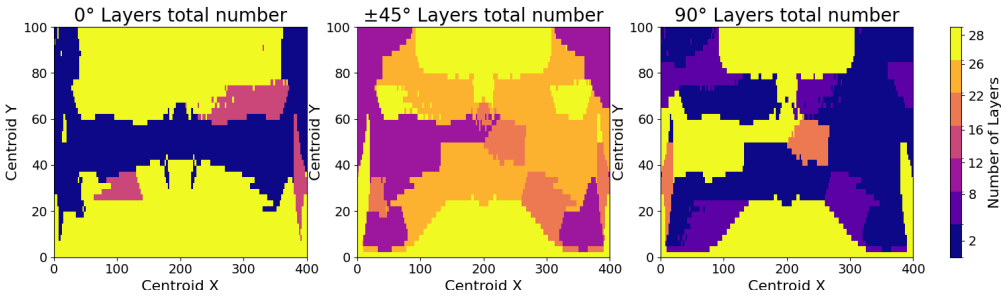

Figure A.1: 16 thickness clusters and 4 stress clusters allowed.

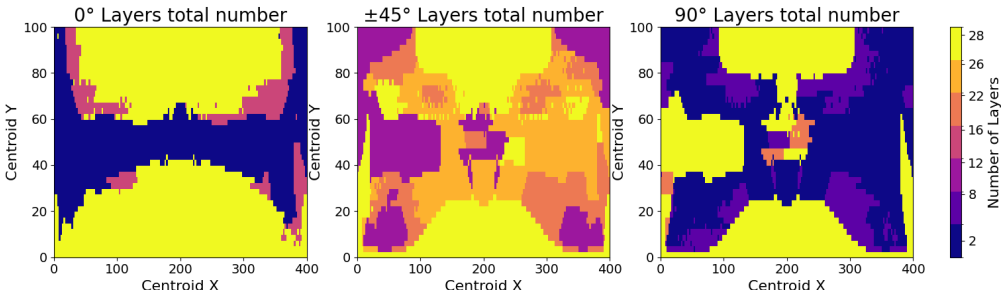

Figure A.2: 16 thickness clusters and 16 stress clusters allowed.

B

Stress Clustered Figures Finer mesh

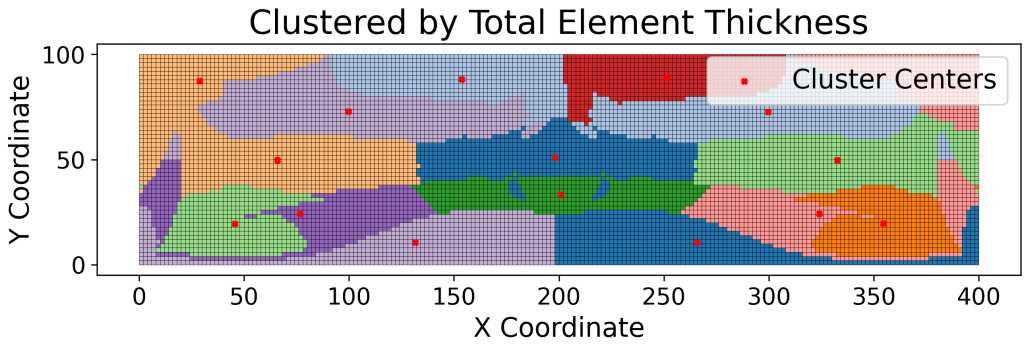

Figure B.1: Caption

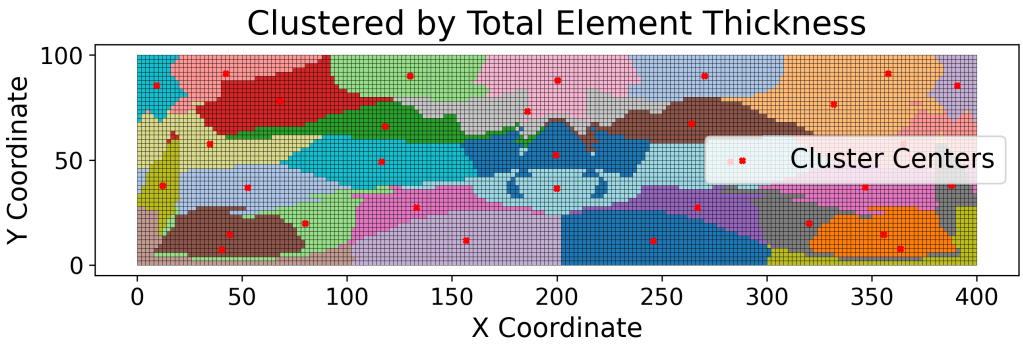

Figure B.2: Thickness clustered

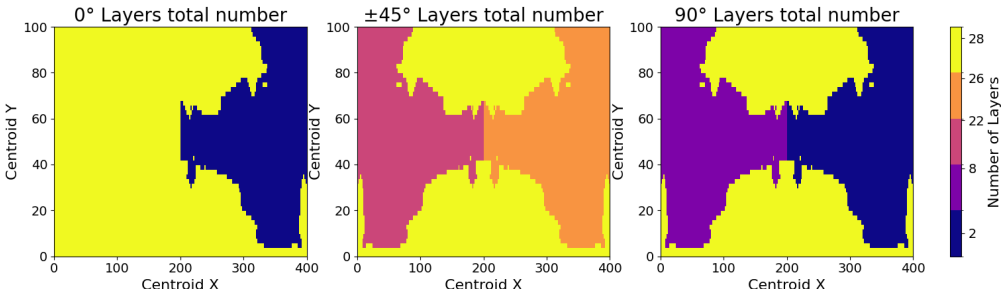

Figure B.3: Stress clustered per orientation finer mesh 4 thickness 1 allowed stress.

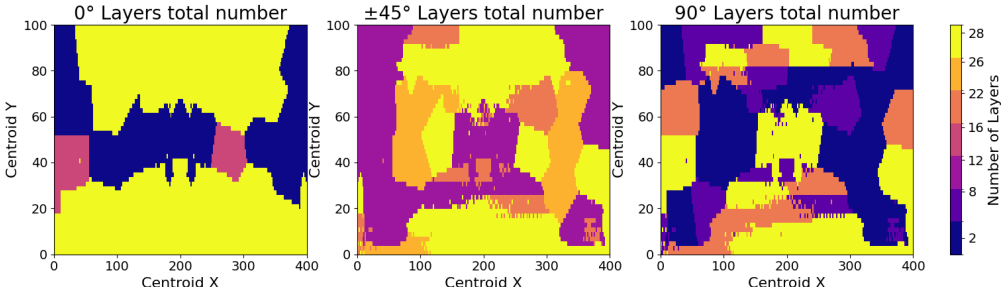

Figure B.4: Stress clustered per orientation finer mesh 4 thickness 16 allowed stress.

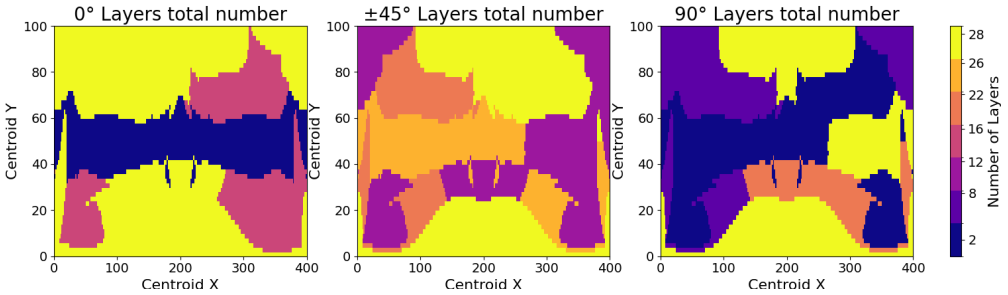

Figure B.5: Stress clustered per orientation finer mesh 16 thickness 1 allowed stress.

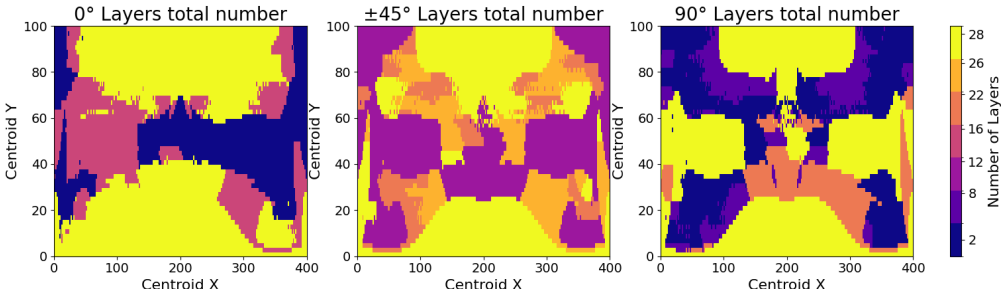

Figure B.6: Stress clustered per orientation finer mesh 16 thickness 16 allowed stress.

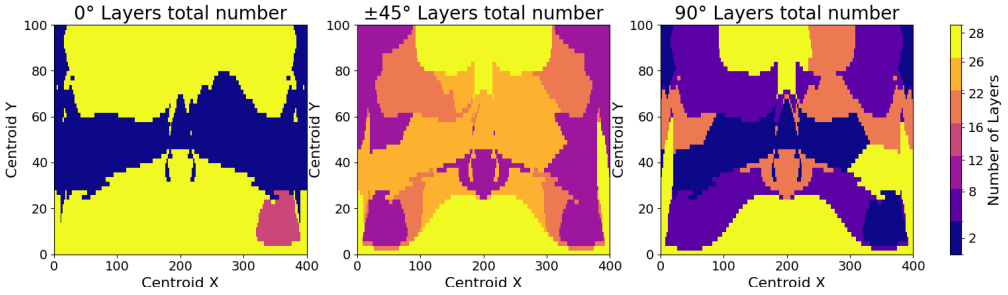

Figure B.7: Stress clustered per orientation finer mesh 32 thickness 1 allowed stress.

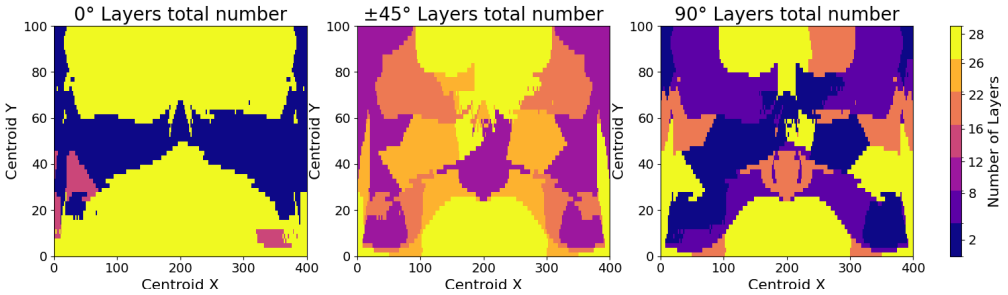

Figure B.8: Stress clustered per orientation finer mesh 32 thickness 4 allowed stress.

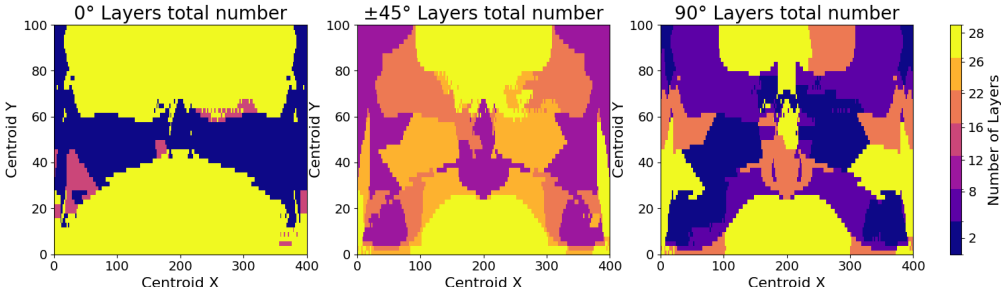

Figure B.9: Stress clustered per orientation finer mesh 32 thickness 16 allowed stress.

C

Error Distribution Graphs.

C.1. Error Distribution Graphs 50mm tape width.

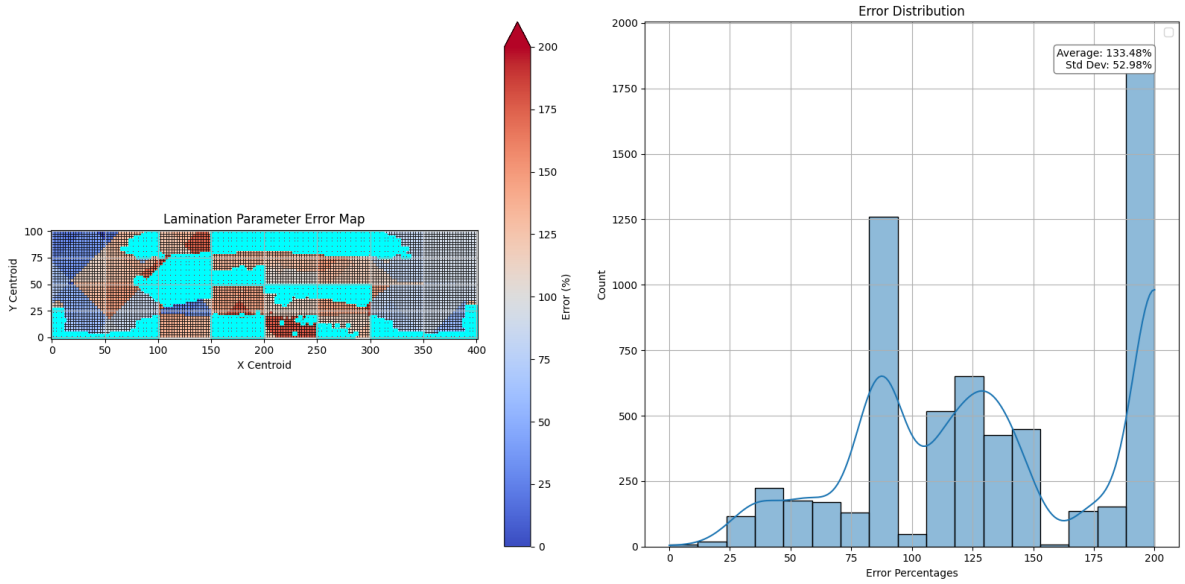

Figure C.1: Error distribution before GA optimization 4 thickness and 4 stress cluster 50mm tape.

C.2. Error Distribution Graphs 25mm tape width.

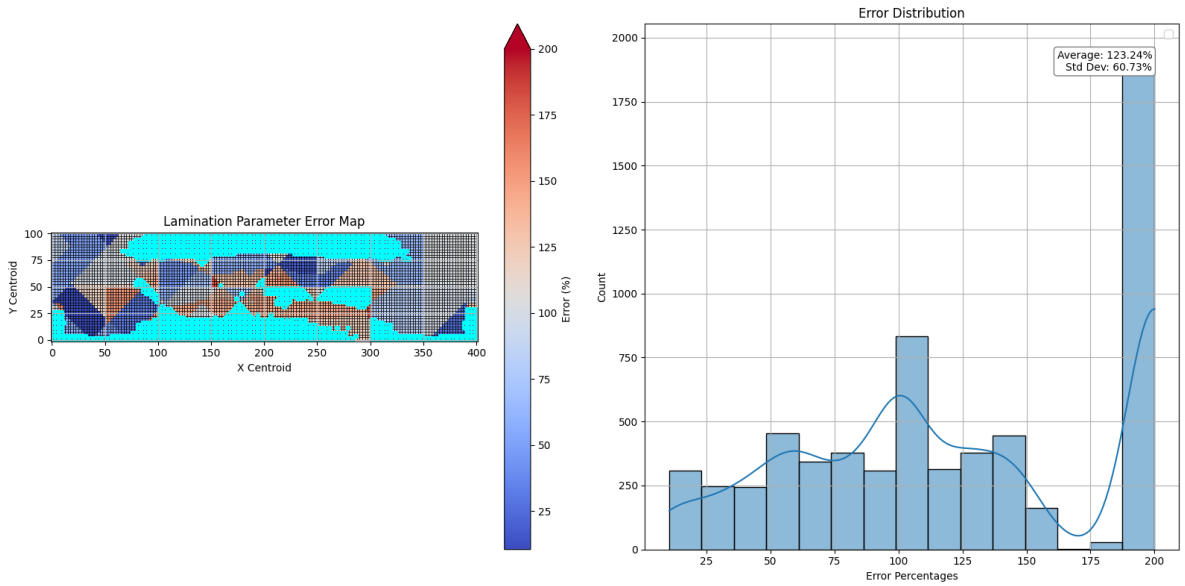

Figure C.2: Error distribution after GA optimization 4 thickness and 4 stress cluster 50mm tape.

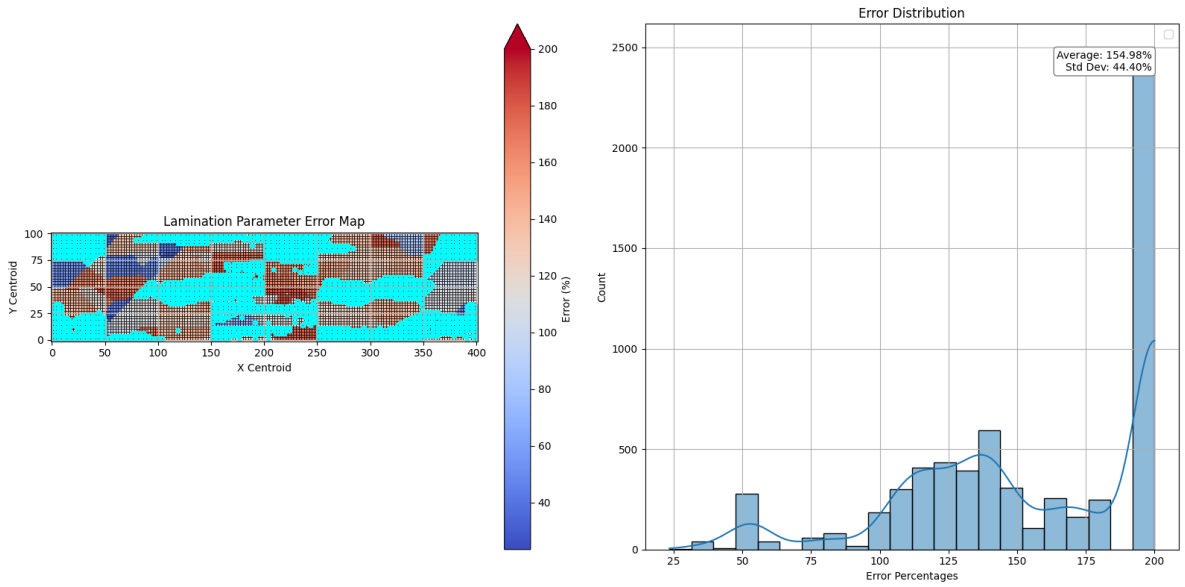

Figure C.3: Error distribution before GA optimization 4 thickness and 16 stress cluster 50mm tape.

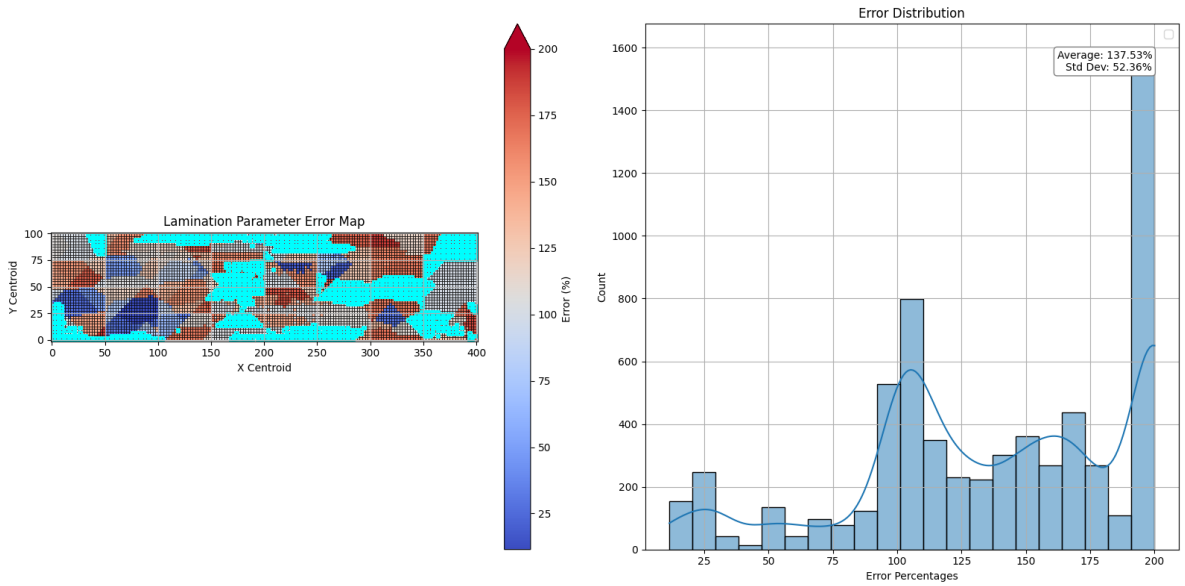

Figure C.4: Error distribution after GA optimization 4 thickness and 16 stress cluster 50mm tape.

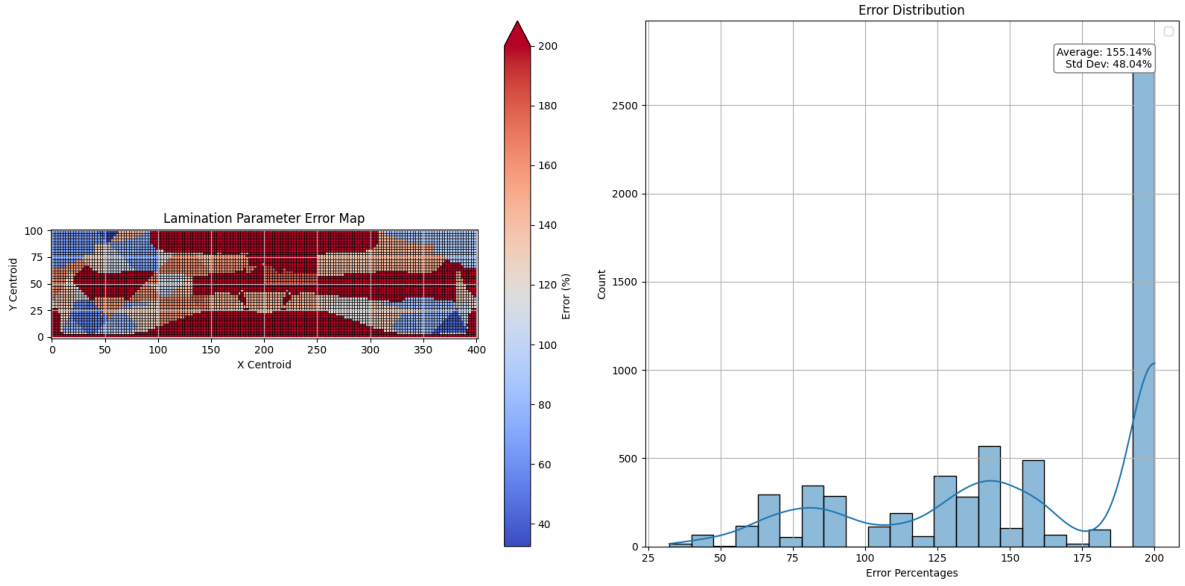

Figure C.5: Error distribution before GA optimization 16 thickness and 1 stress cluster 50mm tape.

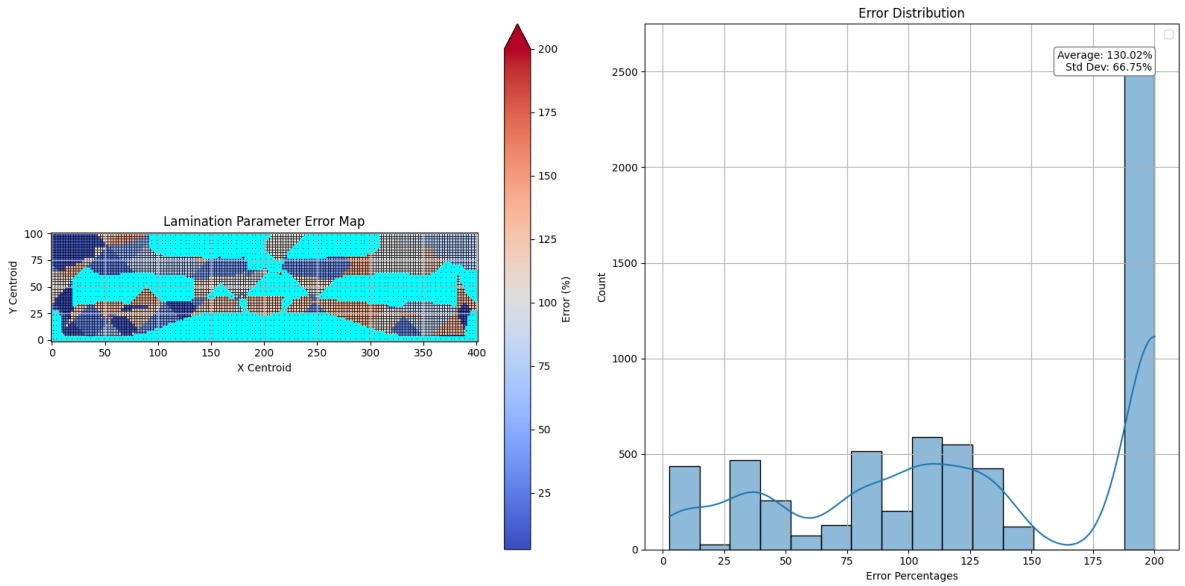

Figure C.6: Error distribution after GA optimization 16 thickness and 1 stress cluster 50mm tape.

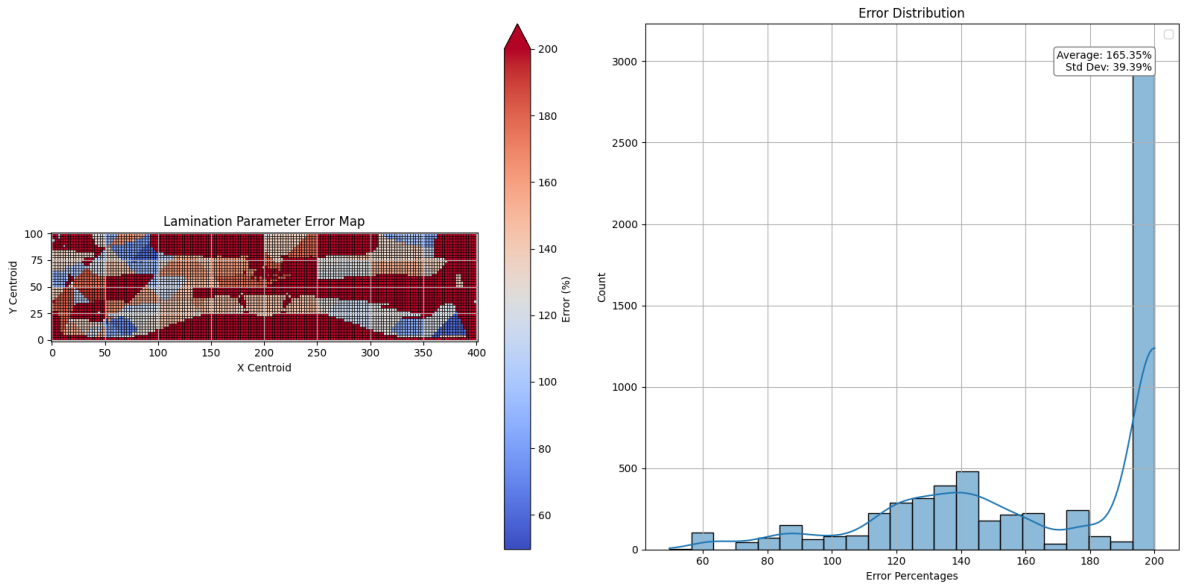

Figure C.7: Error distribution before GA optimization 16 thickness and 4 stress cluster 50mm tape.

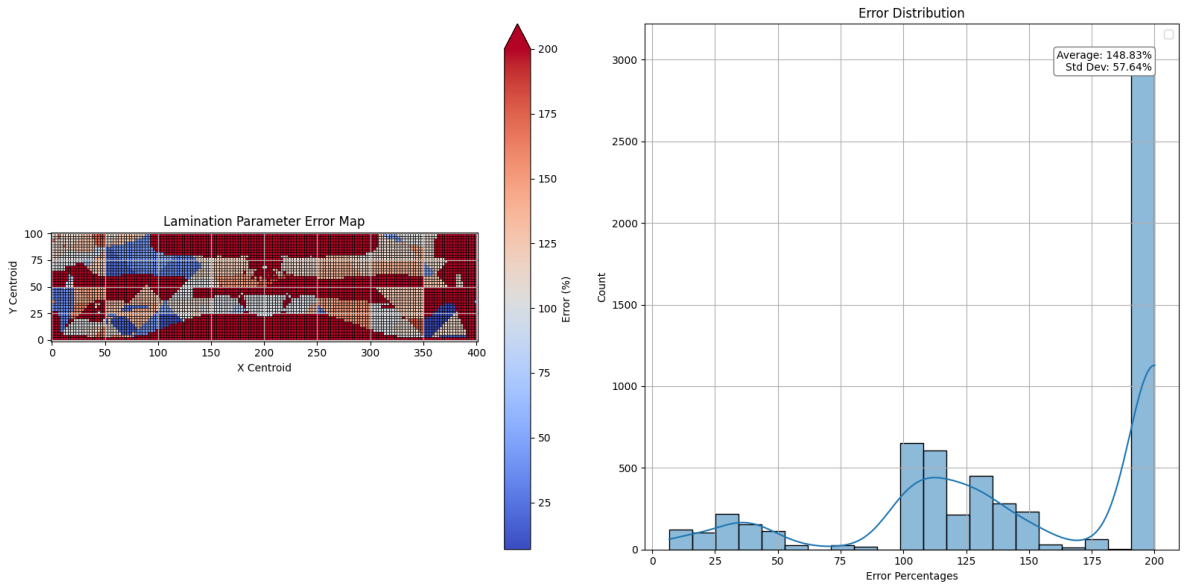

Figure C.8: Error distribution after GA optimization 16 thickness and 4 stress cluster 50mm tape.

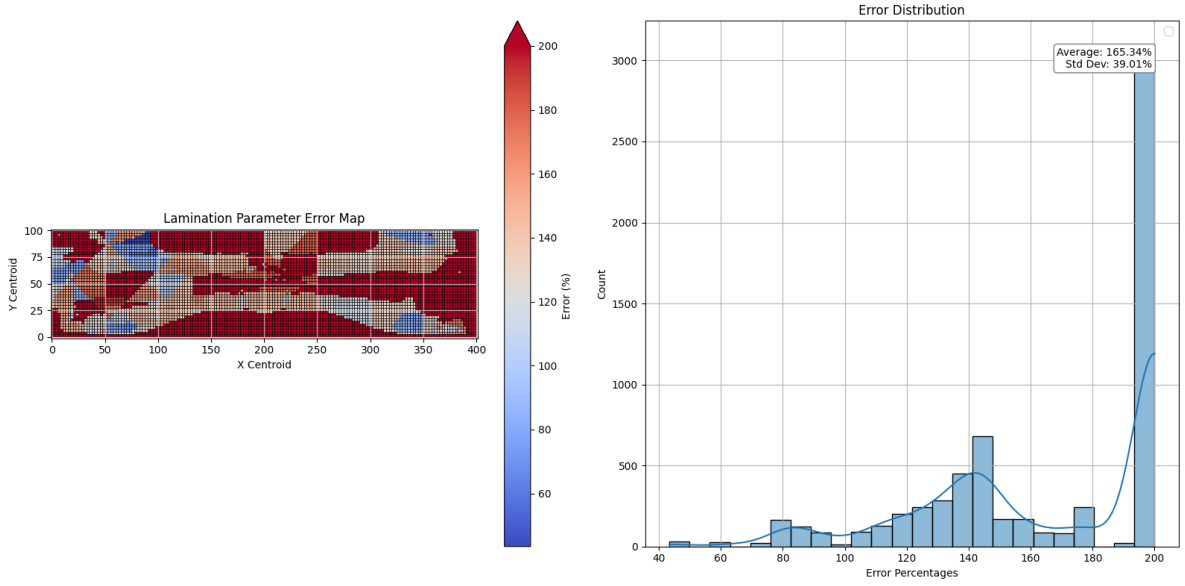

Figure C.9: Error distribution before GA optimization 16 thickness and 16 stress cluster 50mm tape.

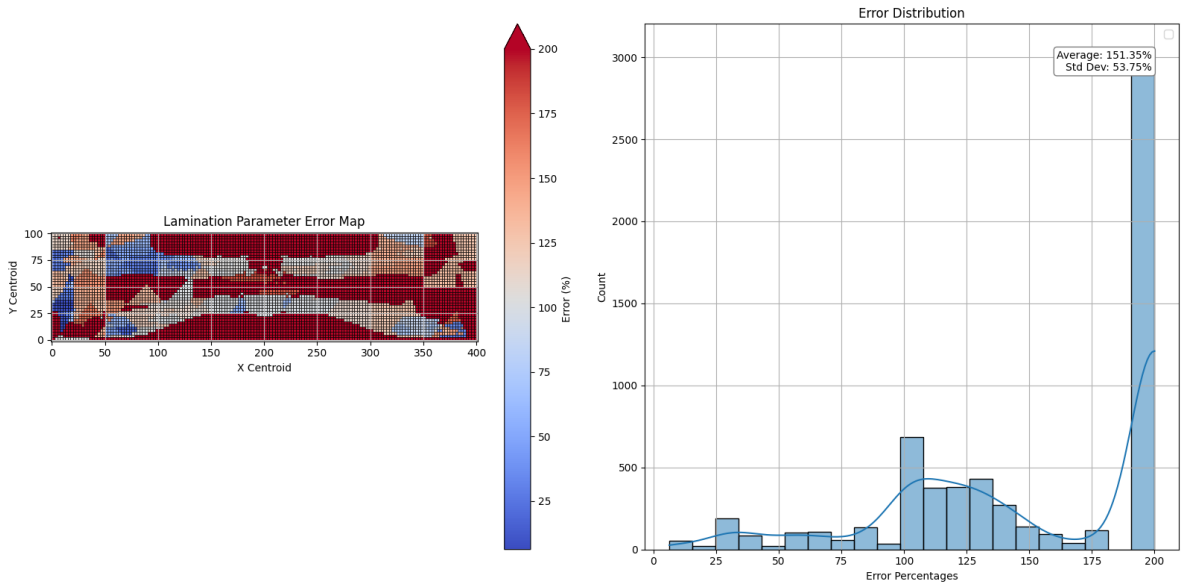

Figure C.10: Error distribution after GA optimization 16 thickness and 16 stress cluster 50mm tape.

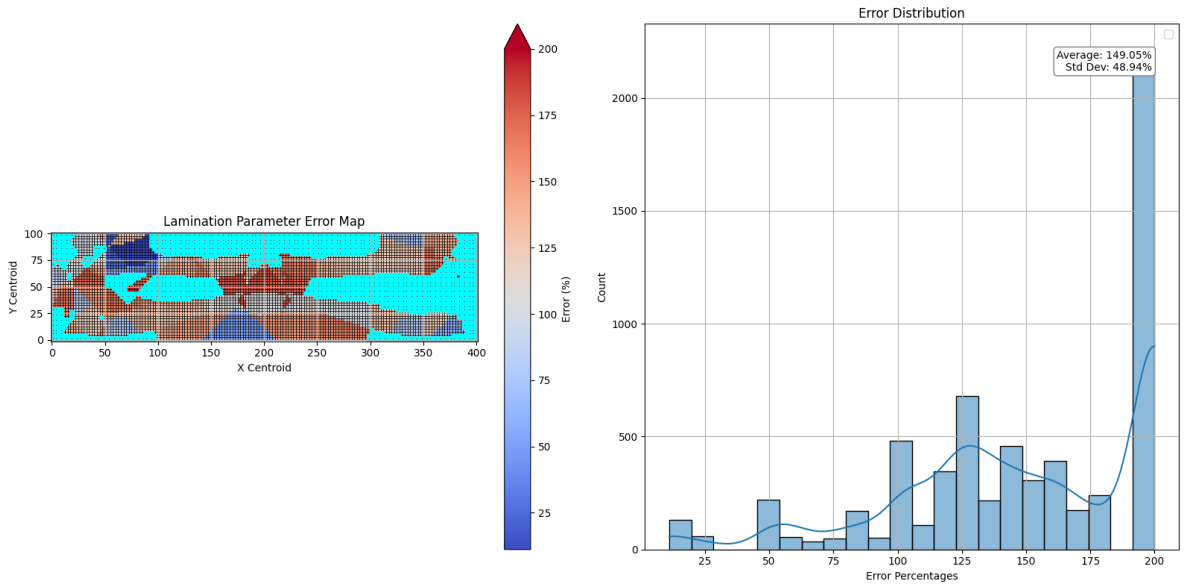

Figure C.11: Error distribution before GA optimization 32 thickness and 1 stress cluster 50mm tape.

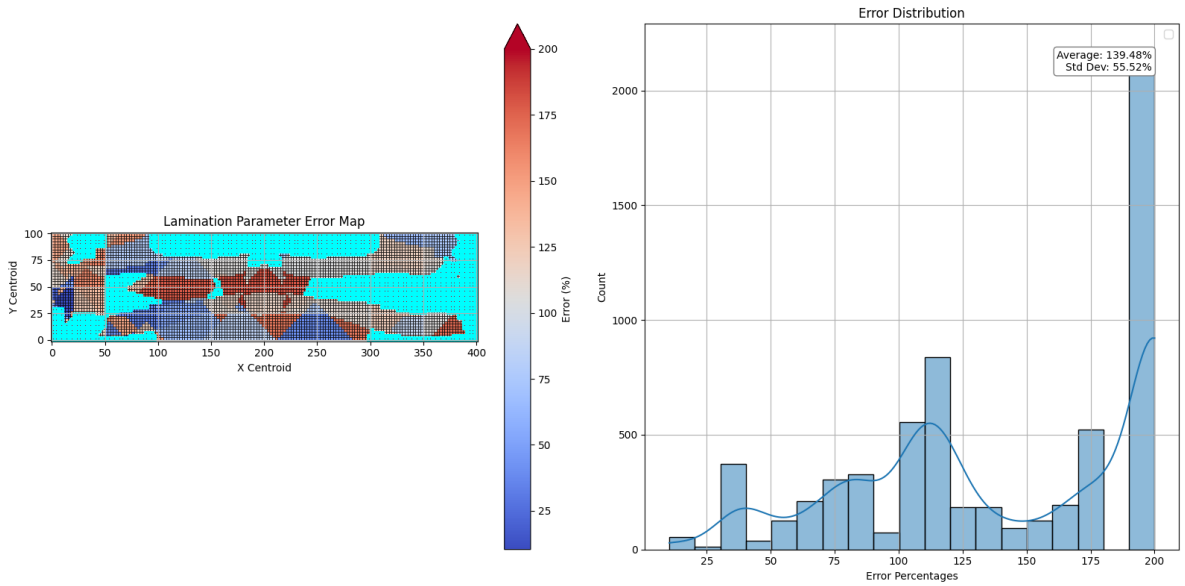

Figure C.12: Error distribution after GA optimization 32 thickness and 1 stress cluster 50mm tape.

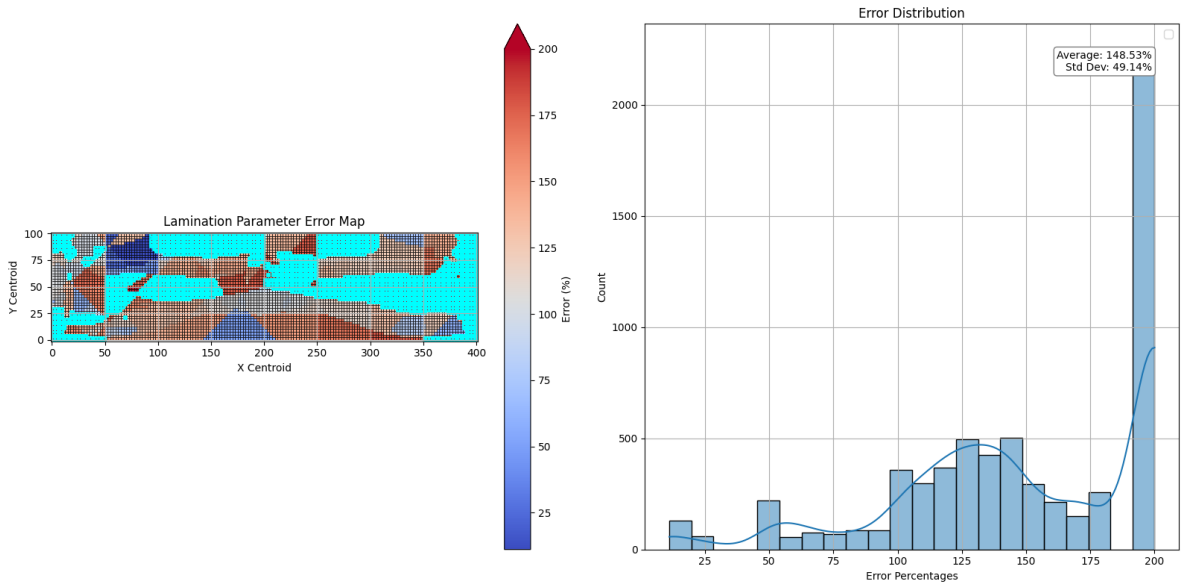

Figure C.13: Error distribution before GA optimization 32 thickness and 4 stress cluster 50mm tape.

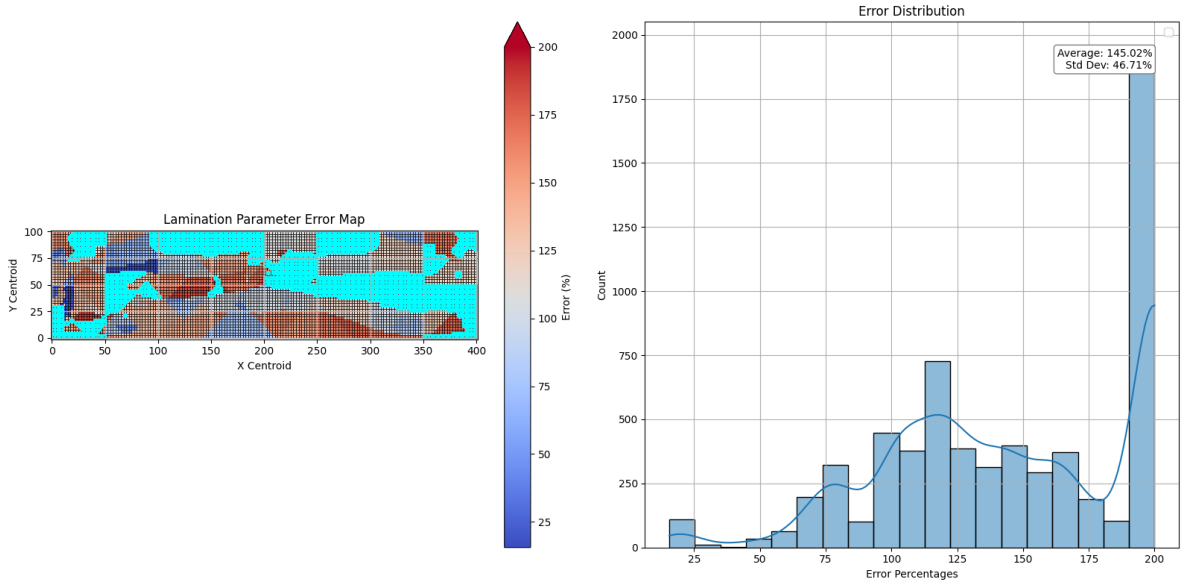

Figure C.14: Error distribution after GA optimization 32 thickness and 4 stress cluster 50mm tape.

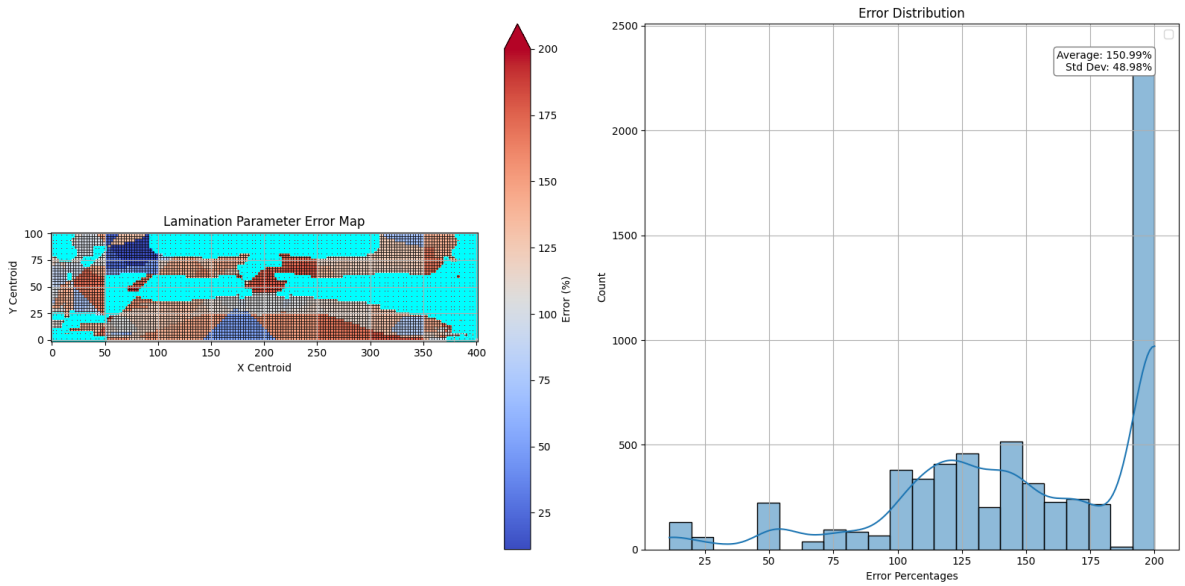

Figure C.15: Error distribution before GA optimization 32 thickness and 16 stress cluster 50mm tape.

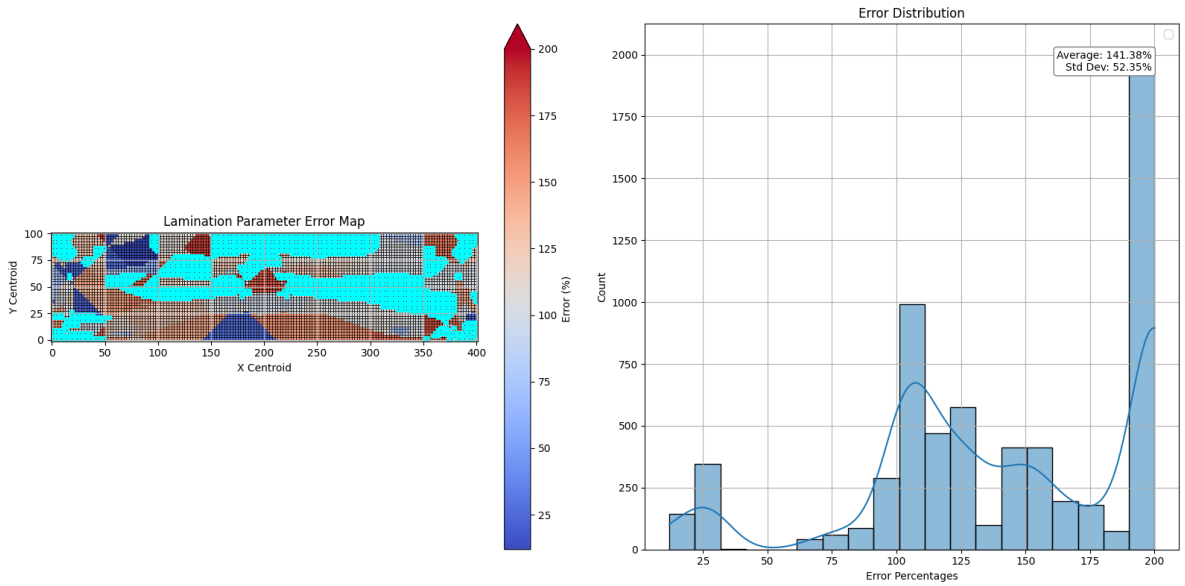

Figure C.16: Error distribution after GA optimization 32 thickness and 16 stress cluster 50mm tape.

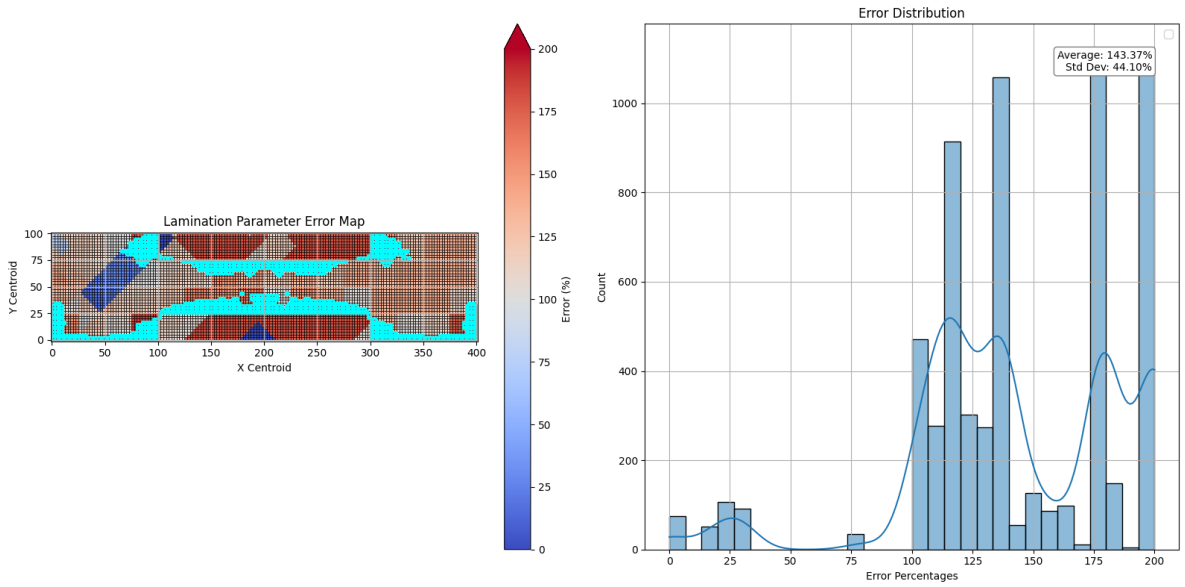

Figure C.17: Error distribution before GA application 4 thickness 1 stress cluster tape width 25mm.

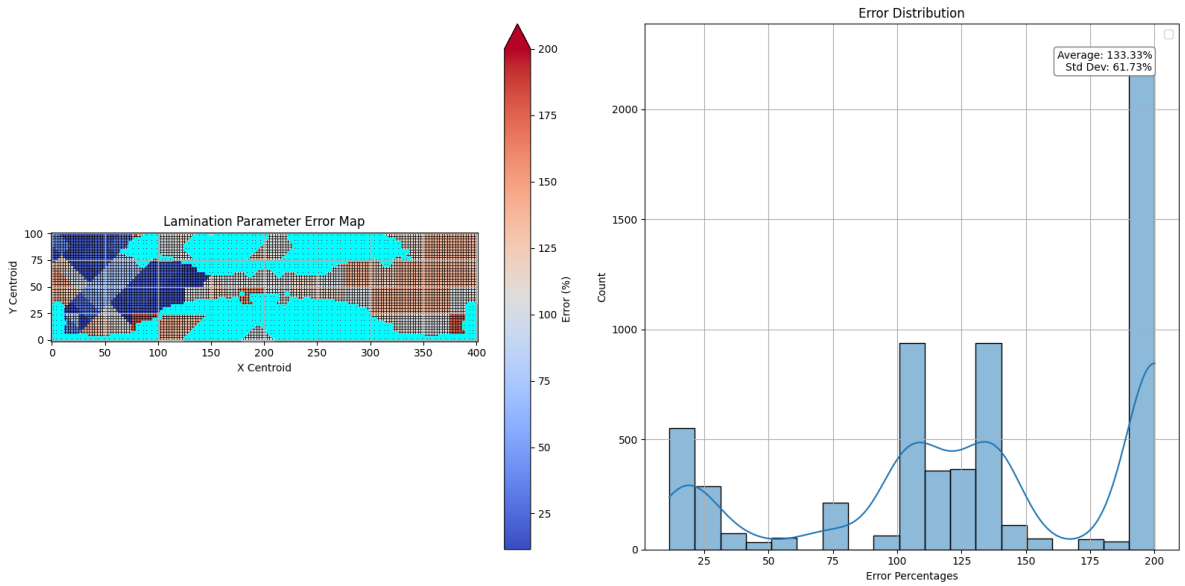

Figure C.18: Error distribution after GA application 4 thickness 1 stress cluster tape width 25mm.

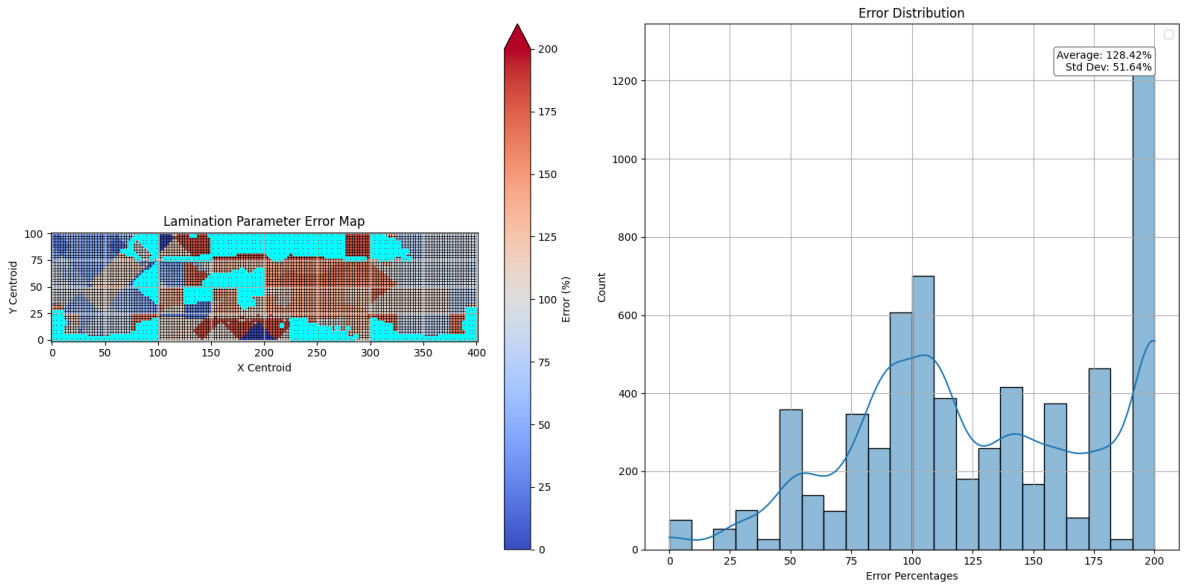

Figure C.19: Error distribution before GA application 4 thickness 4 stress cluster tape width 25mm.

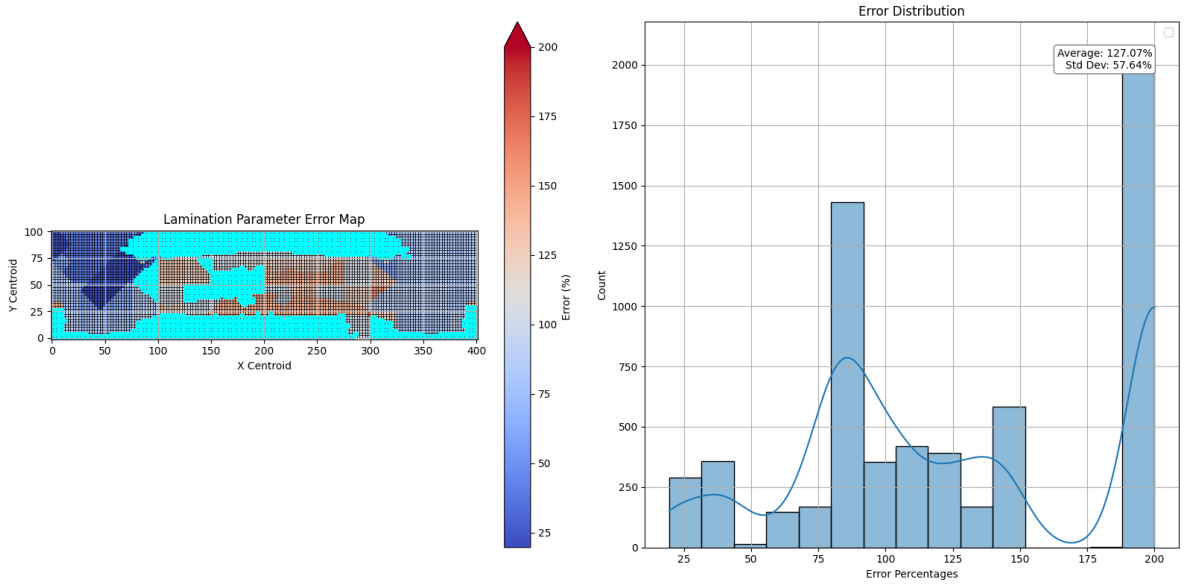

Figure C.20: Error distribution after GA application 4 thickness 4 stress cluster tape width 25mm.

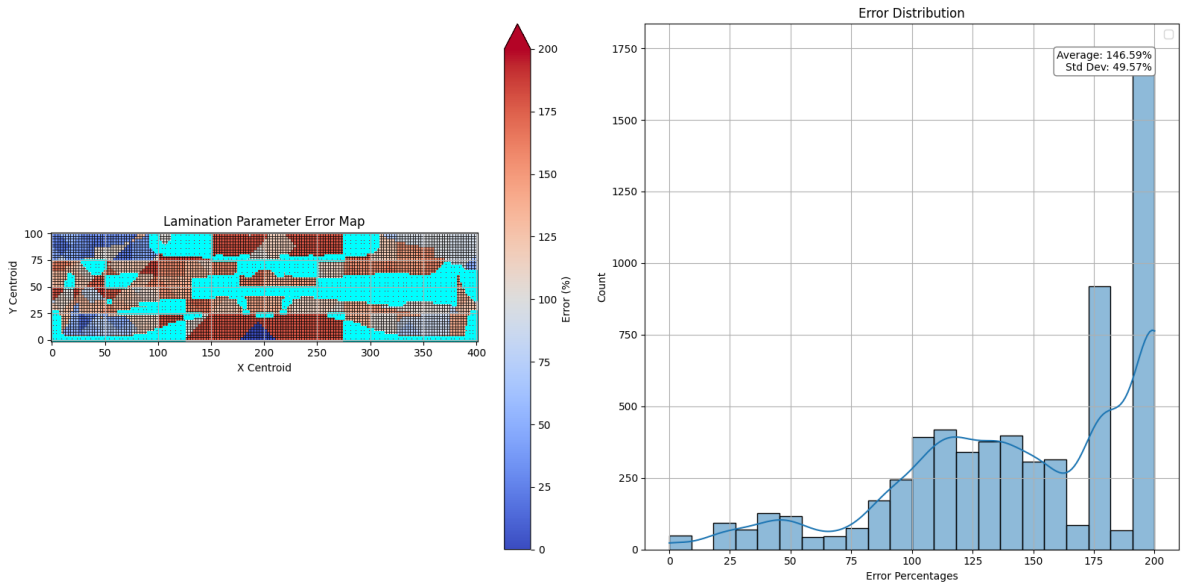

Figure C.21: Error distribution before GA application 16 thickness 1 stress cluster tape width 25mm.

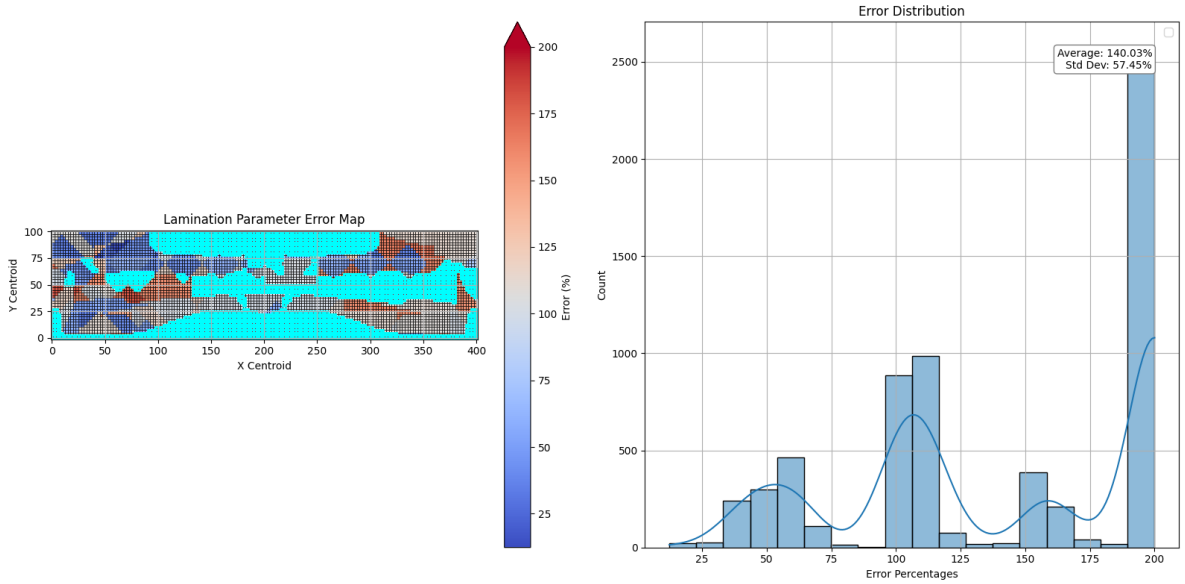

Figure C.22: Error distribution after GA application 16 thickness 1 stress cluster tape width 25mm.

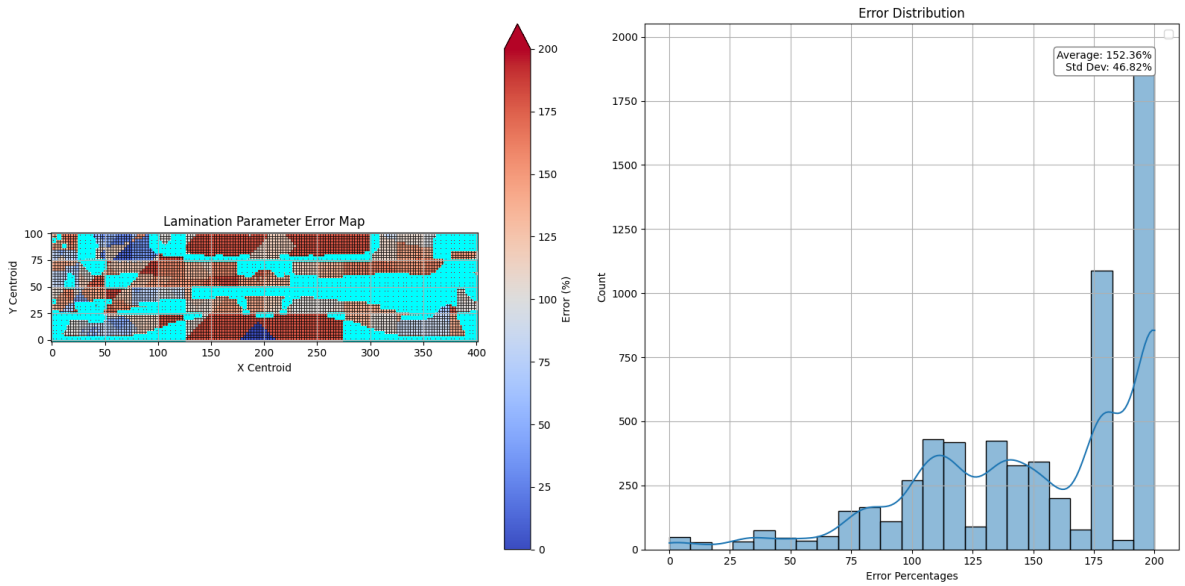

Figure C.23: Error distribution before GA application 16 thickness 4 stress cluster tape width 25mm.

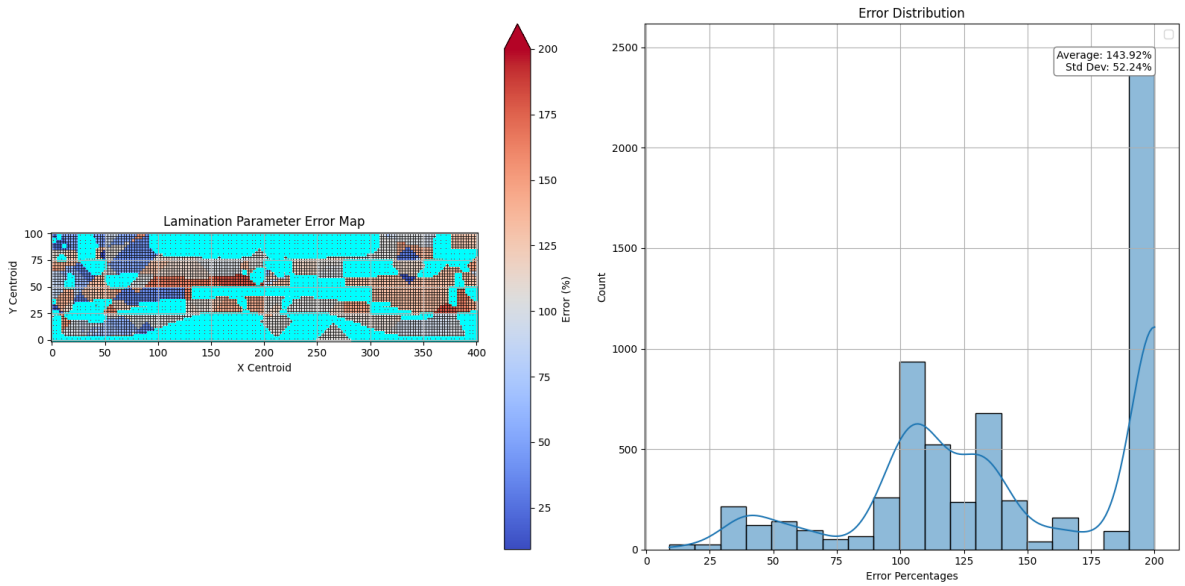

Figure C.24: Error distribution after GA application 16 thickness 4 stress cluster tape width 25mm.

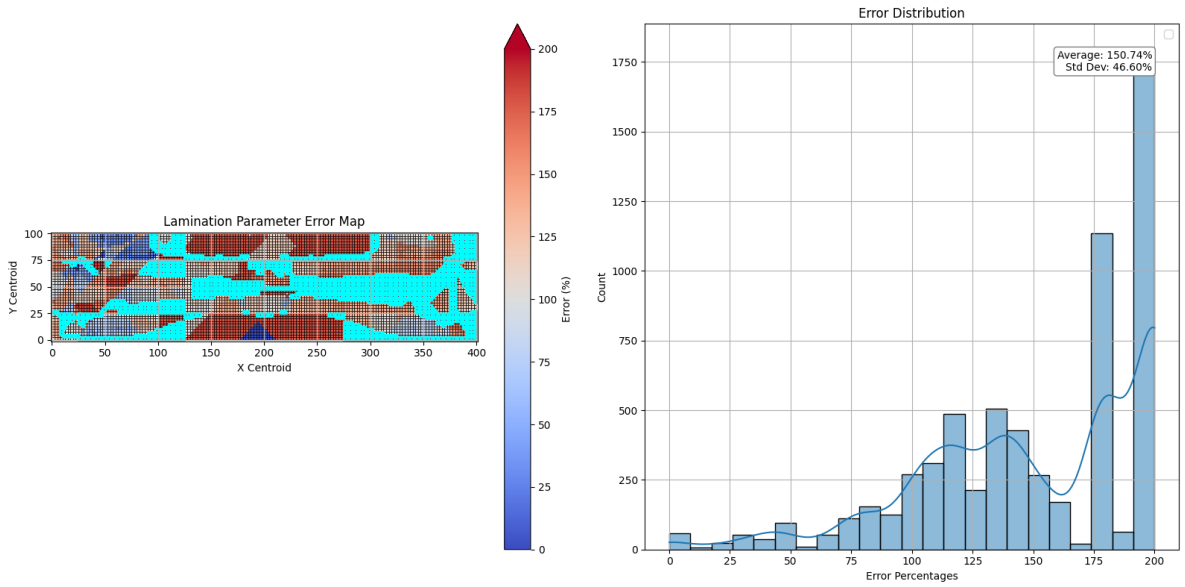

Figure C.25: Error distribution before GA application 16 thickness 16 stress cluster tape width 25mm.

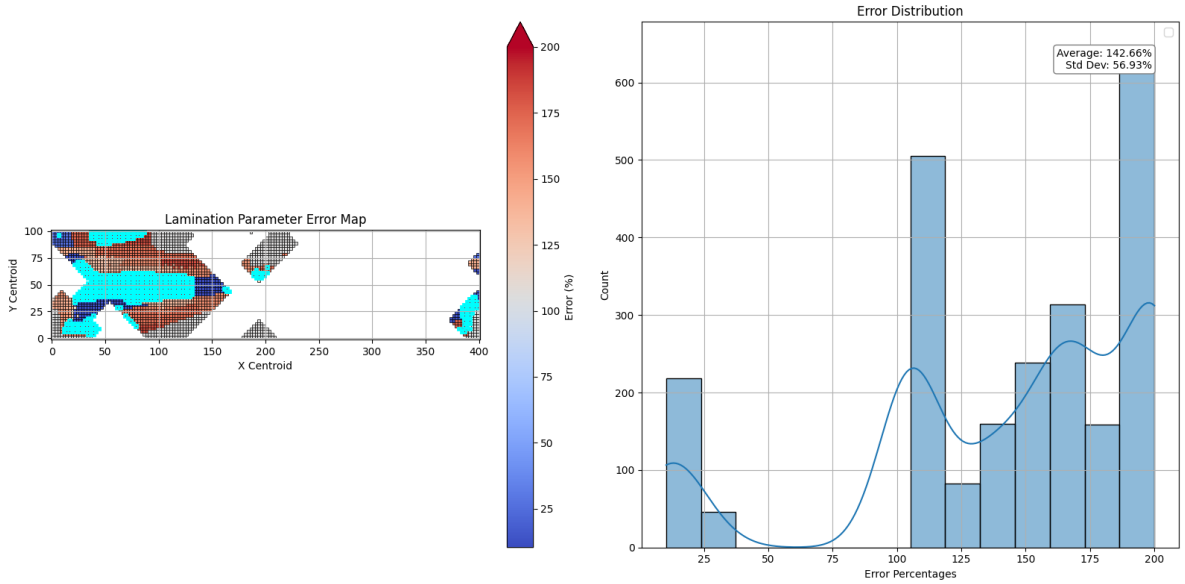

Figure C.26: Error distribution after GA application 16 thickness 16 stress cluster tape width 25mm.

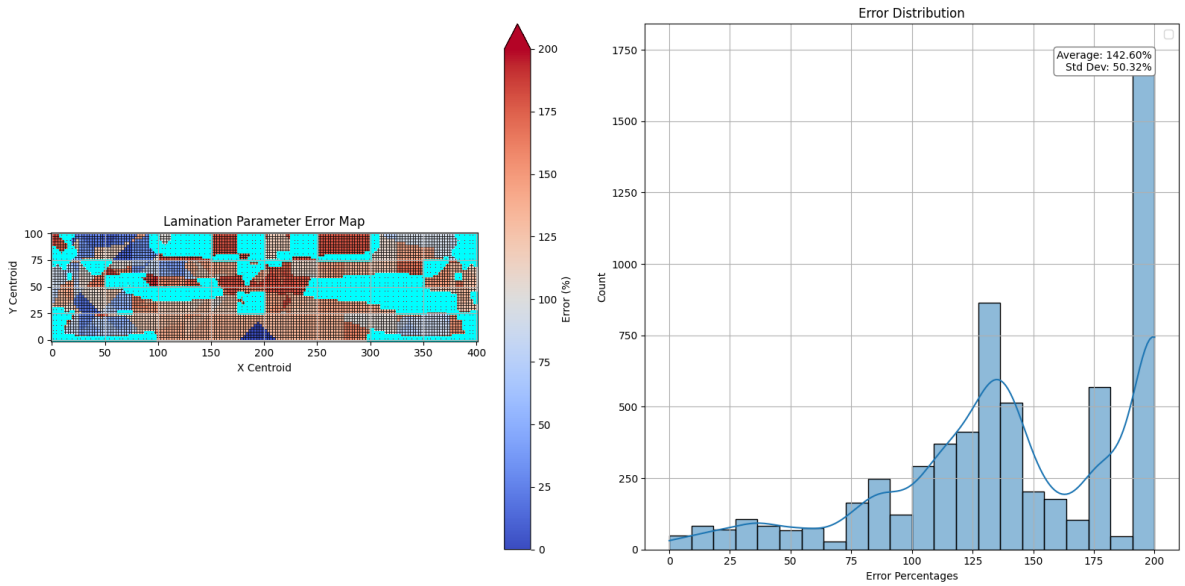

Figure C.27: Error distribution before GA application 32 thickness 1 stress cluster tape width 25mm.

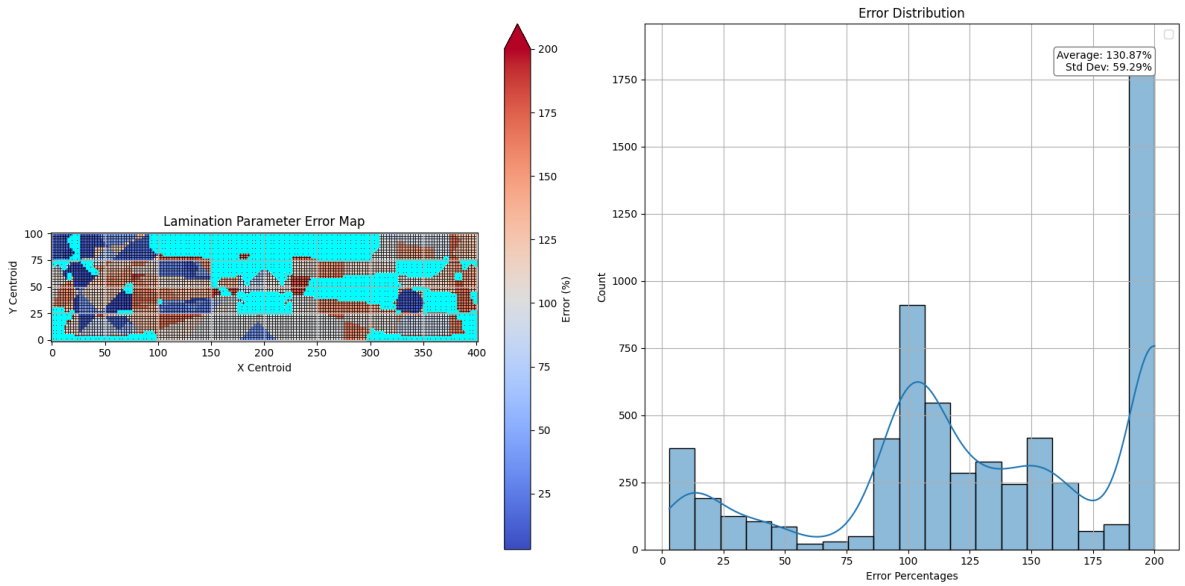

Figure C.28: Error distribution after GA application 32 thickness 1 stress cluster tape width 25mm.

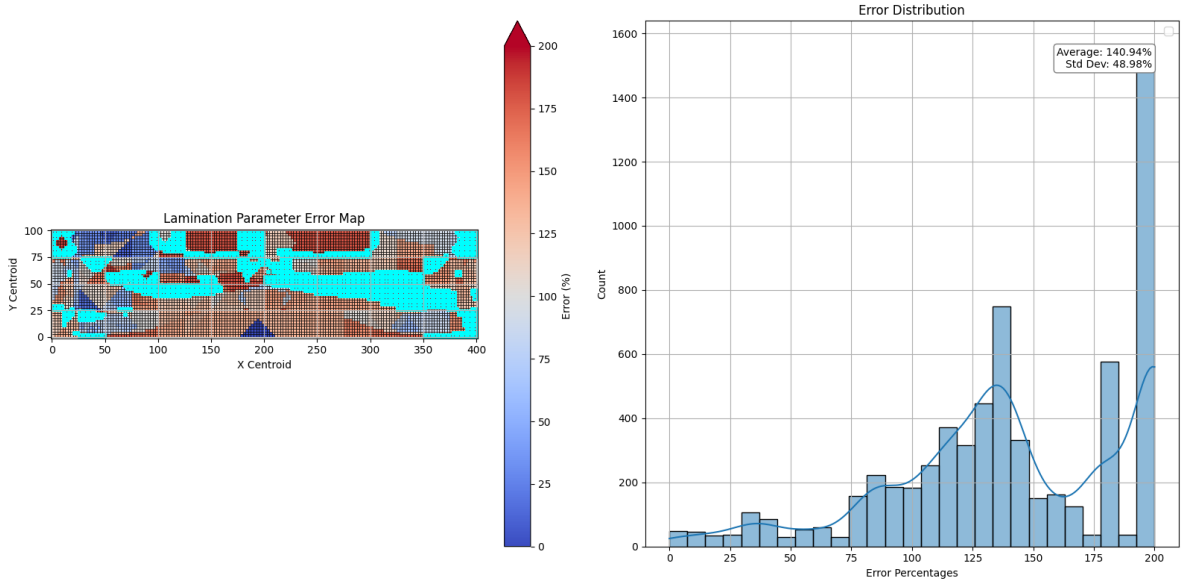

Figure C.29: Error distribution before GA application 32 thickness 4 stress cluster tape width 25mm.

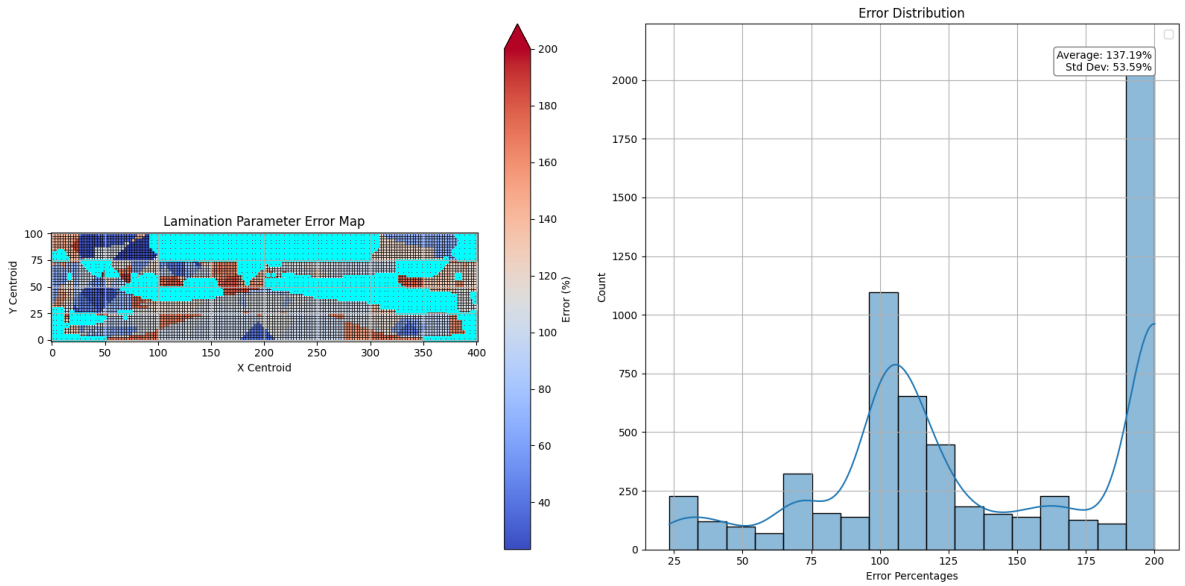

Figure C.30: Error distribution after GA application 32 thickness 4 stress cluster tape width 25mm.

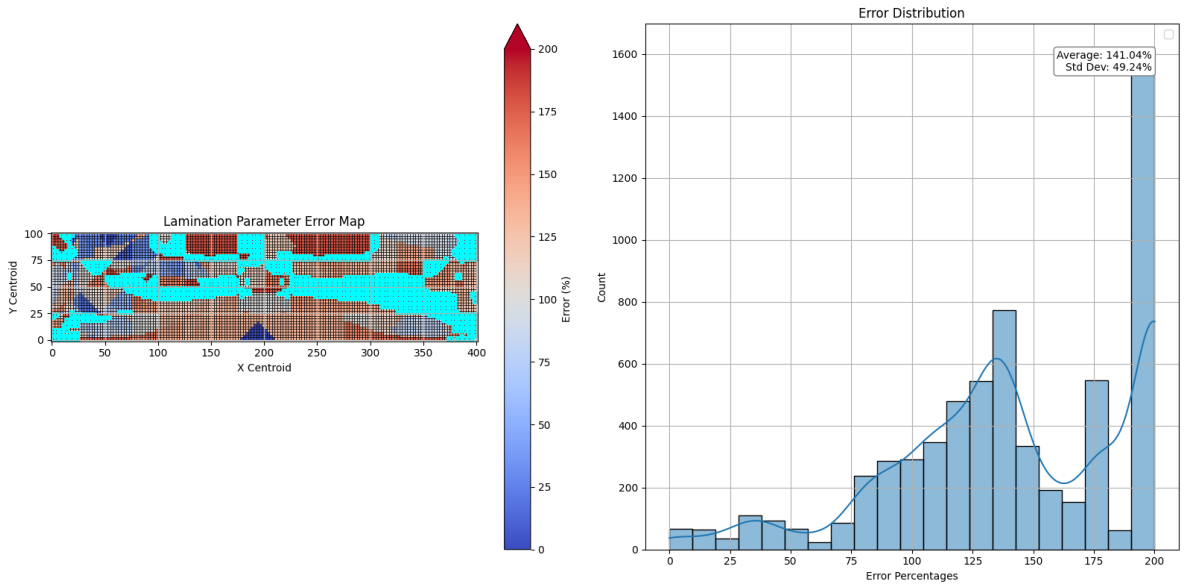

Figure C.31: Error distribution before GA application 32 thickness 16 stress cluster tape width 25mm.

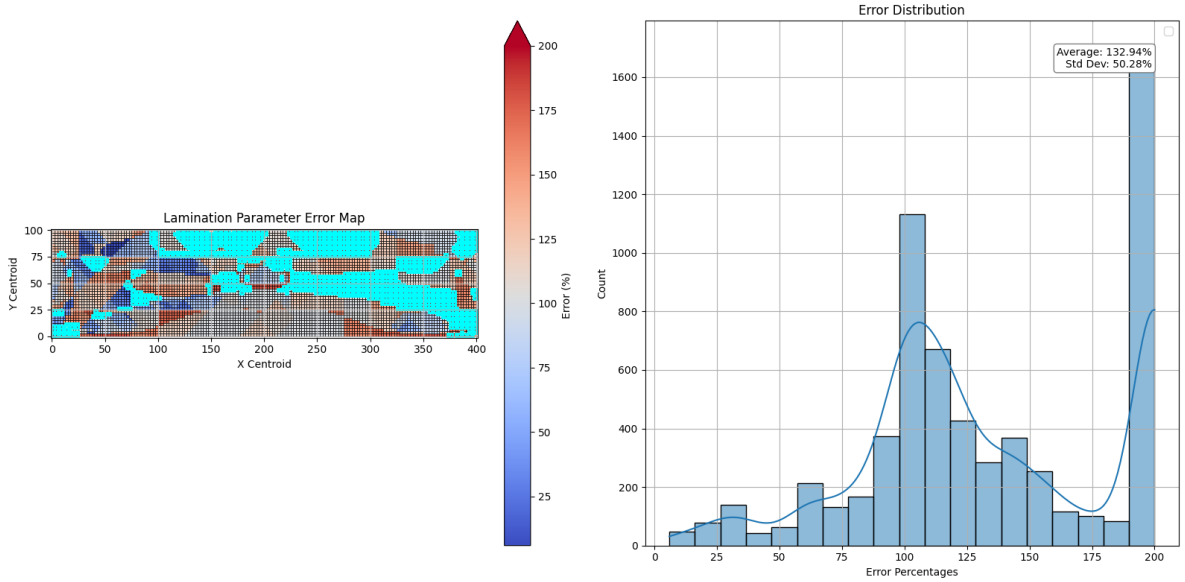

Figure C.32: Error distribution after GA application 32 thickness 16 stress cluster tape width 25mm.

D

Lamination Parameter Distribution Graphs for 25mm tape width.

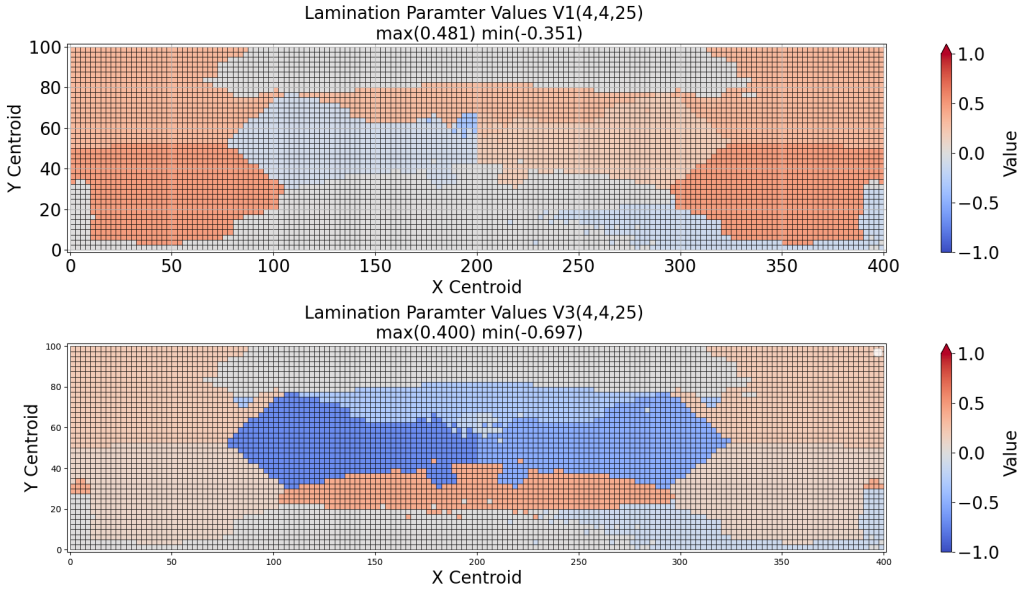

Figure D.1: Finite element model lamination parameter distribution for V1 and V3 in 4 thickness clusters and 4 stress clusters allowed.

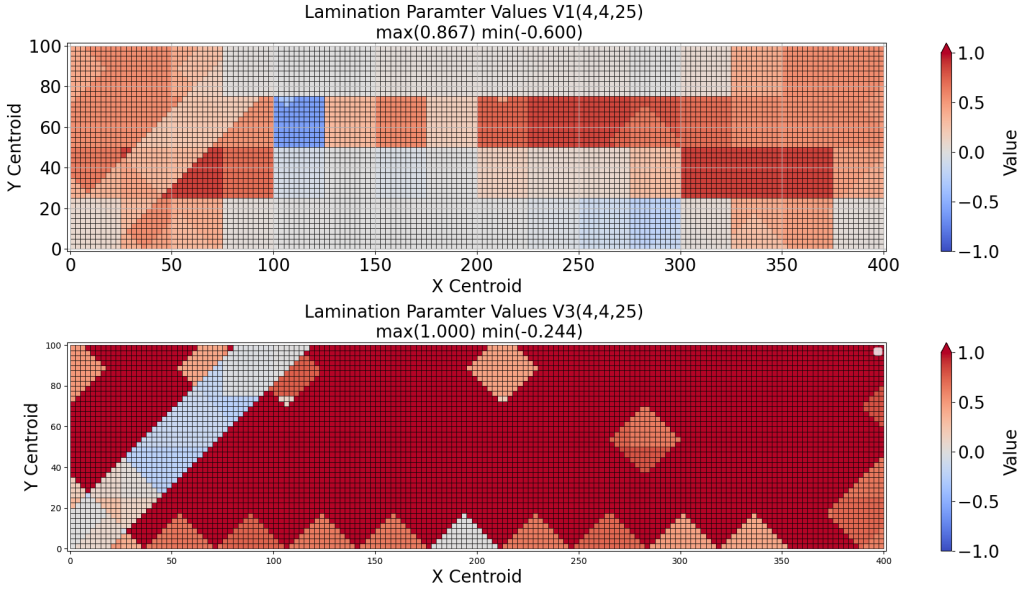

Figure D.2: Patch-wise model lamination parameter distribution for V1 and V3 in 4 thickness clusters and 4 stress clusters allowed before optimization.

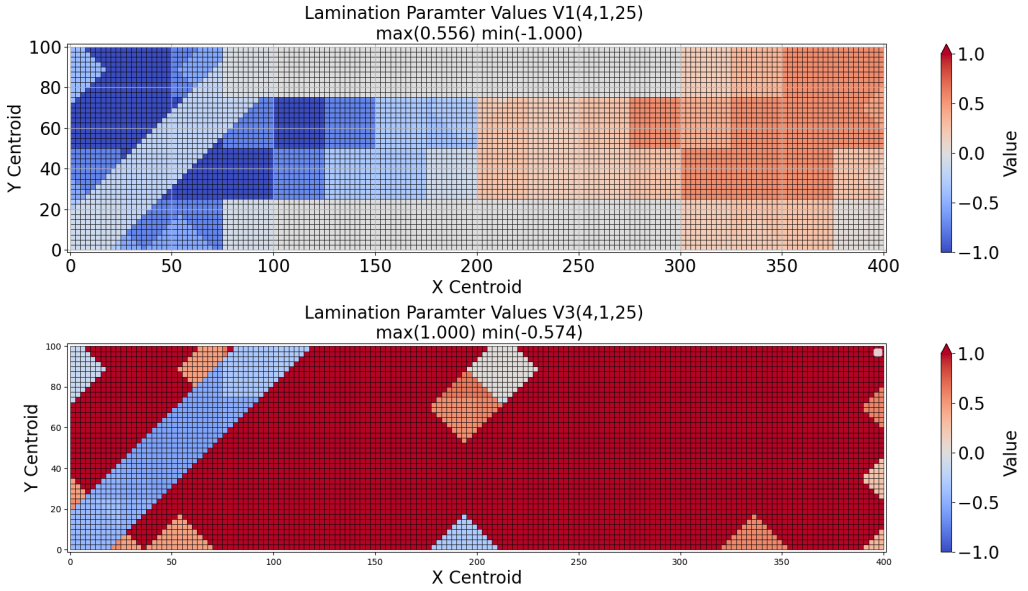

Figure D.3: Patch-wise model lamination parameter distribution for V1 and V3 in 4 thickness clusters and 1 stress clusters allowed after optimization.

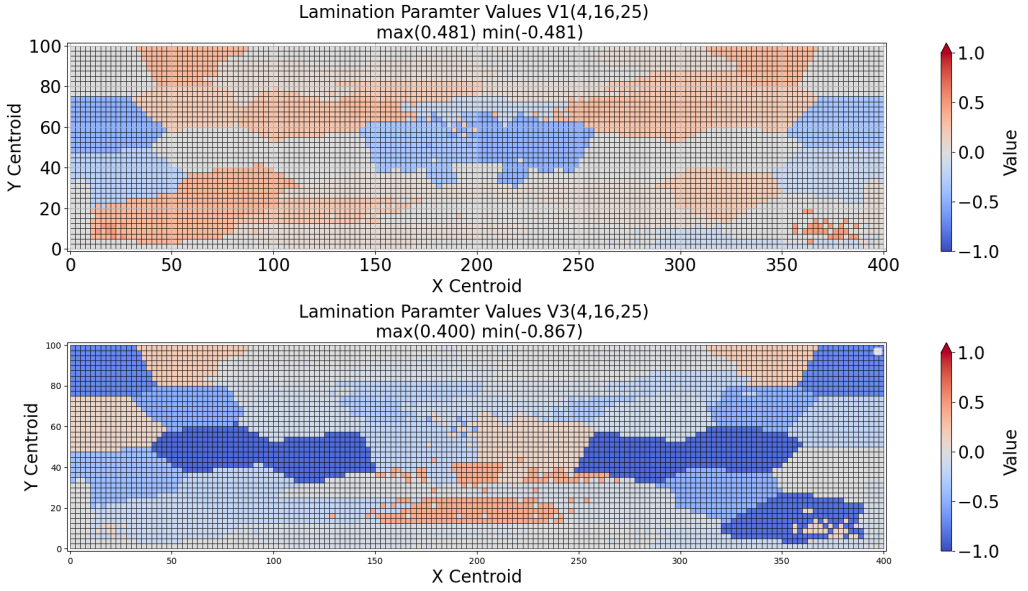

Figure D.4: Finite element model lamination parameter distribution for V1 and V3 in 4 thickness clusters and 16 stress clusters allowed.

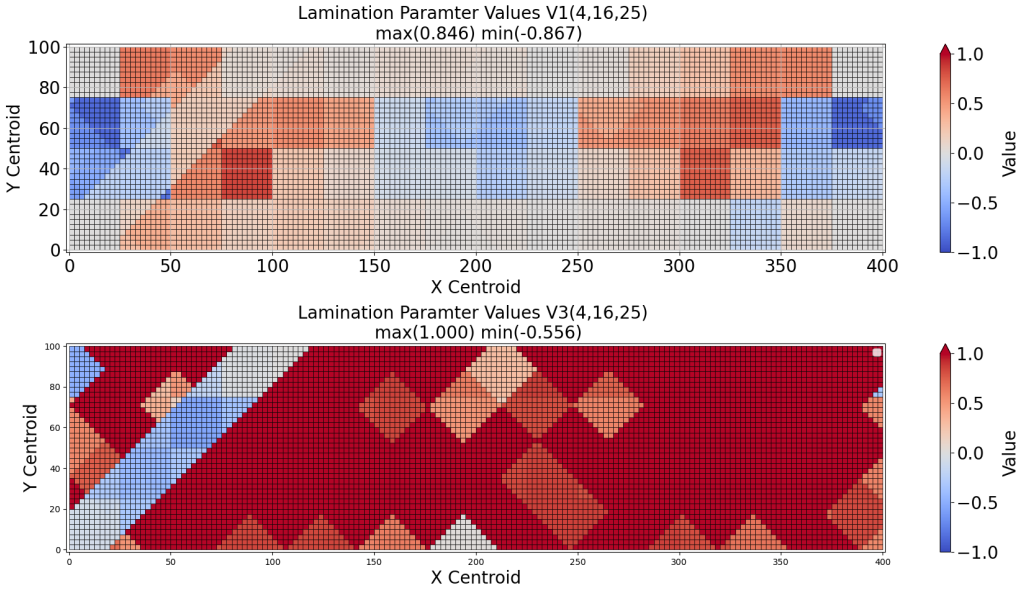

Figure D.5: Patch-wise model lamination parameter distribution for V1 and V3 in 4 thickness clusters and 1 stress clusters allowed before optimization.

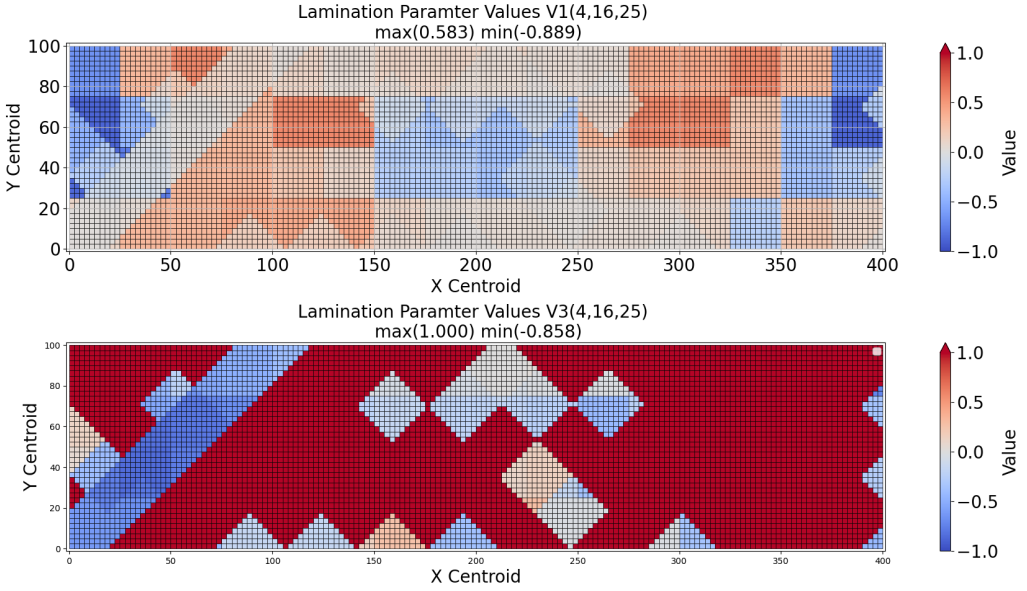

Figure D.6: Patch-wise model lamination parameter distribution for V1 and V3 in 4 thickness clusters and 16 stress clusters allowed after optimization.

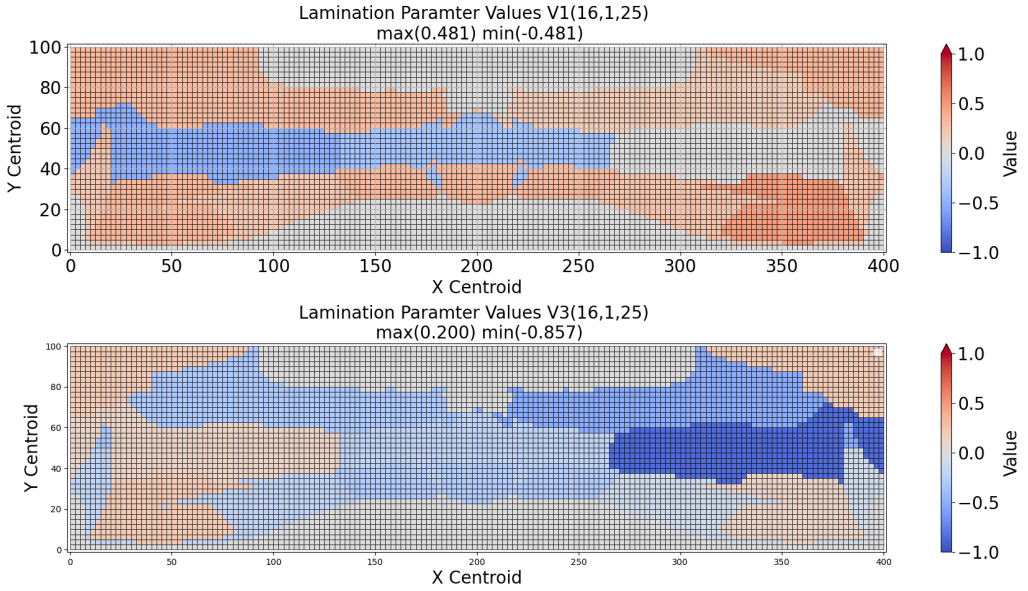

Figure D.7: Finite element model lamination parameter distribution for V1 and V3 in 16 thickness clusters and 1 stress clusters allowed.

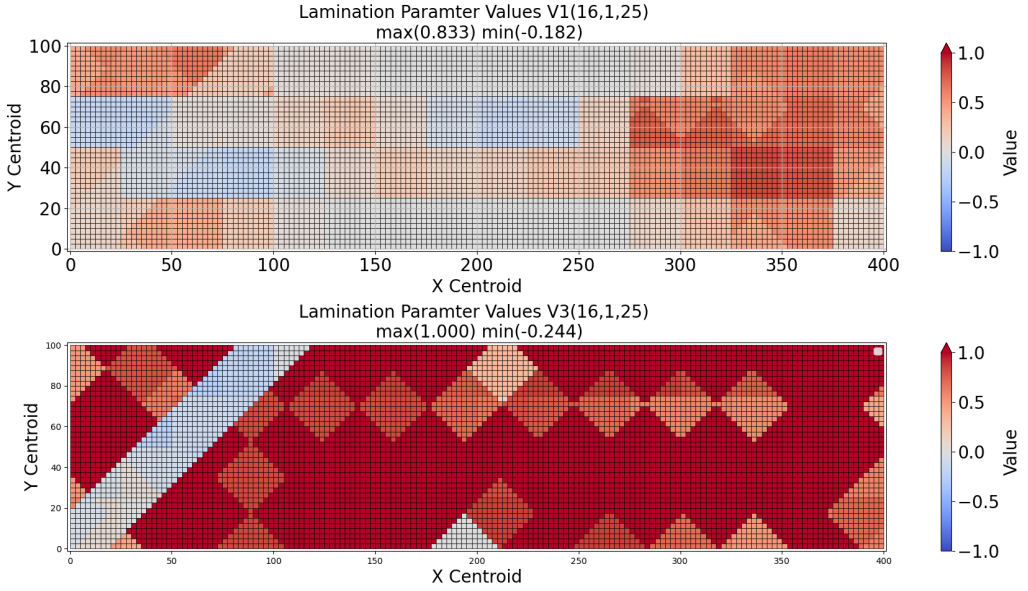

Figure D.8: Patch-wise model lamination parameter distribution for V1 and V3 in 16 thickness clusters and 1 stress clusters allowed before optimization.

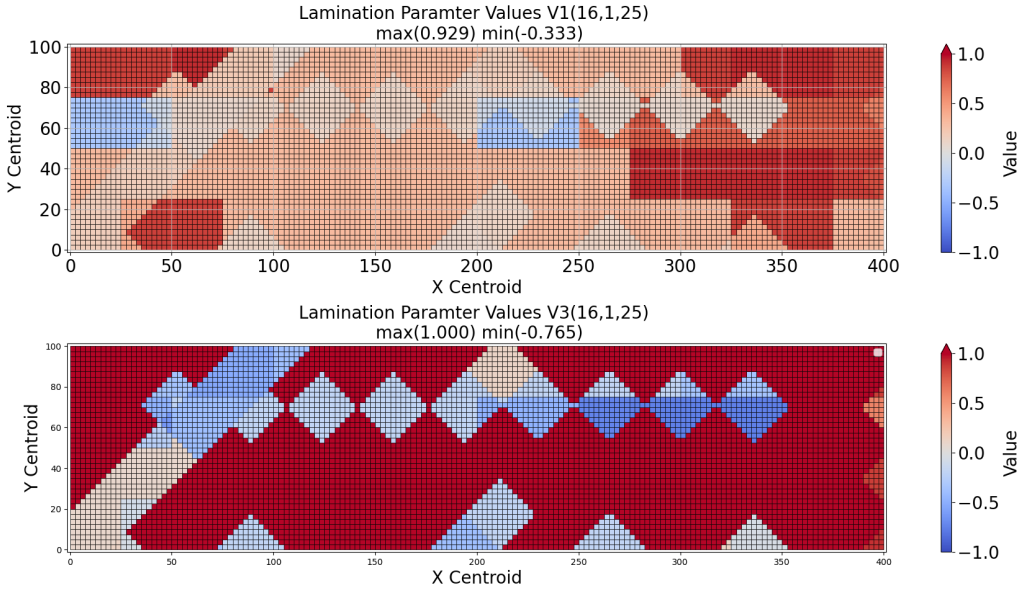

Figure D.9: Patch-wise model lamination parameter distribution for V1 and V3 in 16 thickness clusters and 1 stress clusters allowed after optimization.

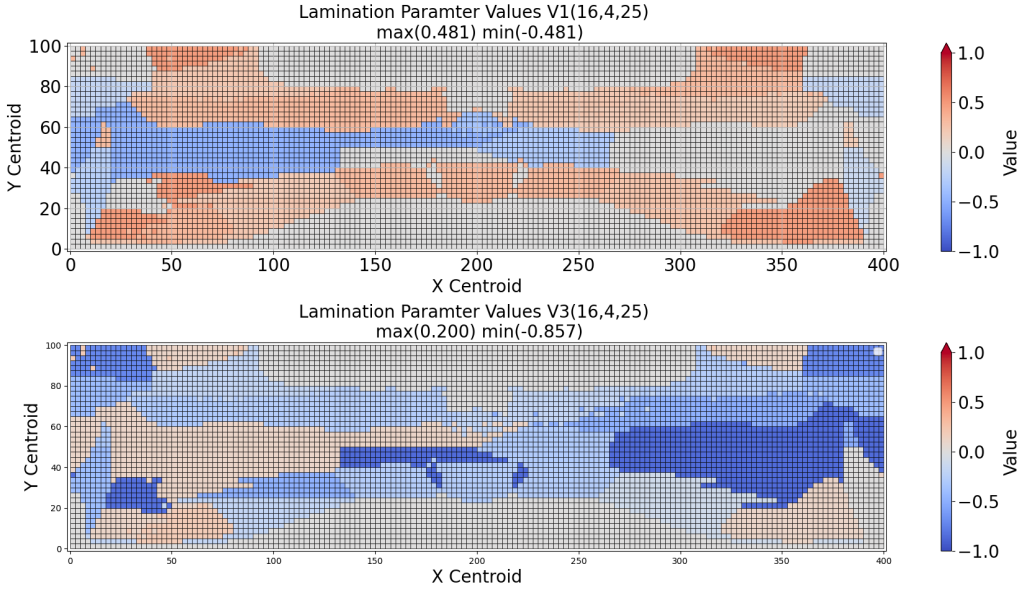

Figure D.10: Finite element model lamination parameter distribution for V1 and V3 in 16 thickness clusters and 4 stress clusters allowed.

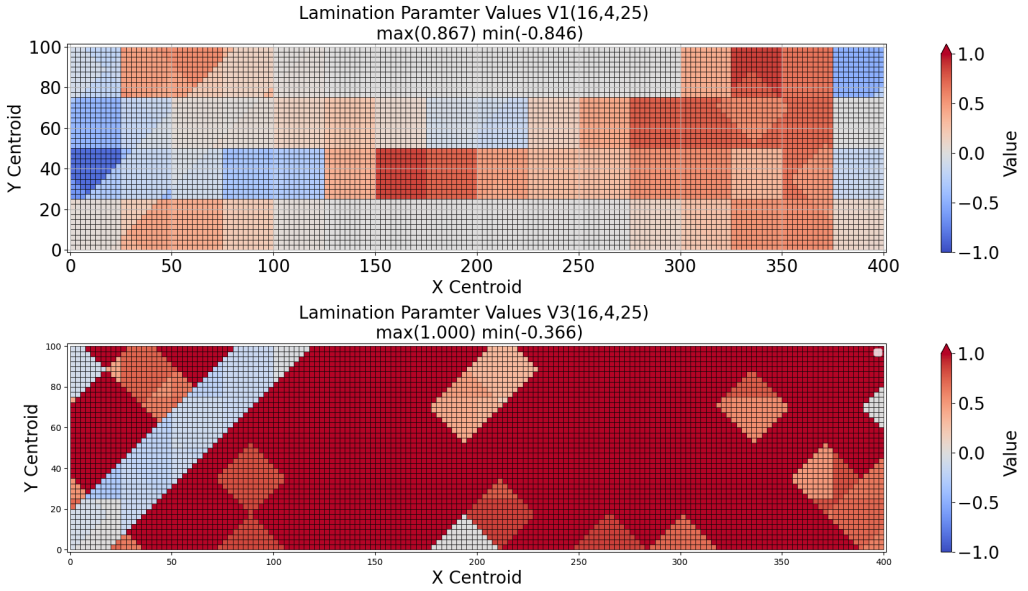

Figure D.11: Patch-wise model lamination parameter distribution for V1 and V3 in 16 thickness clusters and 4 stress clusters allowed before optimization.

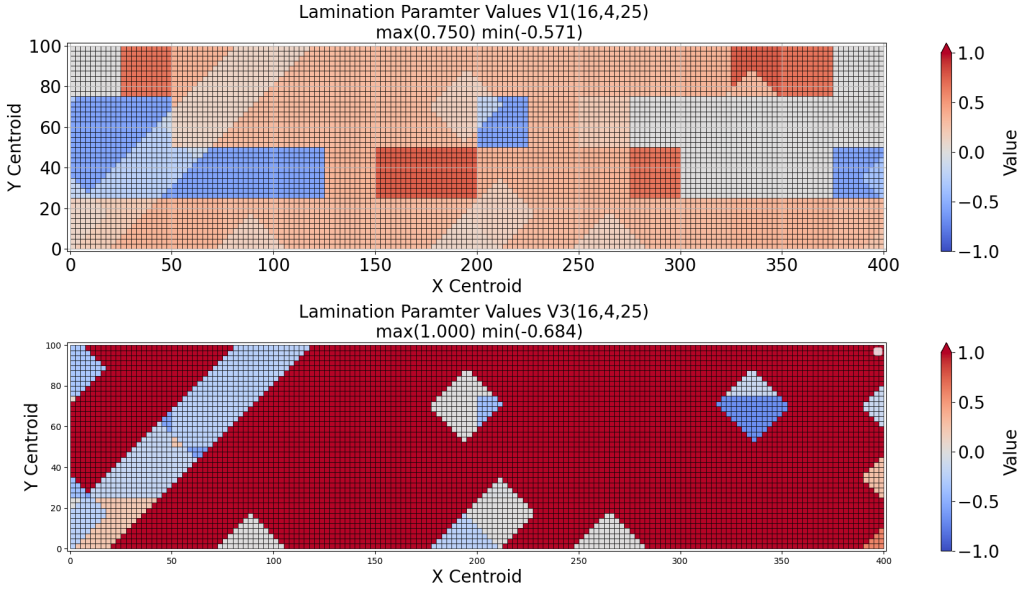

Figure D.12: Patch-wise model lamination parameter distribution for V1 and V3 in 16 thickness clusters and 4 stress clusters allowed after optimization.

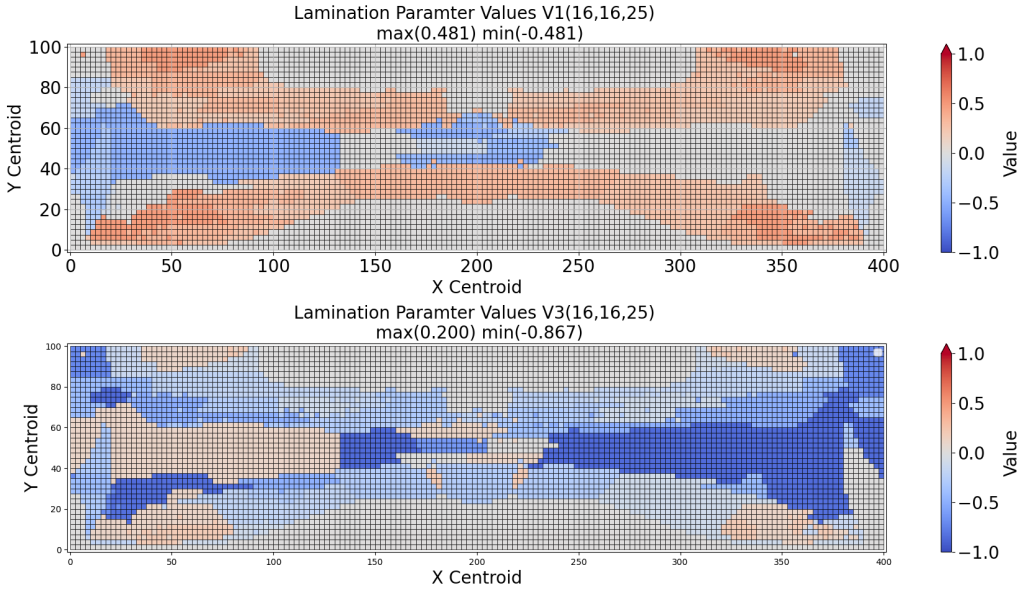

Figure D.13: Finite element model lamination parameter distribution for V1 and V3 in 16 thickness clusters and 16 stress clusters allowed.

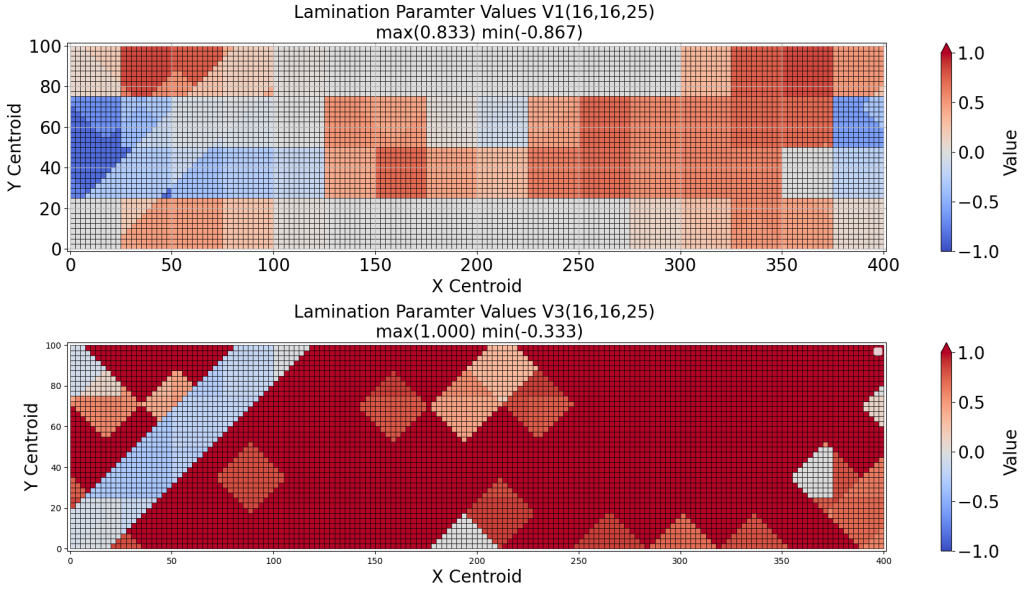

Figure D.14: Patch-wise model lamination parameter distribution for V1 and V3 in 16 thickness clusters and 16 stress clusters allowed before optimization.

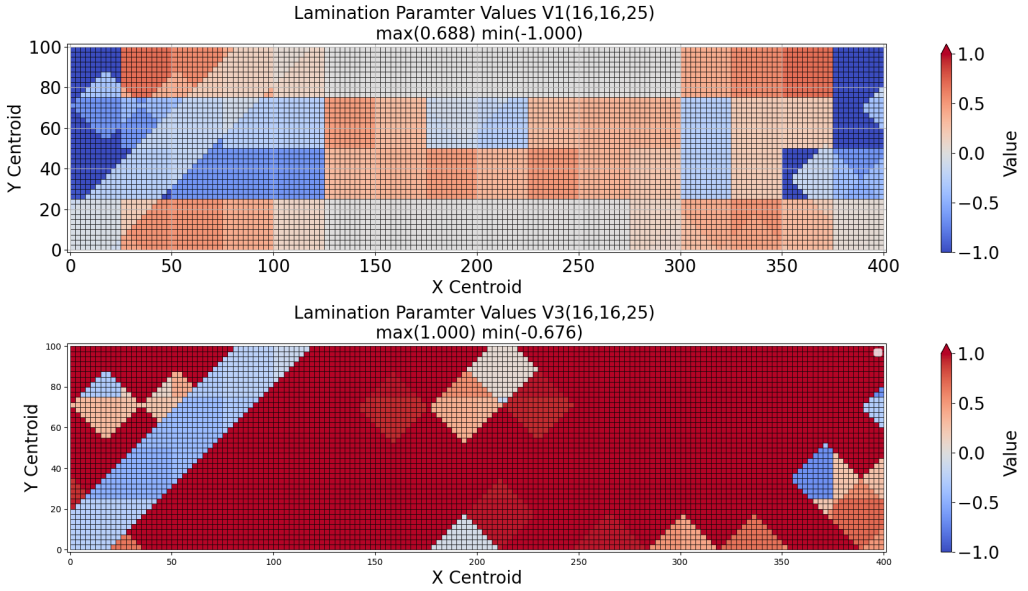

Figure D.15: Patch-wise model lamination parameter distribution for V1 and V3 in 16 thickness clusters and 16 stress clusters allowed after optimization.

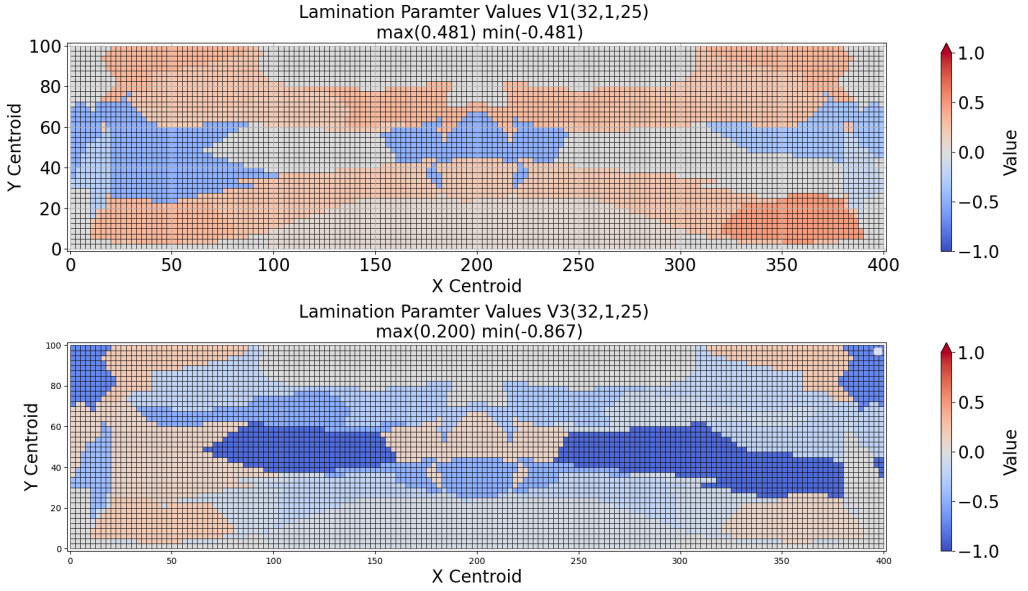

Figure D.16: Finite element model lamination parameter distribution for V1 and V3 in 32 thickness clusters and 1 stress clusters allowed.

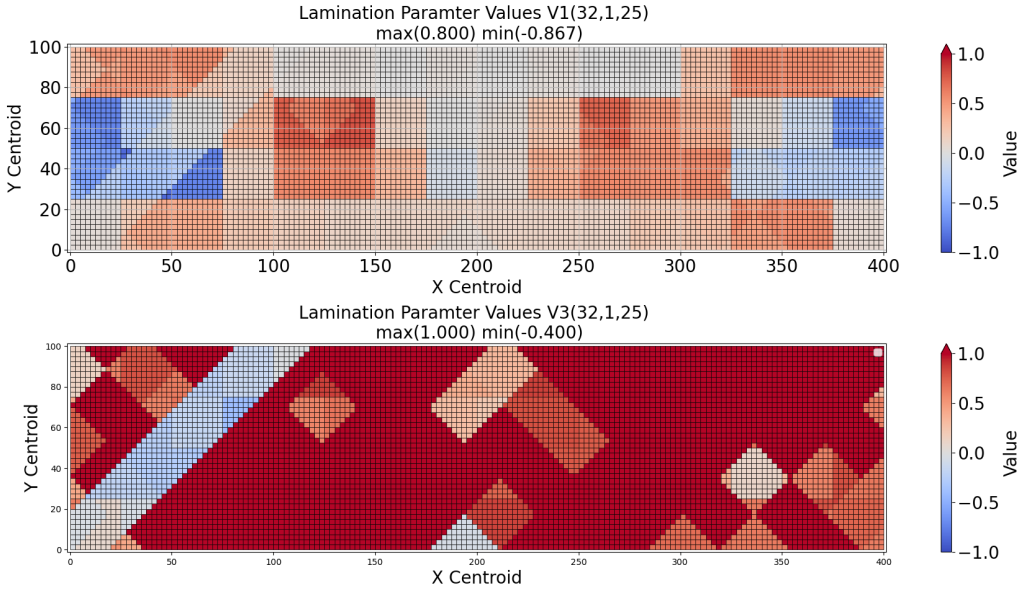

Figure D.17: Patch-wise model lamination parameter distribution for V1 and V3 in 32 thickness clusters and 1 stress clusters allowed before optimization.

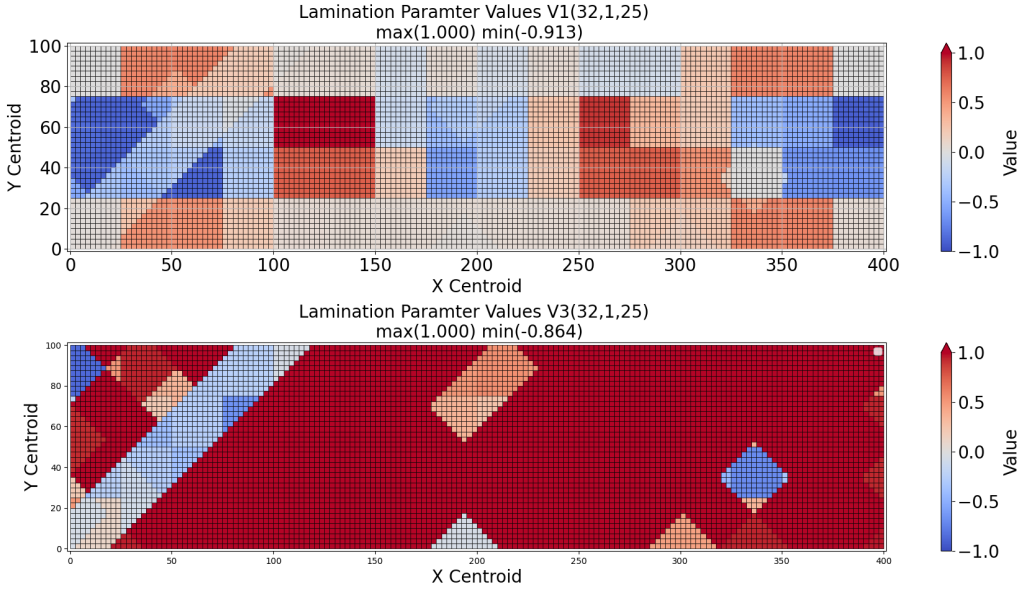

Figure D.18: Patch-wise model lamination parameter distribution for V1 and V3 in 32 thickness clusters and 1 stress clusters allowed after optimization.

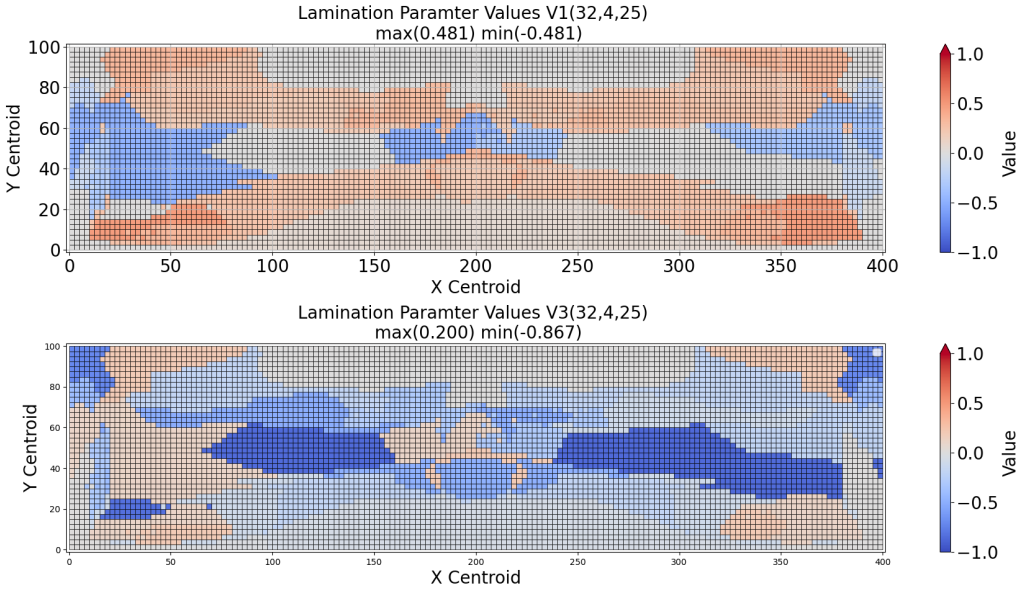

Figure D.19: Finite element model lamination parameter distribution for V1 and V3 in 32 thickness clusters and 4 stress clusters allowed.

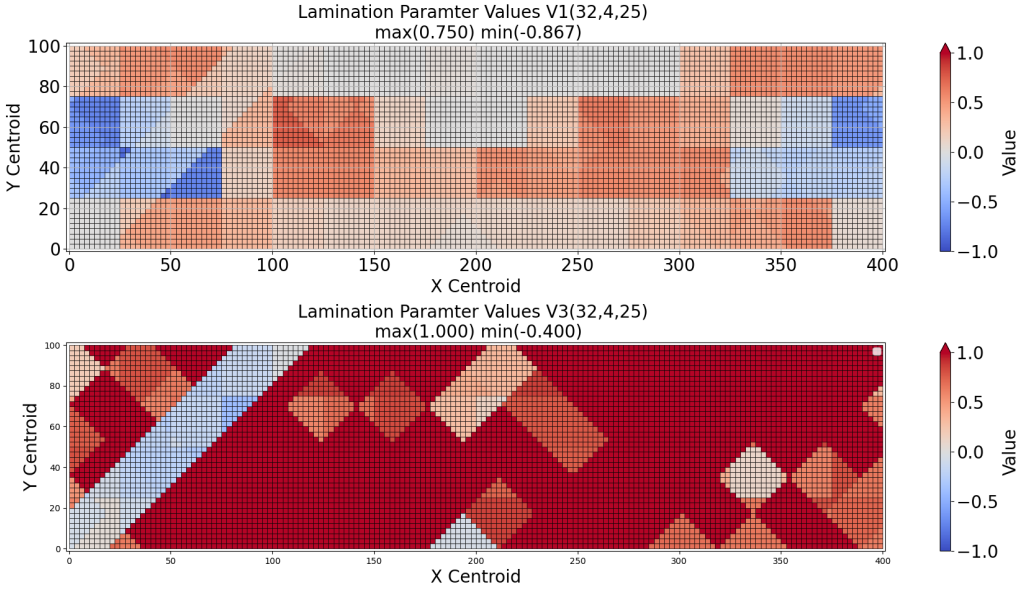

Figure D.20: Patch-wise model lamination parameter distribution for V1 and V3 in 32 thickness clusters and 4 stress clusters allowed before optimization.

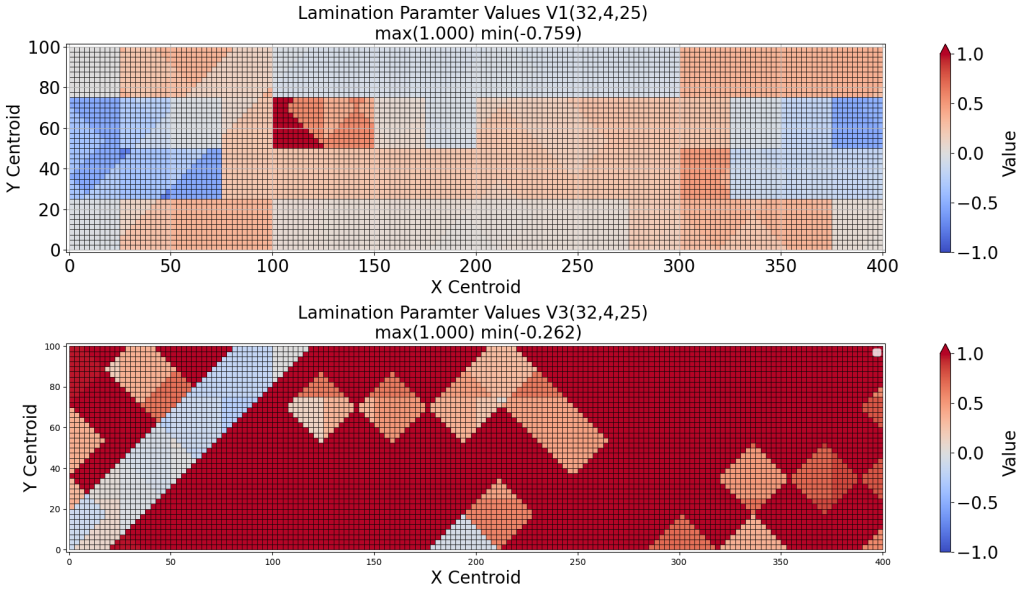

Figure D.21: Patch-wise model lamination parameter distribution for V1 and V3 in 32 thickness clusters and 4 stress clusters allowed after optimization.

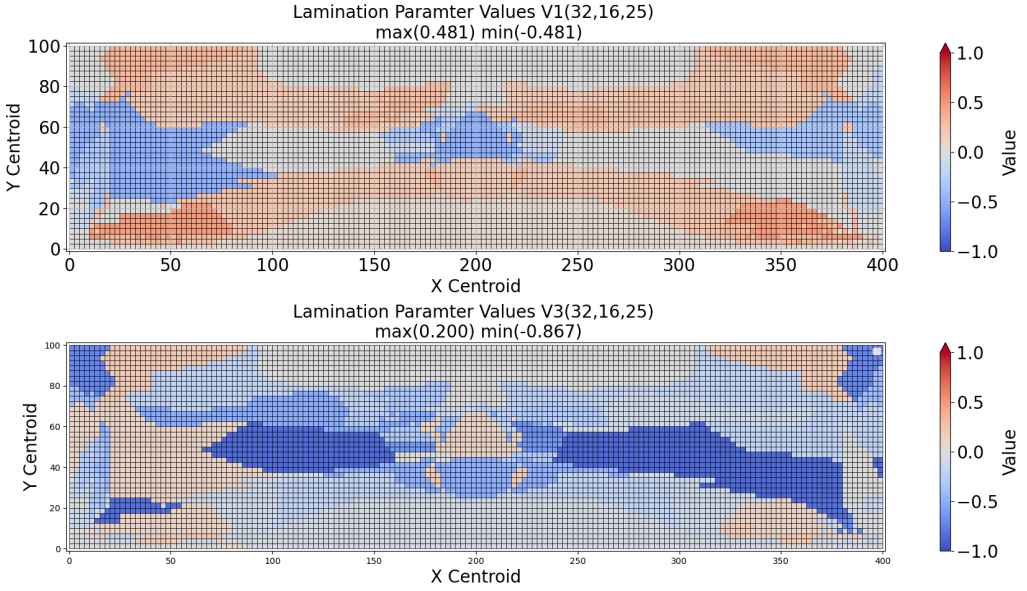

Figure D.22: Finite element model lamination parameter distribution for V1 and V3 in 32 thickness clusters and 16 stress clusters allowed.

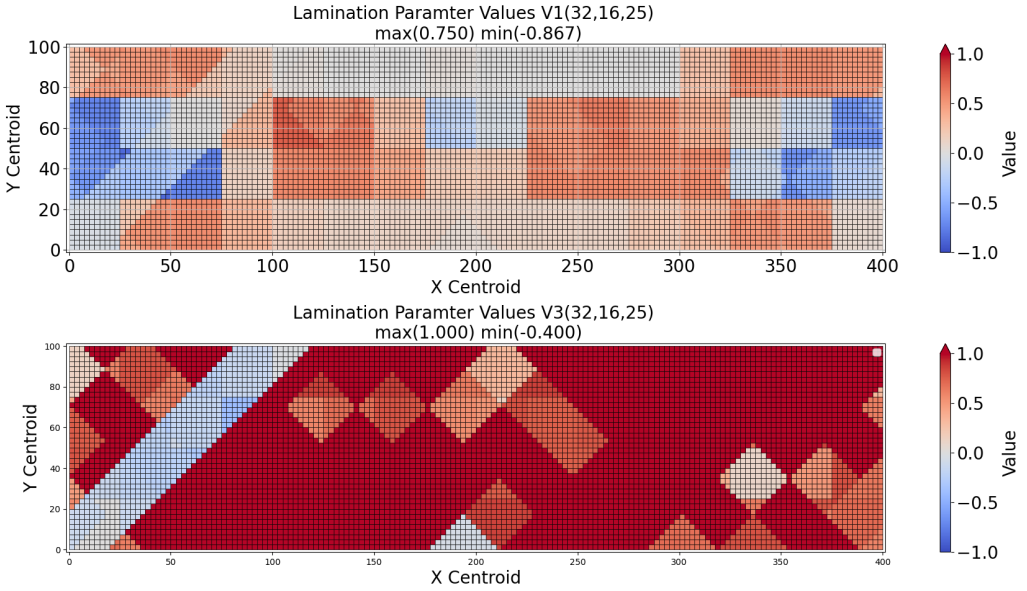

Figure D.23: Patch-wise model lamination parameter distribution for V1 and V3 in 32 thickness clusters and 16 stress clusters allowed before optimization.

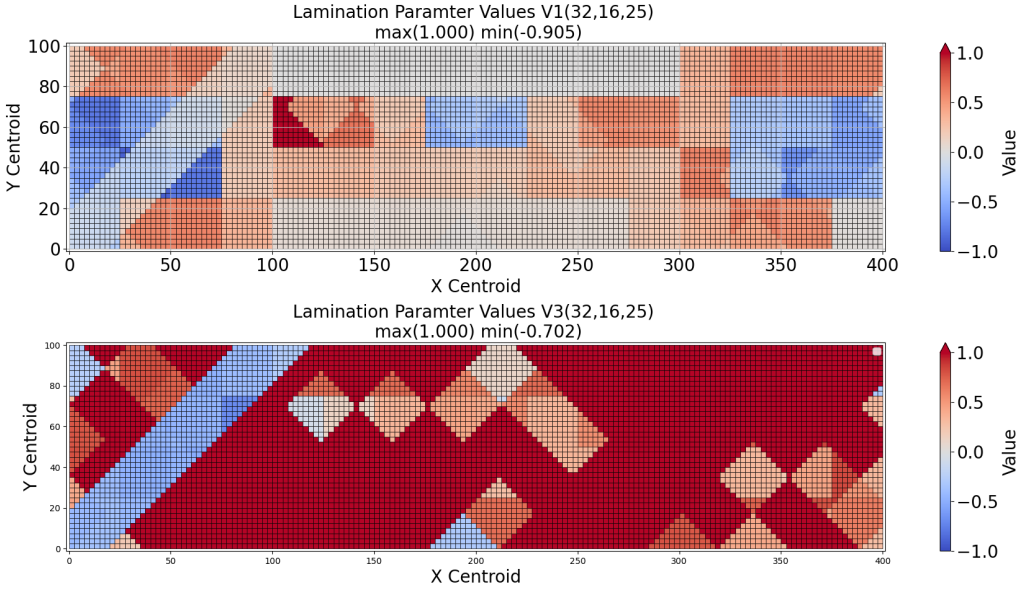

Figure D.24: Patch-wise model lamination parameter distribution for V1 and V3 in 32 thickness clusters and 16 stress clusters allowed after optimization.